THE SOLAR WIND INTERACTION WITH VENUS

J. G. LUHMANN

Institute of Geophysics and Planetary Physics, University of California, Los Angeles, California, U.S.A.

(Received in final form 18 November, 1986)

Abstract. This paper assesses our current understanding of the solar wind interaction with Venus in light of developments since the last major reviews were published in 1983. Suggestions for making further progress in the area of solar wind interactions with planetary atmospheres and ionospheres are offered based on the available observations and techniques, and from the viewpoint of forthcoming missions to Mars.

Table of Contents

1. Introduction

Venus, an effectively nonmagnetic planet, to a first approximation affects the oncoming solar wind plasma as if it were a highly conducting spheroid. On a typical day, the dense ionosphere formed by photoionization of Venus' primarily atomic oxygen upper

Space Science Reviews **44** (1986) 241–306.

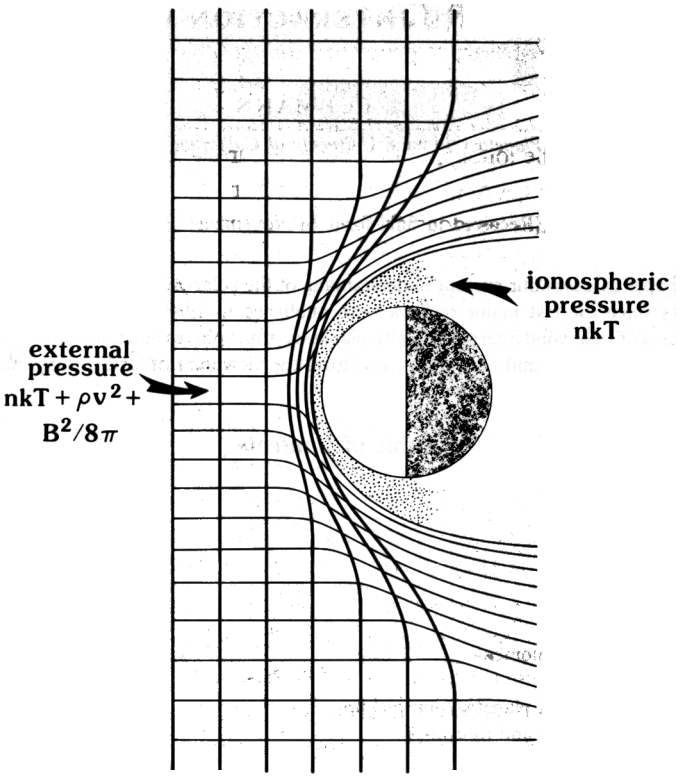

Fig. 1. Simplified illustration (not to scale) of the solar wind interaction with Venus, showing the ionosphere (shaded) 'standing off' the inflowing solar wind at the surface where the dynamic pressure ρv^2 (ρ = density, v = velocity) equals the thermal pressure. The upstream thermal pressure nkT and magnetic pressure $B^2/8\pi$ can usually be neglected compared to ρv^2. Thin lines show streamlines of plasma flow, while the thick lines represent magnetic field lines in the plane of a perpendicular interplanetary field.

atmosphere appears to support currents that largely exclude the interplanetary magnetic field and plasma from altitudes below a few hundred kilometers. In the subsolar region, the ionosphere is observed to have an upper boundary, or 'ionopause', at the location of this shielding current layer. Figure 1 illustrates the observed phenomenology. The solar wind is shocked and diverted around the ionosphere above the ionopause where its incident pressure (mainly dynamic) is approximately balanced by the thermal pressure of the ionospheric plasma, after which it continues along its antisolar route. This flow, which carries with it the interplanetary field, eventually fills the void left by the obstacle. Of course, there are many complications that are neglected in this simple description of the solar wind interaction.

The mere presence of an ionopause attests to the action of processes which must remove the upper ionosphere of Venus. Substantial numbers of neutral exosphere atoms above the dayside ionopause, which are ionized by photoionization, charge exchange with solar wind protons, impact ionization, and possibly by the critical velocity mechanism, can 'mass load' and slow the solar wind via various ion 'pickup' processes.

The ionopause itself is part of a complex boundary layer where the solar wind interaction with the planetary ions appears to produce anomalous heating of the upper ionosphere. Yet, a 'magnetic barrier' seems to effectively separate the plasmas of internal and external origin except on infrequent occasions then the incident solar wind dynamic pressure approaches the ionosphere's peak pressure and the above scenario based on pressure balance no longer applies. The terminator ionosphere generally exhibits signs of waves or irregularities as does the nightside ionosphere, which has a substantial density in spite of the slow rotation of Venus with respect to the Sun. Unlike the situation on the dayside, the upper boundaries of the terminator and nightside ionospheres are usually highly irregular and variable. To distances of at least ~ 12 planetary radii ($1\ R_v \sim 6350$ km) the wake is filled by a magnetic field configuration of interplanetary origin reminiscent of a comet's tail.

Although some of the basic features of the Venus-solar wind interaction were anticipated (cf. Banks and Axford, 1970; Johnson and Midgely, 1969; Wallis, 1974; Cloutier, 1975), our understanding has taken significant leaps as a result of visits by spacecraft during the missions of Mariner 5 and 10, Venera 4, 6, 9, 10, 11, 12, 13, and 14, and Pioneer Venus (see Russell and Vaisberg, 1983). Most recent observational results on the solar wind interaction come from the Pioneer Venus Orbiter, which, at this date, continues its exploration of the Venus environment which it began in 1978. Some of the analyses were made possible only because the mission was allowed to evolve, providing the opportunity for the spacecraft to move into hitherto unexplored regions of the Venus environment. This extended mission, together with the constant reevaluation of previously obtained data, continues to provide an increasingly more complete and complex view of the solar wind interaction.

The subject of this review has already received considerable attention in a post Venera retrospective by Breus (1979), a special Pioneer Venus issue of the *Journal of Geophysical Research* (December, 1980), and a comprehensive 1983 University of Arizona Press volume entitled *Venus*. However, since *Venus* went to press, significant progress has been made. The intention of this review is thus to append to a selective summary of the preceding research the most recent findings from observations, data analyses, and theory. Following a brief reconsideration of the kind of obstacle that Venus represents to the solar wind, the discussion proceeds from the free-stream solar wind to the bow shock, into the region of shocked solar wind that constitutes the magnetosheath, through the boundary layer and into the ionosphere and atmosphere (which are known to affect, and to be affected by, the solar wind interaction), and ends in the wake and magnetotail region. At the conclusion, outstanding questions for future research and exploration are suggested.

2. Nature of the Obstacle

2.1. Intrinsic field

The key difference between the solar wind interaction with Venus and with the Earth is that at Venus, the 'obstacle' is not provided by an intrinsic dipolar magnetic field, but

by a dense ionosphere. The Russell and Vaisberg paper in *Venus* gives a detailed review of work related to the determination of the magnetic field of Venus. Following the 1980 study based on the initial Pioneer Venus observations (Russell *et al.*, 1980), one further effort has been made by Phillips and Russell (1986) to establish the intrinsic field magnitude. This most recent statistical study of Pioneer Venus data obtained in the wake, where fields related to the solar wind interaction with the ionosphere provide their minimal interference, reduces the upper limit of the dipole moment to $\sim 10^{-5}$ that of Earth. As Russell and Vaisberg point out, this field plays no significant role in the solar wind interaction with the planet. Although a suggestion was made by Knudsen *et al.* (1982) that regions of ~ 10 nT sunward and antisunward magnetic fields observed in the antisolar ionosphere were produced by the distorted magnetic field of an intrinsic dipole, studies of the polarities of these fields (Luhmann and Russell, 1983; Marubashi *et al.*, 1985) support the hypothesis of an interplanetary origin. These ionospheric features of the solar wind interaction, also known as holes because of their related depletions in the ionospheric plasma density, will be discussed in a later section.

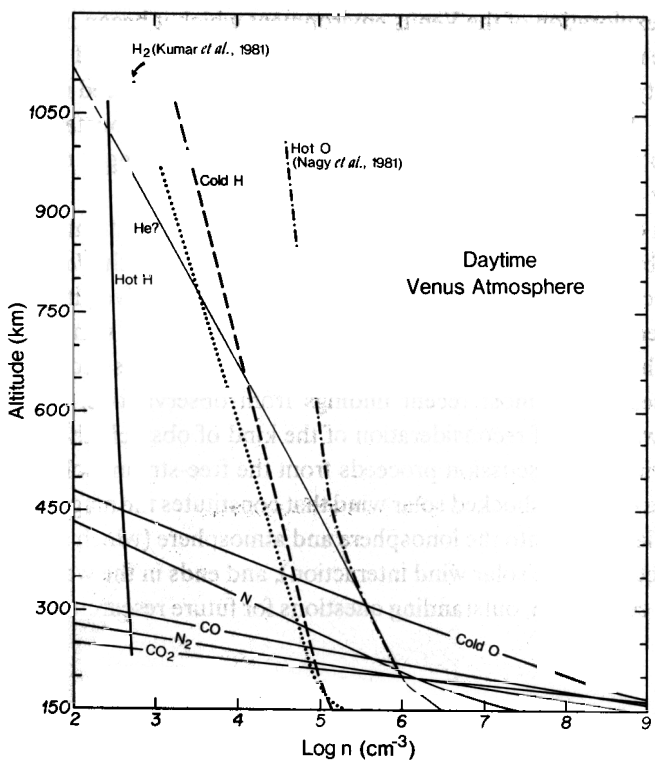

Fig. 2. Altitude profiles of the neutral atmospheric constituents at Venus. The composition below ~ 200 km was measured by Niemann *et al.*. (1980) on the Pioneer Venus Orbiter. The extended exospheres of H and O were inferred from ultraviolet spectrometer data.

2.2. Neutral Atmosphere

Observations at Venus have generally confirmed the importance of the dense dayside ionosphere in standing off the solar wind. The neutral atmosphere, which provides the nominal ionosphere when solar EUV photoionizes its constituents, has been surveyed below ~200 km altitude by the neutral mass spectrometer on the Pioneer Venus Orbiter (Niemann *et al.*, 1980). Ultraviolet spectrometer measurements in H-Lyα and the 1304 Å line of atomic oxygen have increased the altitude range of a subset of these observations to over 1000 km. These data were used (cf. Cravens *et al.*, 1980a; Nagy *et al.*, 1981) to infer the presence of the extended dayside exospheres of hot hydrogen and oxygen illustrated in Figure 2, which also shows the composition detected at the lower altitudes by the neutral mass spectrometer. Oxygen (O) dominates over hydrogen (H) up to ~0.5 R_v where H becomes dominant. The source of this neutral O corona is considered to be dissociative recombination of O_2^+.

Although the planet Venus rotates very slowly in near synchronism with the Sun, the upper atmosphere, like the lower atmosphere, is thought to 'superrotate' in a retrograde sense. Eastward wind speeds of ~100 m s^{-1} are expected to prevail near the altitude of the exobase at ~200 km (Mayr *et al.*, 1980). The details of this neutral exosphere superrotation are, however, poorly known.

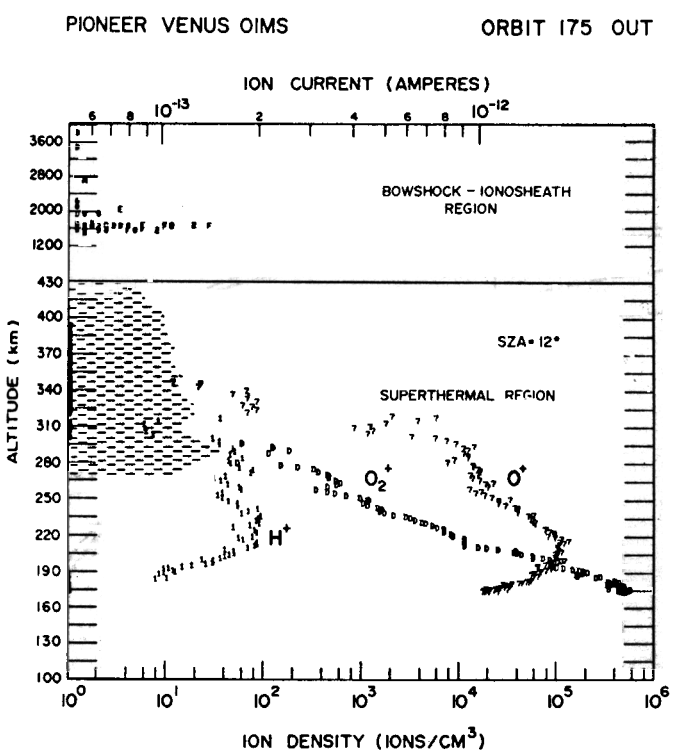

Fig. 3. Pioneer Venus Orbiter ion mass spectrometer observations from one orbit leg displayed as an altitude profile (from Taylor *et al.*, 1980).

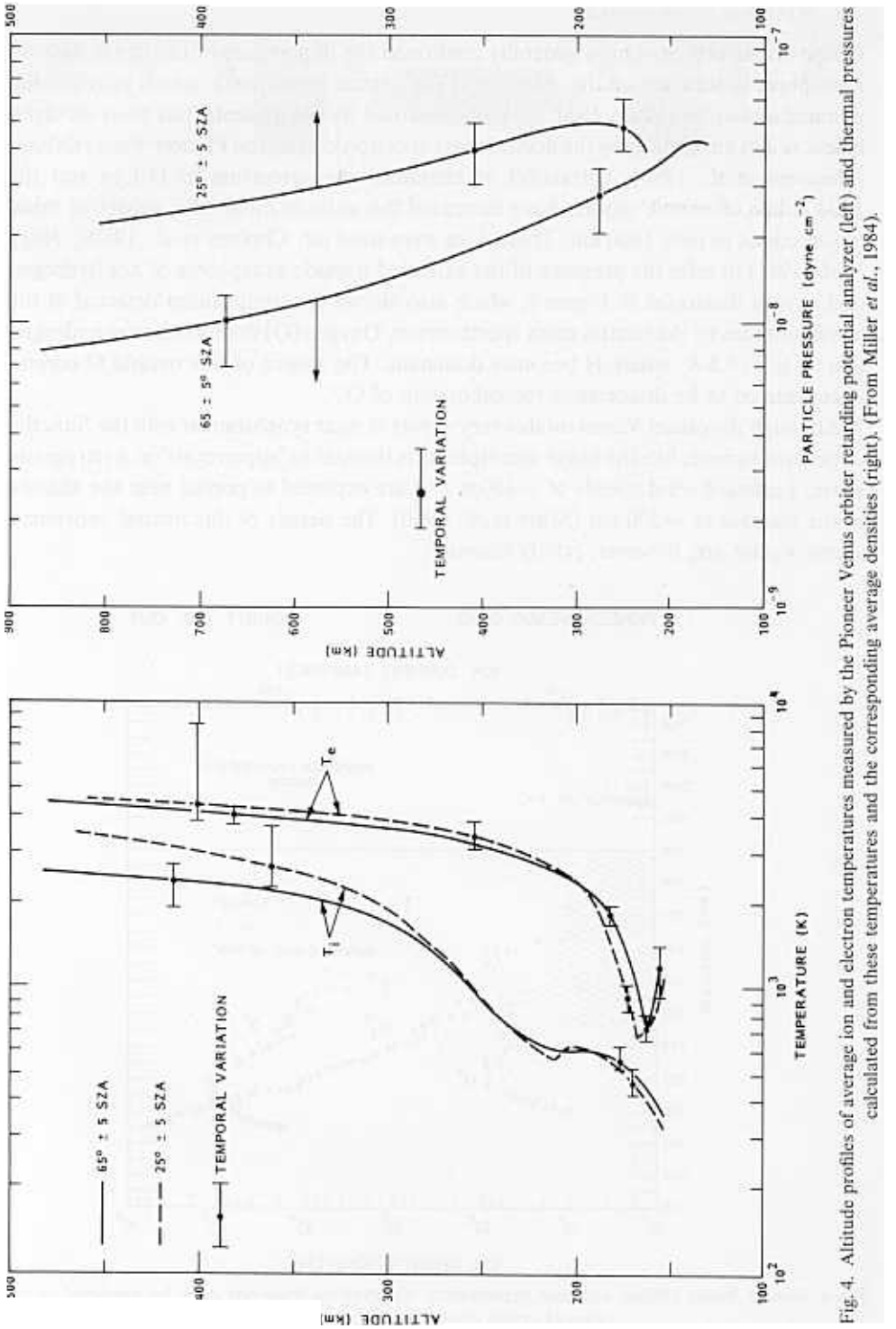

Fig. 4. Altitude profiles of average ion and electron temperatures measured by the Pioneer Venus orbiter retarding potential analyzer (left) and thermal pressures calculated from these temperatures and the corresponding average densities (right). (From Miller *et al.*, 1984).

2.3. IONOSPHERE

The ionosphere produced by the solar EUV incident on the neutral atmosphere has been modelled by Cravens *et al.* (1980b, 1983) and measured by the Langmuir probe (Brace *et al.*, 1980; Theis *et al.*, 1980), the ion mass spectrometer (Taylor *et al.*, 1980) and the retarding potential analyzer (Knudsen *et al.*, 1980a, b; Miller *et al.*, 1980) on the Pioneer Venus Orbiter. Some of the variations observed in the body of the ionosphere reflect both solar cycle and transient changes in the incident solar EUV flux (Bauer and Taylor, 1981; Elphic *et al.*, 1984a; Kar *et al.*, 1986). The ionospheric plasma composition is primarily O_2^+ at low altitudes, and O^+ above $\sim$200 km. An example of an altitude profile of composition obtained along the Pioneer Venus orbit from Taylor *et al.* (1980) is given in Figure 3. Although the ionosphere is absent above the ionopause, ions are still produced there at a rate which can be estimated by multiplying the neutral densities above $\sim$300 km in Figure 2 by $\sim 4 \times 10^{-6}$ s^{-1}. The ionosphere density peak has been measured only indirectly, via radio occultation techniques (cf. Cravens *et al.*, 1981). It

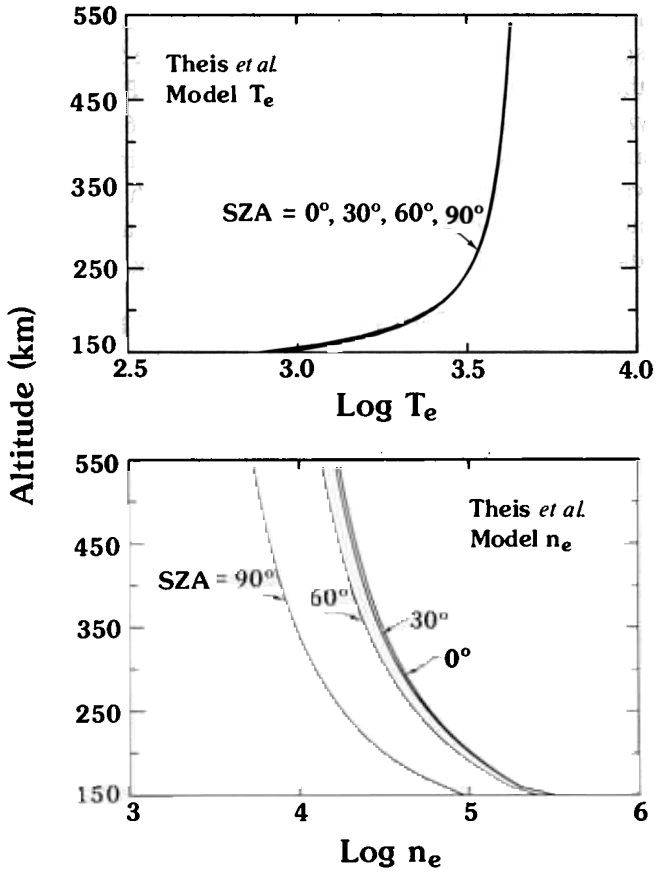

Fig. 5. Altitude profiles of electron density (bottom) and altitude profiles of electron temperature (top) derived from the empirical ionosphere model based on Pioneer Venus Orbiter Langmuir probe data (Theis *et al.*, 1984).

appears to be located at ~140 km altitude and to be characterized by a maximum plasma density of $\sim 5 \times 10^5$–7×10^5 cm^{-3}, depending on the phase of the solar cycle. Ion and electron temperatures at the density peak are not precisely known. However, the *in situ* observations of temperatures reproduced on the left-hand side of Figure 4. indicate that the peak plasma pressure of $\sim 5 \times 10^{-8}$ dynes cm^{-2}, illustrated on the right-hand side of Figure 4, occurs above the density peak at the higher altitude of ~180 km (Miller *et al.*, 1984).

Modelling efforts tell us that photochemical equilibrium prevails below ~170 km (see Nagy *et al.*, 1983). The scale height above the peak pressure appears consistent with diffusive equilibrium except that extra heat sources seem to be required for both ions and electrons (Cravens *et al.*, 1980; Miller *et al.*, 1980; Brace *et al.*, 1983; Nagy *et al.*, 1983). Because this additional heating is probably attributable to the solar wind interaction, it will be addressed in a later discussion. Of course, also because of the solar wind interaction, the ionosphere is absent above the altitude of the ionopause which is typically located at ~300 km in the subsolar region and closer to ~1000 km near the terminator. Theis *et al.* (1984) used the Langmuir probe data to develop a global empirical ionosphere model, which is summarized in Figure 5. This empirical model, together with the observations of ion bulk flow from the Pioneer Venus Retarding Potential analyzer (Knudsen *et al.*, 1981) shown in Figure 6, and several additional modelling efforts (Cravens *et al.*, 1983; Whitten, 1984), indicate that the Venus ionosphere flows anti-sunward with a velocity consistent with pressure gradient driven convection (Knudsen *et al.*, 1981), except, perhaps, for a layer adjacent to the ionopause (Perez-de-Tejada, 1986). This finding is not surprising considering the Sun-

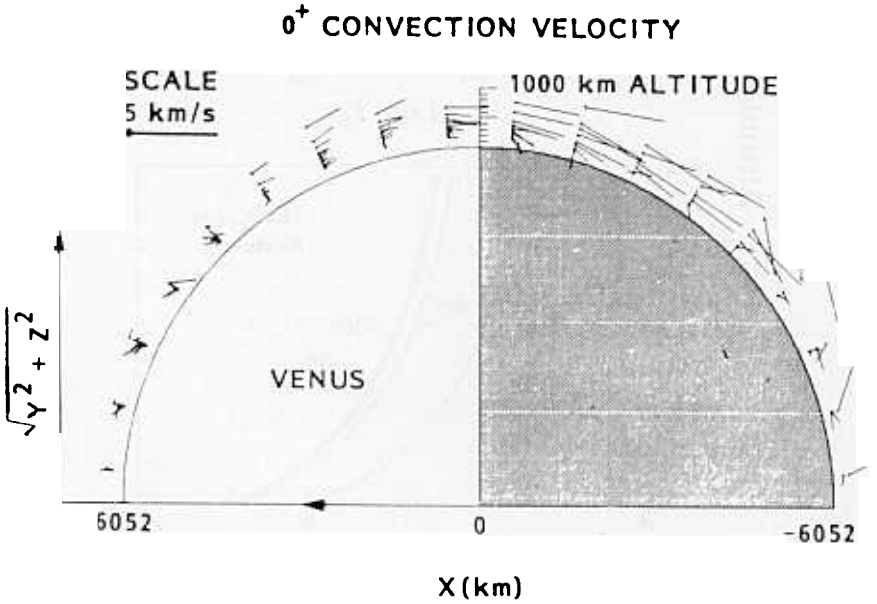

Fig. 6. Average antisolar ionospheric plasma velocity vectors measured by the Pioneer Venus Orbiter retarding potential analyzer (Knudsen *et al.*, 1982).

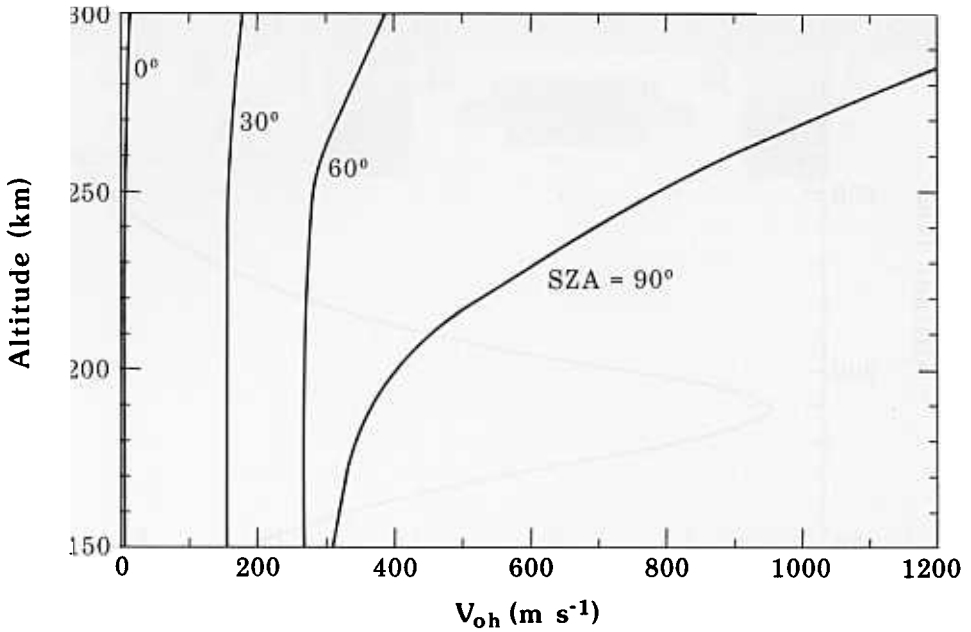

Fig. 7. Altitude profiles of the dayside ionospheric horizontal (antisolar) velocity at several solar zenith angels from the model of Theis *et al.*, 1984.

synchronous rotation of Venus. In simple terms, the photoionization source produces a dayside ionosphere which expands to fill the nightside sink maintained by subsidence and recombination. Figure 7 summarizes one of the current models of the horizontal ionospheric flow. Although collisional coupling of the ions to the superrotating neutral atmosphere (e.g., Schubert, 1983) somewhat distorts this antisolar flow pattern by introducing a dawn-dusk asymmetry (Miller *et al.*, 1984), the global antisolar transport appears adequate to supply the bulk of the nightside ionospheric plasma up to solar zenith angles $\sim 150°$ (Knudsen *et al.*, 1981; Cravens *et al.*, 1983). It is also noteworthy that the km s^{-1} horizontal velocities near the terminator exceed the local sound speed of several hundred m s^{-1}. In addition to this horizontal ionospheric motion, there is a relatively slow vertical convection which is determined by the ionospheric photochemistry, pressure gradients, gravity, polarization electric fields, and the ion-neutral collision rates (Cravens *et al.*, 1984). The altitude profile of this calculated velocity, which is not directly measured due to its small magnitude relative to the horizontal component, is shown in Figure 8. At altitudes below the normal subsolar ionopause (< 300 km), the ionosphere drifts downward with a peak velocity of ~ 60 m s^{-1} at ~ 200 km. The general characteristics of the vertical motion are expected to be similar throughout the dayside ionosphere (cf. Cravens *et al.*, 1983).

A recent overview of the Venus atmosphere and ionosphere has been compiled by Kliore *et al.* (1985) in the *Venus International Reference Atmosphere* volume of *Advances in Space Research*. From the viewpoint of the solar wind interaction, the most important property of Venus' atmosphere and ionosphere is that the peak subsolar ionospheric

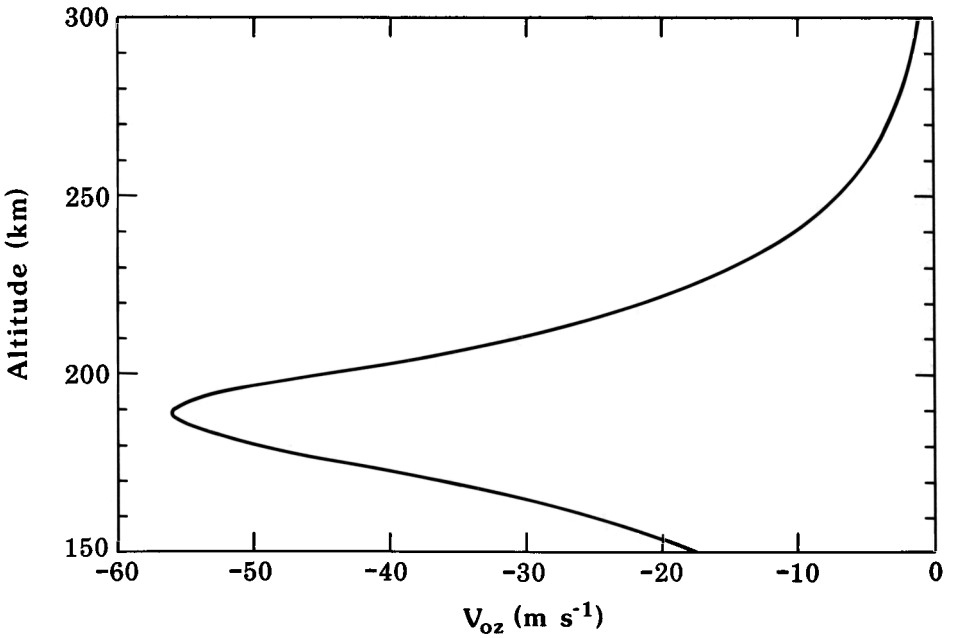

Fig. 8. Altitude profile of the dayside ionospheric vertical velocity from the model of Cravens *et al.* (1984).

plasma pressure generally exceeds the incident solar wind pressure. However, as will be shown, other details such as the intrinsic ionospheric flow properties and the high altitude neutral and ionized population have measurable effects on the solar wind interaction.

3. Solar Wind at 0.7 AU

As at the Earth, the interplanetary medium at Venus is highly variable with the degree of variability reflecting the intensity of solar activity, and, in the case of the interplanetary magnetic field, proximity to the heliospheric current sheet. In addition to the usual corotating stream structure, shocks and other transient disturbances sometimes perturb the local plasma. The details of this behavior can be seen in time series of the plasma and magnetic field data obtained on the Pioneer Venus Orbiter. Figure 9 shows examples of these data for one solar rotation (the apparent rotation period or synodic period is $\sim$28.6 days at Venus). Here, measurements obtained within Venus' magnetosheath have been removed from the magnetic field time series. The plasma data contain some magnetosheath points, but these can be identified as the intervals without simultaneous magnetic data. The local interplanetary magnetic field fluctuates on a broad range of timescales. Its low-frequency variability is dominated by heliospheric current sheet crossings which are sometimes accompanied by corotating interaction regions. The largest field magnitudes and highest densities and ion temperatures

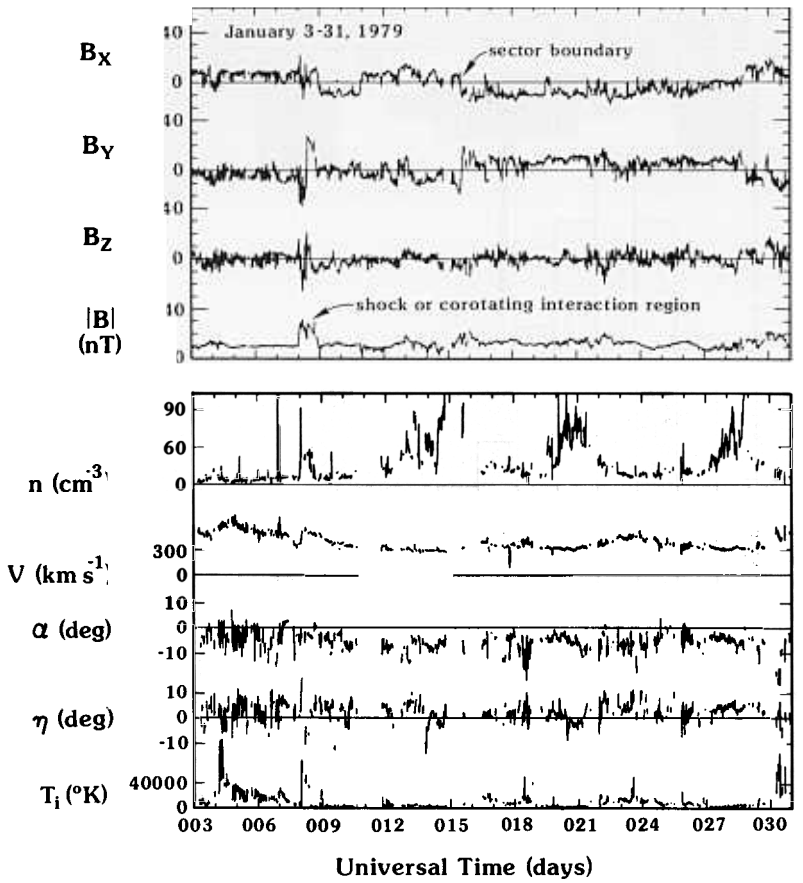

Fig. 9. Example of solar wind parameters measured at Venus during an apparent solar rotation (~28 days) by the Pioneer Venus Orbiter magnetometer and the plasma analyzer. The plasma density, n, bulk velocity v, ion temperature T_i, azimuthal abberation angle α, and polar abberation angle η are shown together with the magnetic field magnitude and components in VSE coordinates.

measured usually occur in conjunction with shocks associated with transient disturbances or corotating interaction regions. However, significant fluctuations of the upstream parameters are also seen in high-speed streams and in occasional long-lived low β (β = thermal pressure/magnetic pressure) regions.

While the aforementioned details are important because they are responsible for the variability of the Venus-solar wind interaction, from the point of view of establishing an 'average' picture it is most useful to examine the statistical properties of the solar wind. Of particular interest for solar wind interaction studies are the dynamic pressure, Mach number, and magnetic field. Figure 10 from Phillips *et al.* (1984) and Figure 11 from Tatrallyay *et al.* (1983) show statistical distributions of the first two quantities obtained on Pioneer Venus near solar maximum. The interplanetary field at Venus has a typical magnitude of ~12 nT and a Parker spiral orientation with a garden hose angle of ~40°.

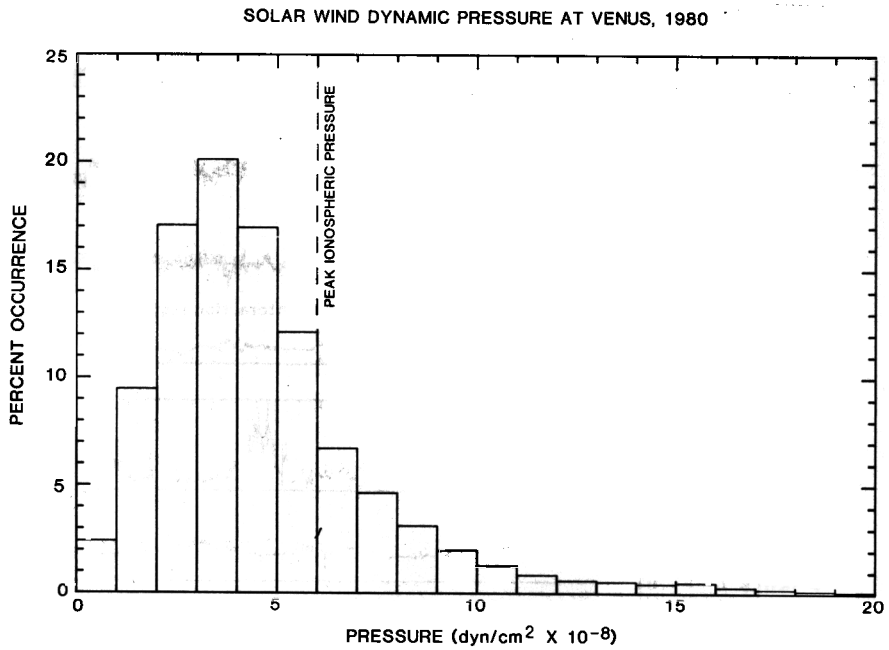

Fig. 10. Histogram of occurrence of solar wind dynamic pressure calculated from the Pioneer Venus plasma analyzer measurements (from Phillips *et al.*, 1984). The peak ionospheric presure is indicated by the dashed line.

It is notable that the average Alfvén Mach number is low in the sense that Spreiter and Stahara (1980a,b) define, suggesting that the interplanetary magnetic field should have a non-negligible effect on the average solar wind interaction with Venus. However, it is even more important, for the nature of the interaction, that the dynamic pressure is usually less than the peak ionospheric plasma pressure observed on Pioneer Venus (see Figure 4). The vertical dashed line in Figure 10 is adjusted to allow for the fact that the stagnation pressure of the solar wind is actually ~ 0.85–0.88 of the upstream dynamic pressure.

4. Solar Wind Interaction Phenomena

4. Bow shock

4.1.1. *Global Effects of Planetary Ion Pickup*

A fast magnetosonic shock and its foreshock are the outermost signatures of an obstacle to the solar wind flow. The presence of a bow shock at Venus was detected by the earliest probes (cf. references in Gringauz, 1983; and Russell and Vaisberg,1983). These observations provided the first clues about the planetary obstacle. In particular, gasdynamic modelling of hypersonic flow around blunt obstacles (cf. Spreiter and Stahara, 1980a) provides a tool for inferring the shape of an obstacle from the position

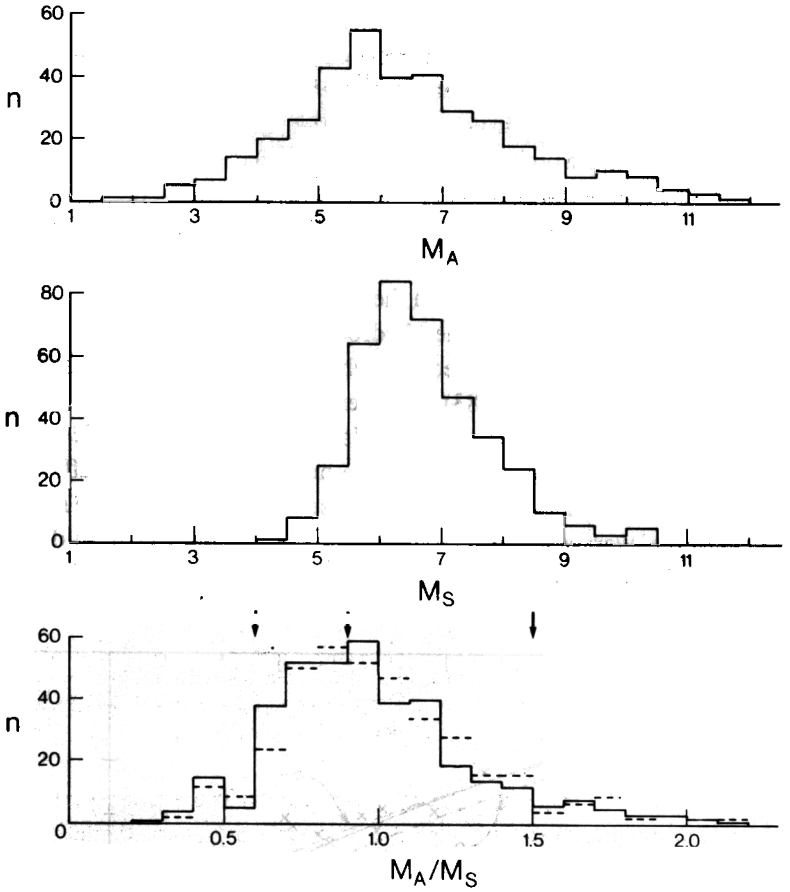

Fig. 11. Histograms of solar wind Mach numbers derived from Pioneer Venus Orbiter plasma analyzer data (from Tatrallyay *et al.*, 1983). The Alfvén Mach number, M_A, sonic Mach number, and their ratio (equal to the square root of the plasma β) are shown.

and shape of its bow shock. When these early measurements were compared with model results (cf. references in Slavin *et al.*, 1983), it was apparent that the effective Venus obstacle nose is located at a distance from the planet center comparable to the planetary radius.

The extensive Pioneer Venus coverage greatly improved the data base for studying the bow shock position and behavior. For example, Slavin *et al.* (1980) extrapolated the well-determined shock position at larger solar zenith angles (where orbital coverage was available) to estimate a subsolar shock position at ~ 2300 km above the surface under solar maximum conditions. This estimate was later verified by Russell *et al.* (1985a) using new data obtained at lower solar zenith angles and a technique utilizing a calculation of the probability of observing the shock location at various solar zenith angles. These analyses showed that the suggestion (Russell, 1977) that the bow shock might be occasionally 'attached' to the Venus obstacle at the nose was not correct, at least at solar maximum, since the subsolar ionopause is typically inferred to be located

~2000 km below the shock altitude (cf. Brace *et al.*, 1983). With this extrapolation, it was considered that the shock shape could be used to investigate the extent of solar wind absorption by Venus' atmosphere. Both Slavin *et al.* (1980, 1983) and more recently Russell *et al.* (1985) made efforts to model the shock shape determined from magnetometer data using Spreiter and Stahara's (1980a) gas dynamic treatment and thereby deduce the altitude of the obstacle nose. This altitude would be near or above the subsolar ionopause if absorption was unimportant, and well within the observed ionopause if the opposite was true. Unfortunately, because the bow shock location is affected by the solar wind interaction with the neutral atmosphere above the ionopause, and because the interaction is magnetohydrodynamic and not gas dynamic, these studies were by their nature limited in what they could accomplish. Another investigation by Tatrallyay *et al.* (1983), which examined the variation of the bow shock position with solar wind parameters such as Mach number and dynamic pressure, was similarly undermined by its neglect of what we now know about the effect of Venus' exosphere on the bow shock shape. However, these authors provided the most accurate measurement of the average shock shape to date. Their result, based on data from the years 1978–1983, is displayed in Figure 12.

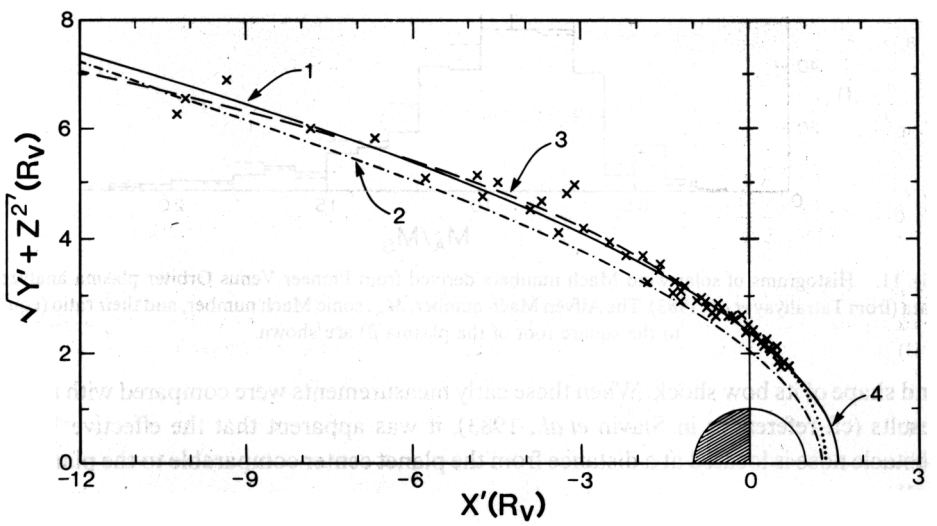

Fig. 12. Several conic section fits to Venus bow shock positions obtained from Pioneer Venus Orbiter magnetometer measurements (from Tatrallyay *et al.*, 1983).

Our current understanding of the Venus bow shock took shape when several Pioneer Venus investigators (Slavin *et al.*, 1980; Mihalov *et al.*, 1982), noted that the shock observed during the early mission could be produced with an ionopause-shaped obstacle in the gas-dynamic calculations only if an unrealistically low sonic Mach number (~3) was invoked. These authors realized that the solar plasma flow around the Venus obstacle could be significantly modified by the addition of planetary ions produced

above the ionopause. Slavin *et al.* (1980) further realized that the observed difference between the bow shock position measured on the Pioneer Venus Orbiter and the earlier Venera spacecraft was due to solar cycle changes in the effective obstacle that Venus presents to the solar wind. The duration of the Pioneer Venus mission permitted the detailed study of the position of the bow shock as the current solar cycle progressed to maximum and then declined. Using the Orbiter magnetometer data to identify the shock, Alexander and Russell (1985) obtained the result shown in Figure 13, which clearly

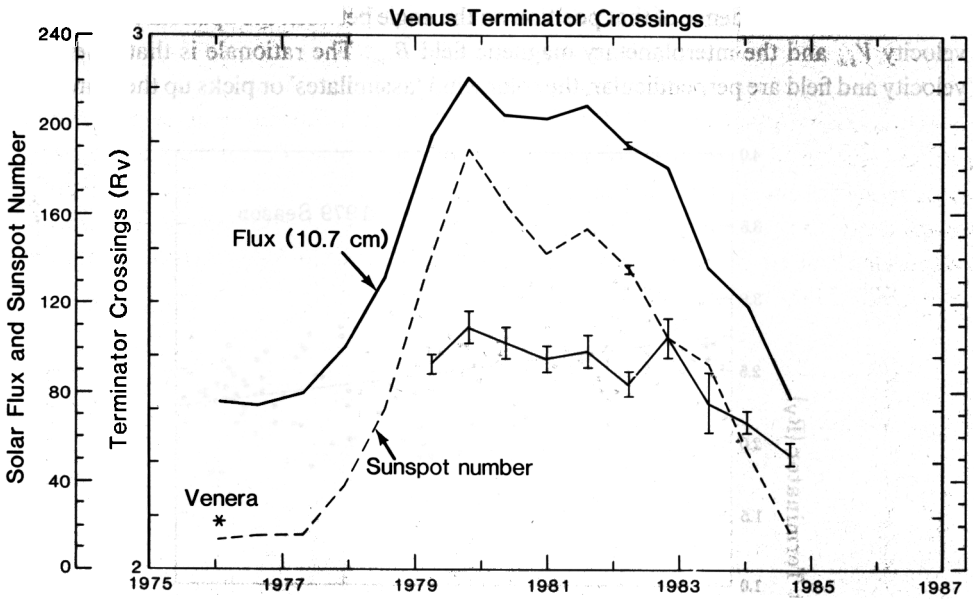

agreement with the observational results, that the bow shock is located further from the planet at the terminator in the model with the source term than it is for gas dynamic models without the source term.

While the mass-loaded gas dynamic models indeed represent an advancement in our ability to simulate the Venus-solar wind interaction, there are further subtleties of the Venus obstacle which are not taken into consideration in such macroscopic models. A recent observational analysis by Alexander *et al.* (1986) of the terminator position of the bow shock specifically considers the effects of planetary ions in the magnetosheath by examining the dependence of that position on the angle between the upstream solar wind velocity $\overline{V}_{sw}$ and the interplanetary magnetic field $\overline{B}_{sw}$. The rationale is that when the velocity and field are perpendicular, the solar wind 'assimilates' or picks up the planetary

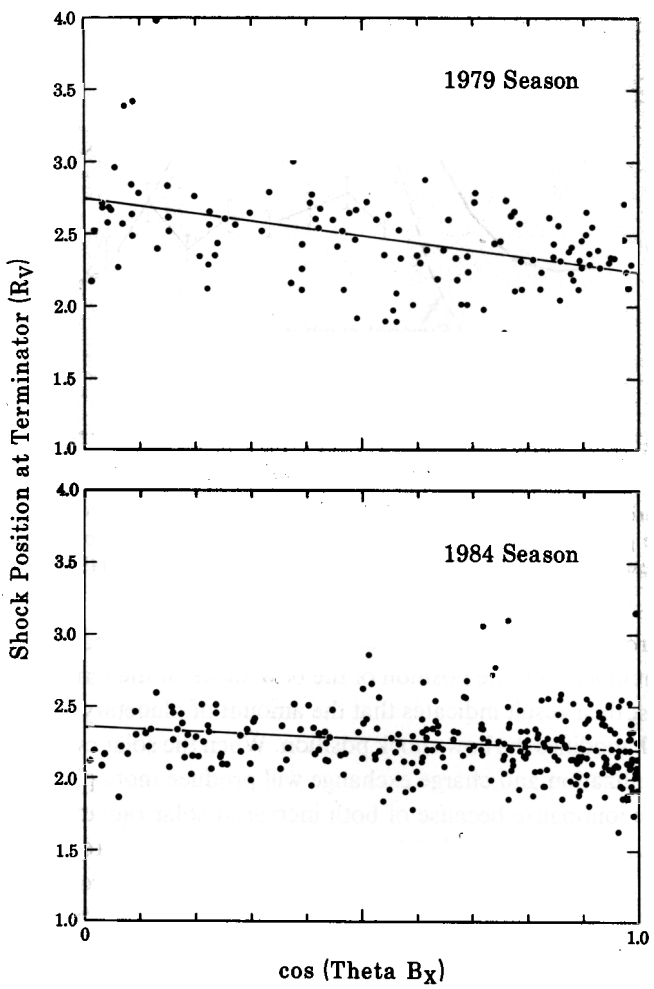

Fig. 14. Pioneer Venus extrapolated terminator crossing positions of the bow shock for periods around solar maximum (top) and near solar minimum (bottom), plotted as a function of the cosine of the angle between the upstream magnetic field and plasma velocity (from Alexander *et al.*, 1986).

ions by accelerating them in the large-scale convection electric field ($\overline{E} = -\overline{V}_{sw} \times \overline{B}_{sw}$) at the expense of the solar wind energy. The large-scale electric field disappears, and thus this coupling mechanism ceases to operate, when the upstream velocity and field are coaligned. This same behavior extends into the magnetosheath although the flow field and magnetic field are distorted from their upstream orientations. Hence, one expects the planetary ions' effect on the bow shock to be greatest for perpendicular upstream field and flow. Figure 14 displays the position dependence on the angle between the upstream field and velocity (e.g., 'cone' angle). The shock is furthest from

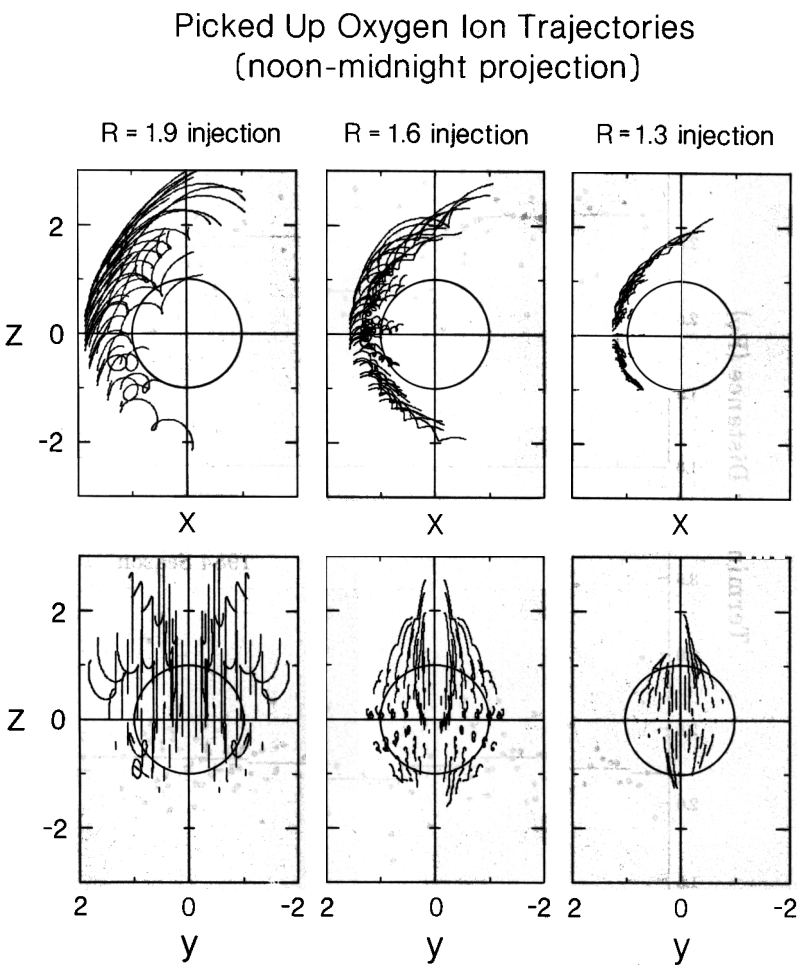

Fig. 15. Projected views of trajectories of initially cold (10 eV) O^+, started at a grid of points at the radial distances (R) indicated, in a gas dynamic magnetosheath magnetic and convection electric field model for an upstream Mach number 4.5 flow and a perpendicular magnetic field of 10 nT pointing out of the page. The views at the top are in the noon-midnight plane with the Sun at the left. Corresponding views from the Sun are shown at the bottom. The trajectories end either at the point where they interesect the ionospheric obstacle in the model or at a point where the total time of integration reaches a specified maximum value.

the planet during solar maximum for perpendicular upstream conditions in agreement with the large-scale motional electric field pickup mechanism.

Ion pickup by the motional electric field should also introduce some shock shape asymmetry in a sense that is controlled by the interplanetary magnetic field orientation in the plane perpendicular to $\bar{V}_{sw}$ (cf. Cloutier and Daniell, 1974). In Figure 15, calculated O^+ ion trajectories in the gas dynamic magnetosheath model (to be discussed in more detail later), illustrate how the diverted flow and draped magnetic field geometry in the magnetosheath produce asymmetry because picked-up ions escape loss into the atmosphere only in the hemisphere toward which the convection electric field points.

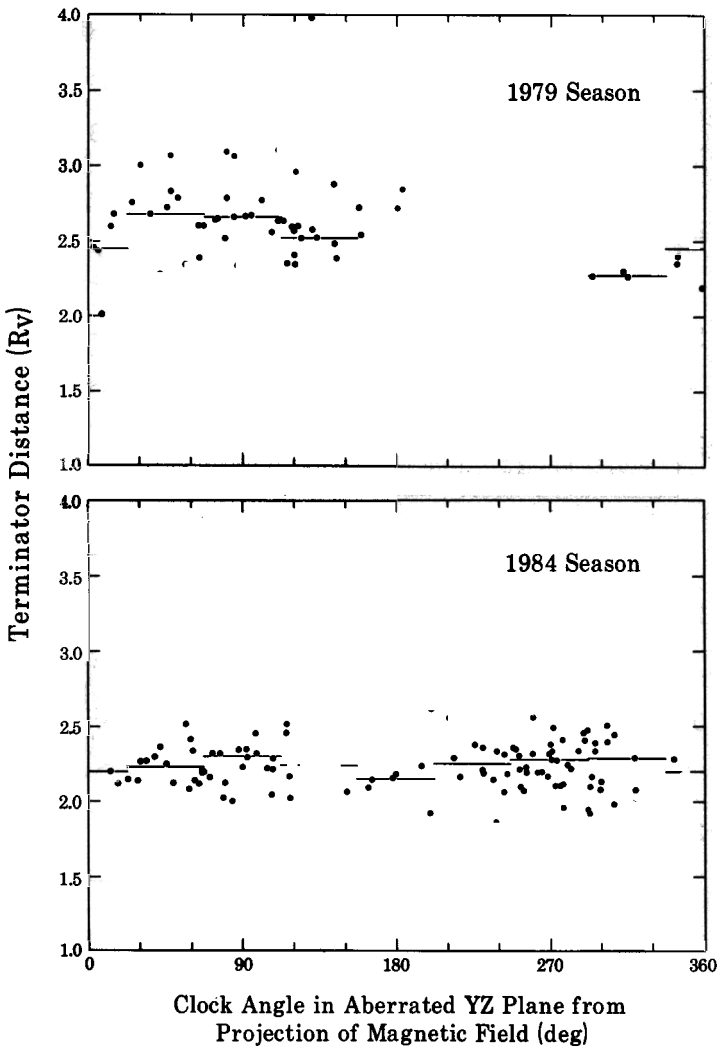

Fig. 16. Pioneer Venus extrapolated terminator shock crossing positions plotted versus the angle between the radial through the shock position and the perpendicular component of the upstream interplanetary magnetic field. The plot at the top and bottom show solar maximum data and near-solar minimum data, respectively. (From Alexander *et al.*, 1986).

The bow-shock position is expected to reflect this difference, which can be attributed to the large gyroradii of the picked up ions relative to the obstacle size. Figure 16 shows the trends that appeared in Alexander *et al.*'s (1986) results for solar maximum conditions compared to near-solar minimum conditions. During solar maximum, when mass loading effects are most prominent, the shock position for perpendicular upstream field cases is organized by the site of the observation relative to the field direction (made common here by rotating the shock data). The shock is farthest away in the 'northern' hemisphere (clock angles 0–180°) where the picked up ions escape into the magnetosheath to large distances (see Figure 15). From these results one can also infer that, at solar minimum, the Venus exosphere is so rarefied that planetary ion pickup has relatively little effect on the bow shock position. The weak pole-equator asymmetry, which is in the sense noted by Romanov (1978), is most probably from magneto-hydrodynamic forces in the magnetosheath.

As illustrated by Figure 17, if one considers the sourceless gas dynamic model results for an upstream Mach number of 5 (a typical magnetosonic Mach number at Venus), and the observed minimum terminator position of 2.1 planetary radii, one deduces an obstacle shape quite similar to the observed shape of the Venus ionopause. The contamination of this type of analysis by planetary ion pickup effects on the shock positions is thus not a source of error as long as the data are preselected to avoid it. Indeed, Verigin *et al.* (1978), who worked only with the Venera solar minimum results, correctly concluded from the shock position that there was very little absorption of the

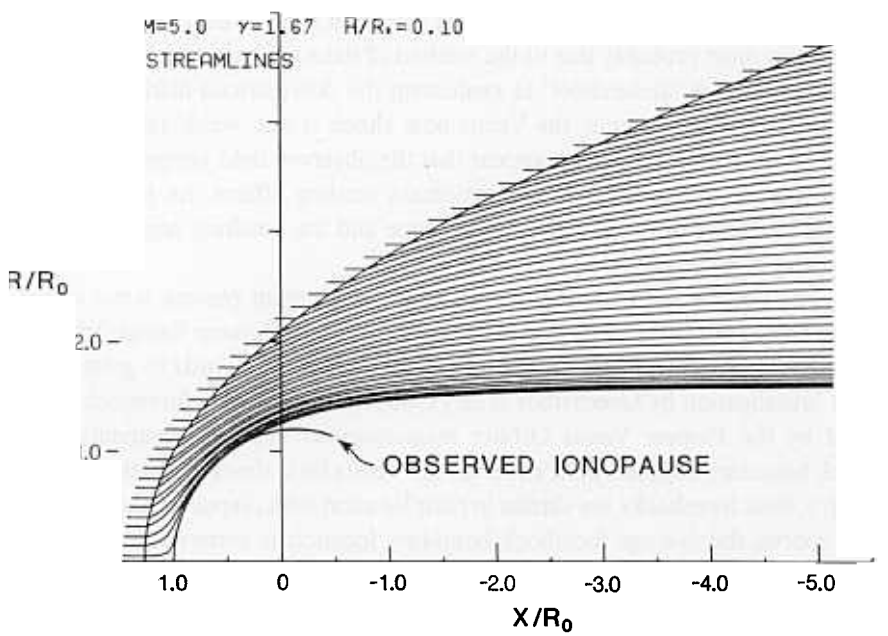

Fig. 17. Gas dynamic model of the bow shock and streamlines of magnetosheath flow calculated by Stahara *et al.* (1980) for a Mach 5 solar wind and the obstacle shape shown. The average observed ionopause current layer position (Phillips *et al.*, 1984) is superposed for comparison.

solar wind at Venus. Only at solar minimum and at times when the interplanetary field is nearly parallel to the solar wind velocity can the technique of fitting the observed shock shape to the gas dynamic model without atmospheric ion sources provide an accurate assessment of the obstacle shape. In this regard, it should be mentioned that Slavin *et al.* (1983) suggested that solar cycle changes in the ionopause height could be responsible for the solar cycle effect on the bow shock position. The results of Figures 14 and 16, together with the near-absence of a solar cycle effect at small cone angles, verify that changes in the 'hard' obstacle size are unimportant relative to changes in the exosphere, which are caused by both enhanced scale heights and photoionization (e.g., see Elphic *et al.*, 1984a). However, it is possible that a small solar maximum decrease in average ionopause height can also substantially affect the number of planetary ions in the magnetosheath (see Figure 2) by exposing more of the cold atmosphere to the solar wind. Whereas this effect has been modelled (e.g., Wolff *et al.*, 1979) it has not been established by measurements.

4.1.2. *Local Properties and Foreshock*

While the above work examined the global properties of the bow shock, some efforts have focussed on its local attributes. For example, Tatrallyay *et al.* (1984) compared the magnetic field jumps for several hundreds of shock crossings observed on the Pioneer Venus Orbiter with the values predicted by the Rankine–Hugoniot relations and the observed solar wind properties. This study found that the upstream magnetosonic Mach number is the best predictor of shock strength if a value of the ratio of specific heats of about 1.8 is assumed. The departure from the usual specific heat ratio of $\frac{5}{3}$ obtained in this study is most probably due to the method of data analysis which did not always avoid the post-shock 'undershoot' in evaluating the downstream field. Thus, at least away from the subsolar region, the Venus bow shock is not 'weak' (cf. Russell *et al.*, 1979) in the sense that it does not appear that the observed field jumps are affected by upstream mass-loading. The downstream mass loading affects the jumps, but only through its alteration of the shock's global shape and the resulting angles of incidence of the upstream flow.

Scarf *et al.* (1980) first remarked on the intense upstream plasma wave activity at 30 kHz observed out to the $\sim 12\ R_v$ dayside apoapsis of the Pioneer Venus Orbiter. This finding showed that the influence of Venus on the solar wind extends to great altitudes. A recent investigation by Greenstadt *et al.* (1986) focusses on the foreshock region as observed by the Pioneer Venus Orbiter magnetometer. Their determination of the foreshock boundary suggests that, although the Venus bow shock is much smaller than the Earth's, their foreshocks are similar in their location with respect to the tangent field line. Of course, the average foreshock boundary location is somewhat altered by the smaller garden hose angle at Venus. Little work has been done on the specific properties of the upstream waves other than in a comparative planetary foreshock study where Hoppe and Russell (1982) established their frequency dependence on the interplanetary field magnitude.

Another recent investigation by Winske (1986) considers theoretically the response

of the Venus subsolar shock structure to the presence of O^+ ions. This author finds that modifications of the waves in the immediate vicinity of the shock can occur only if the concentration of O^+ ions upstream of the shock is far above that which is expected at Venus under ordinary circumstances. All of these studies indicate that the ion pickup process around Venus, which produces a marked effect on the macroscopic shock shape, has little apparent effect on the microscopic properties of the bow shock. In this regard, Venus contrasts sharply with the cometary obstacle (cf. Omidi *et al.*, 1986). Because Venus' gravitational field keeps the atmospheric scale height small, its atmosphere is evidently too sparse at the usual shock altitude to modify the local structure significantly.

4.2. MAGNETOSHEATH

4.2.1. *Plasma and Magnetic Field*

In the magnetosheath, the region of shocked solar wind inside of the bow shock, the solar wind interaction with Venus exhibits a combination of planetary magnetosphere and comet-like features. This is not surprising, given the dense, highly-conducting dayside ionospheric obstacle with the extended, though gravitationally bound, neutral atmosphere extending far above the ionopause.

Several detailed comparisons of plasma data obtained on Venera 9, 10, and Pioneer Venus spacecraft with the gas-dynamic model of flow past an obstacle have found basic agreement between the two (cf. Verigin *et al.*, 1978; Spreiter and Stahara, 1980b) with the greatest exceptions in the low altitude regions near the ionopause (Vaisberg *et al.*, 1976) and at the bowshock due to the shock shape mismatch (Mihalov *et al.*, 1982). Evidently, the gross characteristics of the interaction of the solar wind with the Venus obstacle are not unlike its interaction with a magnetospheric obstacle. Although the temporal and thus spatial resolution of the largest collection of plasma data obtained (on the Pioneer Venus Orbiter) was not very high, the average bulk velocity pattern shown in Figure 18 follows the streamlines expected for flow around an ionospheric obstacle (Mihalov *et al.*, 1980).

More detailed comparisons with the gas dynamic model have been possible with the rapidly sampled magnetic field data (cf. Spreiter and Stahara, 1980b; Luhmann *et al.*, 1986; Phillips *et al.*, 1986)). A case study from Luhmann *et al.* (1986), in Figure 19, illustrates the occasional remarkable agreement between the draped, frozen-field configuration of the steady gas dynamic magnetosheath model (see Spreiter and Stahara, 1980a, for a detailed description of the model) and the observed field along the Pioneer Venus Orbiter trajectory. A statistical field draping pattern obtained by Phillips *et al.* (1986a), shown in Figure 20 (see also Marubashi *et al.*, 1985), similarly matches the morphology of the model results in the magnetosheath region. The dawn-dusk asymmetry introduced into the magnetosheath by the radial component of the average interplanetary field is clearly seen in this display. Moreover, Phillips *et al.* (1986a) found that the largest upstream Mach numbers produce the greatest compression of the field within the magnetosheath, as expected from theory. Individual

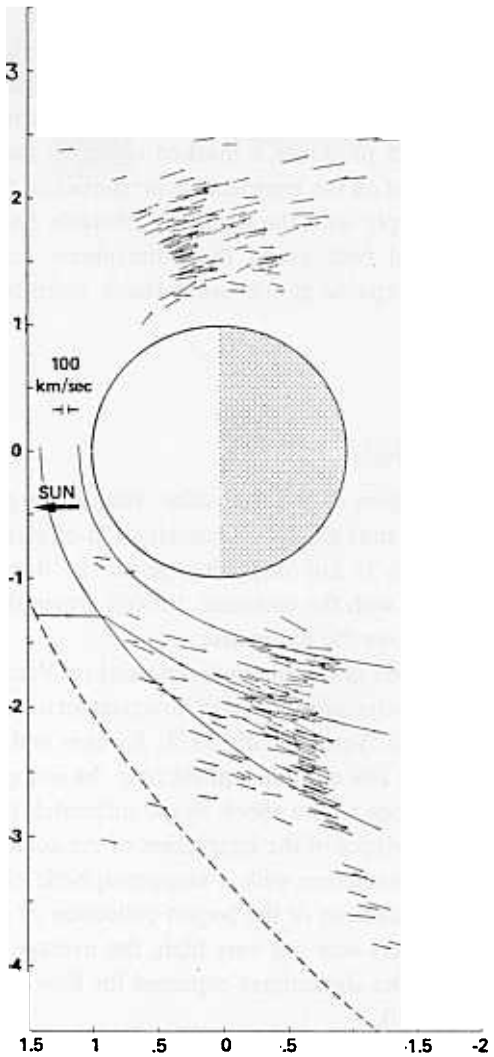

Fig. 18. Magnetosheath flow vectors measured by the Pioneer Venus Orbiter plasma analyzer (from Mihalov *et al.*, 1980).

orbit comparisons like that in Figure 19 are not generally possible because the interplanetary field usually changes during the ~ 2 hr that it takes the Pioneer Venus Orbiter to traverse the magnetosheath. Of course, the statistical studies avoid this problem. Nevertheless, to investigate the typical conditions of a temporally varying interplanetary field, Luhmann *et al.* (1986a) generalized the gas dynamic model for unsteady boundary conditions on the field. Their examples of the evolution of the model magnetosheath field draping pattern during the passage of simple isolated rotations of the upstream field give some feeling for the typical complexity of the magnetosheath field configuration.

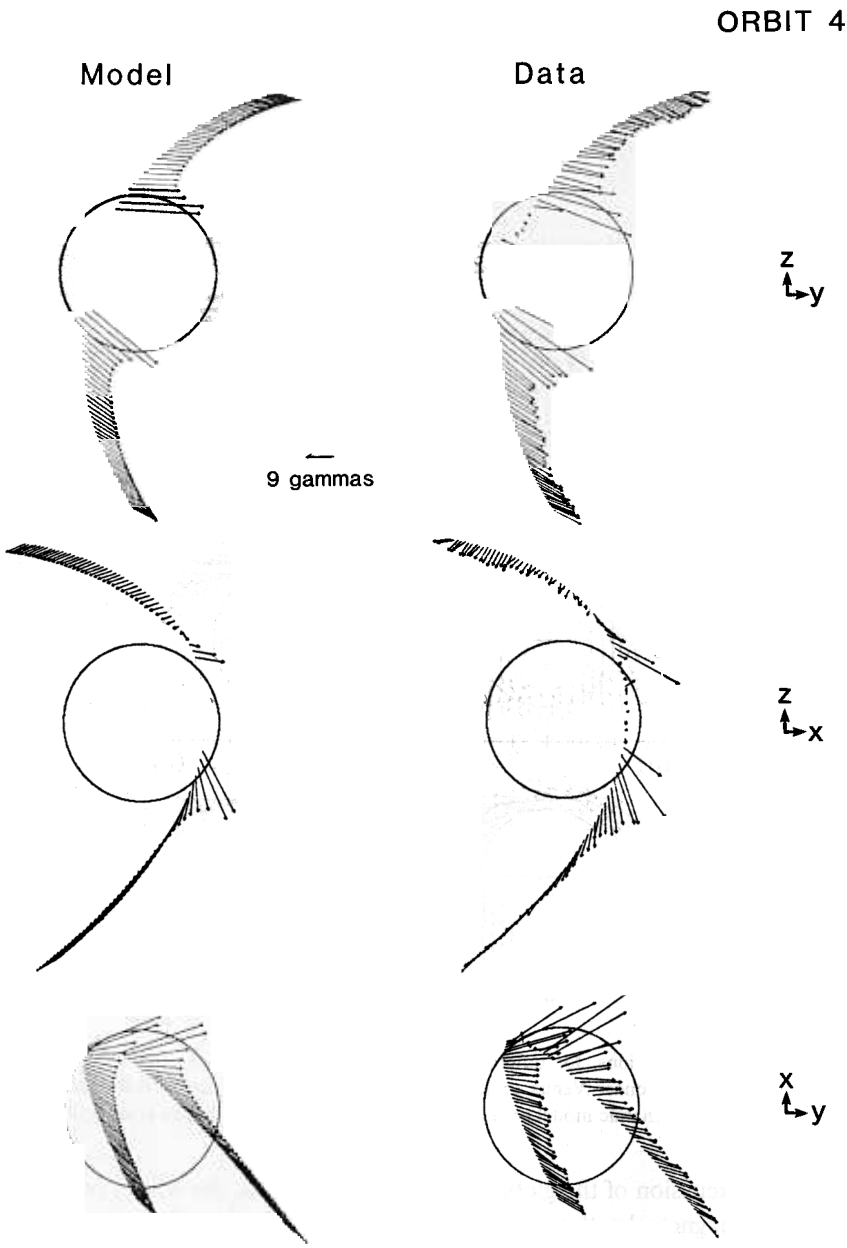

Fig. 19. Comparison of magnetic field vectors along a Pioneer Venus orbit segment form the data (right) with the gas dynamic magnetosheath field model for the observed upstream field (left). Three projections are shown: the Sun's view (top), the noon midnight view (center) and the ecliptic plane (bottom). (From Luhmann *et al.*, 1986.)

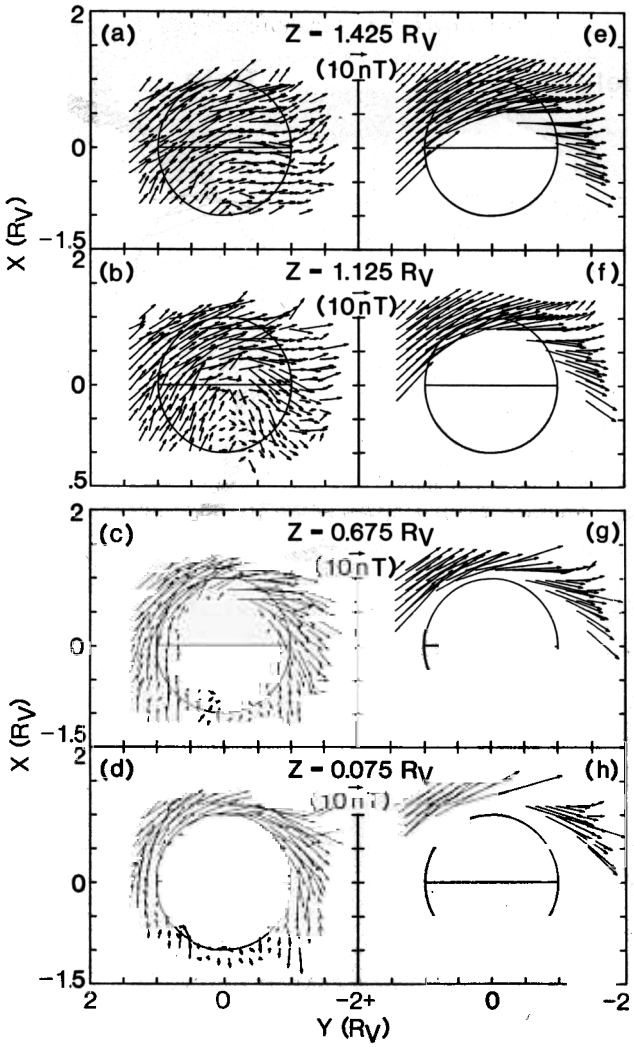

Fig. 20. Ecliptic plane projections, for different latitude intervals, of average magnetic field vectors obtained by rotating many Pioneer Venus orbits so as to coalign their upstream fields (left) and the corresponding gas dynamic model results (right) from the study by Phillips *et al.* (1986).

In the above discussion of the global bow shock properties, the effects of planetary ion pickup in the magnetosheath on the shock shape were described. These results prove that planetary ion pickup by the large-scale convection electric field in the magnetosheath alters the solar wind flow around the Venus obstacle. However, as indicated in the foregoing paragraph, the magnetosheath field and flow characteristics bear a close resemblance to sourceless gas dynamic models. Since more than $\sim 10^{26}$ O^+ ions s^{-1} are produced in the dayside magnetosheath (a number obtained by integrating the hot O-distribution shown in Figure 2 above $\sim$250 km over a hemispherical shell and assuming that $\sim 4 \times 10^{-6}$ s^{-1} of the neutrals are ionized), one

expects to observe some direct evidence of the inferred ion pickup in the magnetosheath data. Figure 15, first mentioned in the section on the bow shock, illustrates how initially cold (~ 10 eV) O^+ ions, created at various altitudes in the dayside magnetosheath and just upstream of the bow shock, behave in the gas dynamic magnetosheath model magnetic field and convection electric field for an interplanetary field in the $+y$-direction. It was also pointed out that the asymmetry of the trajectories is organized by the perpendicular (to the flow) component of the upstream magnetic field, which produces an electric field that accelerates the picked up ions into the atmosphere in one hemisphere and into the magnetosheath in the other hemisphere. This asymmetry in the magnetosheath ion pickup causes the bow shock to be located at a greater altitude in the hemisphere where the ion trajectories do not preferentially intersect the atmosphere. If the bow shock shows an asymmetry it would be surprising not to find some corresponding asymmetry in the magnetosheath. Indeed, Phillips *et al.* (1986a) found that, on the average, the magnetic field strength in the magnetosheath hemisphere where the ions move freely is larger than that in the opposite hemisphere when the data are rotated to coalign the perpendicular components of the upstream fields. This result is shown in Figure 21 as the ratio of the field strengths measured in the 'north' and 'south' hemispheres. (In this study the rotations placed the escaping particles in the south.) The average magnetosheath field strength asymmetry is most pronounced at solar zenith angles nearest the terminator at an altitude of ~ 1000 km. Possible

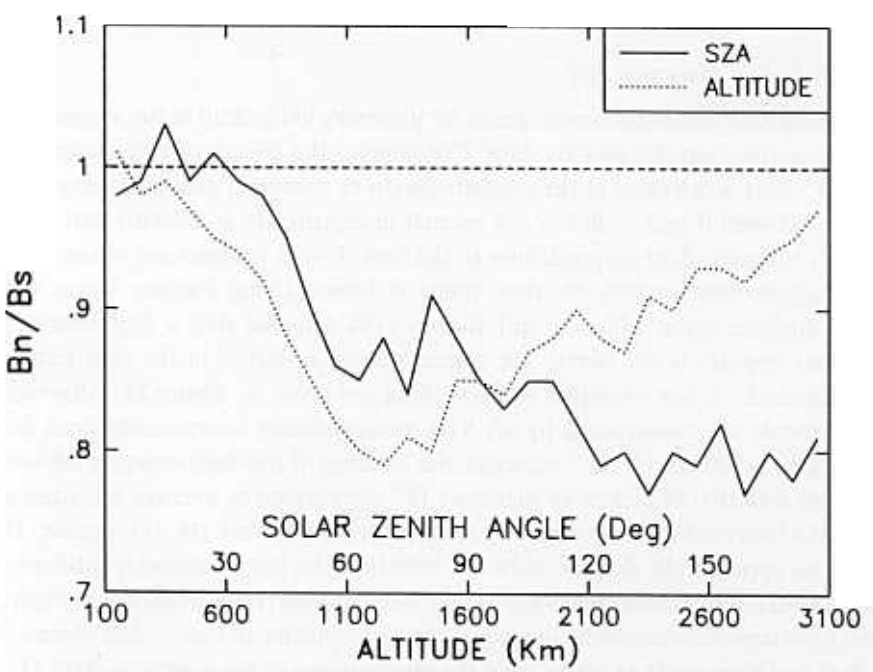

Fig. 21. Ratio of the average magnetosheath magnetic field magnitudes in the northern and southern hemispheres obtained after rotating the data so as to coalign the upstream fields versus altitude and solar zenith angle (from Phillips *et al.*, 1986).

explanations include an effectively larger obstacle in the preferred hemisphere for ion pickup (produced by related effects in the boundary layer above the ionosphere), or a slowing of the magnetosheath flow in the preferred hemisphere by the combination of mass pickup and momentum conservation. The magnetosheath data analyses have so far not distinguished between these two interpretations, although the ionopause height was found to be insensitive to those factors which organize the bow shock and magnetosheath observations (Phillips *et al.*, 1986b).

Also mentioned above was the only model that has attempted to simulate the effects of mass loading on the bow shock and the magnetosheath. Breus *et al.* (1986) obtained a more distant bow shock than the sourceless gas dynamic model, as is observed, but they also find an altered magnetosheath magnetic field with an enhanced field magnitude at large solar zenith angles and a weakened field in the subsolar region. Their model results are thus consistent with the observations in Figure 21 which indicate that the mass-loading asymmetry in the field strength grows with solar zenith angle. However, because the subsolar magnetosheath is not generally observed from the Pioneer orbit, the data used in the study by Phillips *et al.* (1986a) do not allow one to test Breus *et al.*'s predictions for small solar zenith angles. One would presumably get different results if one compared the model with data from the preferred hemisphere for ion pickup than one would get for the opposite hemisphere. Yet, Alexander *et al.*'s (1986) results on the shock asymmetry indicate that the solar maximum shock is further from the solar minimum position in *both* hemispheres. The low-altitude ion pickup must then affect the magnetosheath even where the ions are eventually lost to the obstacle.

4.2.2. *Picked-up Planetary Ions*

Perhaps the most unambiguous evidence for planetary ion pickup in the magnetosheath is found in the energetic plasma data. Considering the effects of convection electric fields, O^+ ions accelerated in the magnetosheath or upstream can attain energies that oscillate between 0 and ~ 30 keV for normal interplanetary conditions and an interplanetary magnetic field perpendicular to the flow. Lower energies are obtained in the inner magnetosheath where the flow speed is lower. Using Pioneer Venus Orbiter plasma analyzer data, Mihalov and Barnes (1981) found that a high-energy peak sometimes appears in the energy per charge spectra observed in the near terminator magnetosheath. A few examples of these data are given in Figure 22. Although the measurements are constrained by an 8 kV energy/charge instrumental limit (corresponding to ~ 300 km s^{-1} O^+ velocity), the location of this high energy peak is often consistent with that of picked up planetary O^+ accelerated to average velocities up to that of the observed lower energy magnetosheath proton peak (cf. Intriligator, 1982). These ions appear to be slowest and most intense at the lowest altitudes (Mihalov and Barnes, 1981). While these observations may well represent the ions shown in Figure 15, which have been accelerated by the large-scale magnetosheath convection electric field, no effort has been made as yet to see if the observations of the magnetosheath O^+ are organized by the prevailing orientation of the interplanetary magnetic field.

In the preceding discussion, the implication is that planetary ion pickup should not

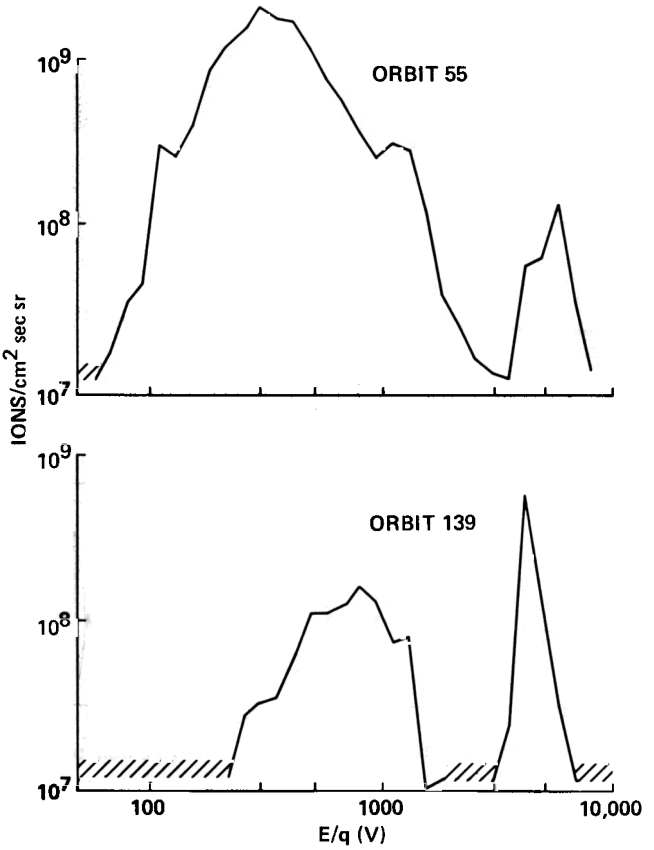

Fig. 22. Examples of Pioneer Venus Orbiter plasma analyzer energy/charge spectra obtained in the terminator magnetosheath, showing the slowed solar wind proton plasma (left hand peaks), and the higher energy peak attributed to picked up O^+ (from Mihalov and Barnes, 1981). Similar spectra are observed in the wake at $\sim 12\,R_v$.

occur if the upstream field is aligned with the solar wind flow. Indeed, both bow shock and magnetosheath studies indicate that a perpendicular field component causes ion pickup by the large scale convection electric field in the manner illustrated by Figure 15. Nevertheless, observations suggest that there is an alternate mode of pickup that operates in the aligned situation although it does not produce either the major effect on the shock shape, or the large-scale gyroradii and hemispheric asymmetry association with the perpendicular field mode of ion pickup. It has been demonstrated (Luhmann *et al.*, 1983; Phillips *et al.*, 1986a) that the Venus magnetosheath field is disturbed on streamlines of plasma flow that intersect the quasiparallel portion of the bow shock. When the upstream plasma velocity and magnetic field are within $\sim 45°$ of coalignment, the disturbed region fills the dayside magnetosheath, as illustrated by Figure 23, because fluctuations generated by the shock are convected inward. One consequence of this is poor comparisons of magnetic field observations with the gas dynamic magnetosheath field model for small cone angles. Another is that efficient ion acceleration can occur

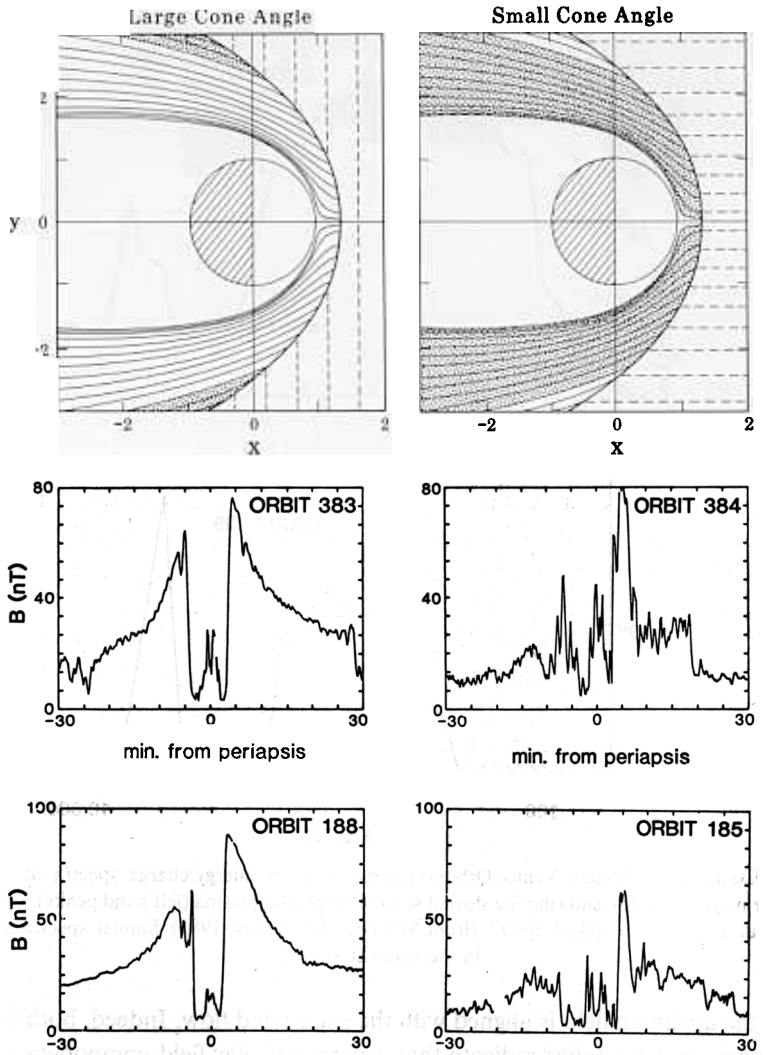

Fig. 23. Magnetic field magnitude measured along dayside periapsis orbits of Pioneer Venus showing the two types of magnetosheaths encountered, and the suggested interpretation (bottom) in terms of turbulence (shading) convected downstream from the quasiparallel bow shock. (From Luhmann *et al.*, 1986).

in the fluctuating convection electric fields associated with the observed convected low frequency transverse magnetic field fluctuations (Luhmann *et al.*, 1985b; Winske, 1986). The major difference between this ion pickup mechanism and the large-scale convection electric field mechanism is that the electric field in this case fluctuates. This introduces some stochasticity in the ion trajectories such that the smooth gyromotion and resulting large-scale hemispherical organization of Figure 15, found for more perpendicular upstream fields, is lost. The magnetic field fluctuation-related ion pickup can be invoked to explain the slight departure of the bow shock position at solar maximum for coaligned

upstream field and flow from the solar minimum bow shock position (cf. Alexander *et al.*, 1986), while the conventional ion pickup described above produces the major displacements of the shock position compared to the early gas dynamic models.

Although comet-like ion-pickup related instabilities (cf. Wu *et al.*, 1986; Ip and Axford, 1986) could in principle produce both waves in the magnetosheath plasma and planetary ion pickup as suggested by Hartle *et al.* (1973), the evidence for such activity near Venus is not apparent. As discussed above, the spatial distribution of the magnetic field fluctuations in the magnetosheath is consistent with a source at the quasi-parallel bow shock. Moreover, the recent simulations by Winske (1986) indicate that the characteristics of the observed fluctuations in the small cone angle case are consistent with the shock source, and that oxygen ion densities in excess of those expected in the magnetosheath are necessary for the rapid growth of strong waves in the narrow (relative to an ion gyroradius) region between the subsolar bow shock and ionopause. Of course it is possible that the picked up ions could generate some plasma turbulence downstream of the region where they are picked up (by either the large-scale or fluctuating convection electric fields), but this possibility is difficult to test since the magnetotail exhibits a great deal of variability. However, Intriligator and Scarf (1982) do find evidence for ion acoustic turbulence in the tail plasma wave data. An additional candidate for ion pickup instability effects is the higher frequency (100 Hz–30 kHz) plasma wave activity observed on Pioneer Venus close to the ionopause (Scarf *et al.*, 1980), but the details of these waves have not yet been investigated except for their correlation with superthermal planetary ions in the boundary layer (Taylor *et al.*, 1981; Kasprzak *et al.*, 1983). These latter observations will be discussed further in conjunction with the next topic, which is the boundary layer.

4.3. Boundary Layer

4.3.1. *Definitions*

One of the most complicated regions of the Venus environment, from the viewpoint of constructing theories and models, is the boundary layer on the dayside between the magnetosheath and the lower ionosphere (where photochemical equilibrium maintains a fairly constant state of the plasma). The boundary layer is a particularly comet-like feature because it is where most of the heavy, cold ion production and pickup occur. This region includes phenomena which are associated in the literature with the mantle, the magnetic barrier, and the ionopause. The definitions of these components of the boundary layer are in fact somewhat ambiguous. For example, the ionopause has been defined as the altitude where the thermal electron density falls to $\sim 10^2\ \mathrm{cm}^{-3}$ (Theis *et al.*, 1980), the altitude where the magnetosheath magnetic pressure gradient is balanced by the thermal plasma pressure gradient (Elphic *et al.*, 1981; Phillips *et al.*, 1985), or the location where the thermal ions disappear and a superthermal ion component is sometimes observed to take its place (Taylor *et al.*, 1981). These latter definitions usually differ by $\sim$ 10s of km but may differ by $\sim$ 100s of km at solar zenith angles near the terminator, or when the solar wind dynamic pressure is extraordinarily

high. Because of this ambiguity, the term ionopause is probably best regarded as referring to a somewhat loosely defined interface between the magnetosheath plasma and field on one side and the ionospheric thermal plasma on the other. The mantle is sometimes associated with the location of superthermal (1–40 eV) electrons observed just above the dayside interface between solar wind and ionospheric plasmas (cf. Spenner *et al.*, 1980). Alternatively, the term has been used to refer to the magnetic barrier, which is a volume of space above the ionospheric plasma within which magnetic pressure, having a magnitude reflecting the incident solar wind dynamic pressure, apparently dominates all other pressure contributions (Vaisberg and Zeleny, 1984). Although all of these terms are used below, their exact definitions will generally not be crucial to the discussion.

In the simplest pictures of the Venus-solar wind interaction, the ionopause is assumed an impenetrable surface or tangential discontinuity inside of which the ionosphere is

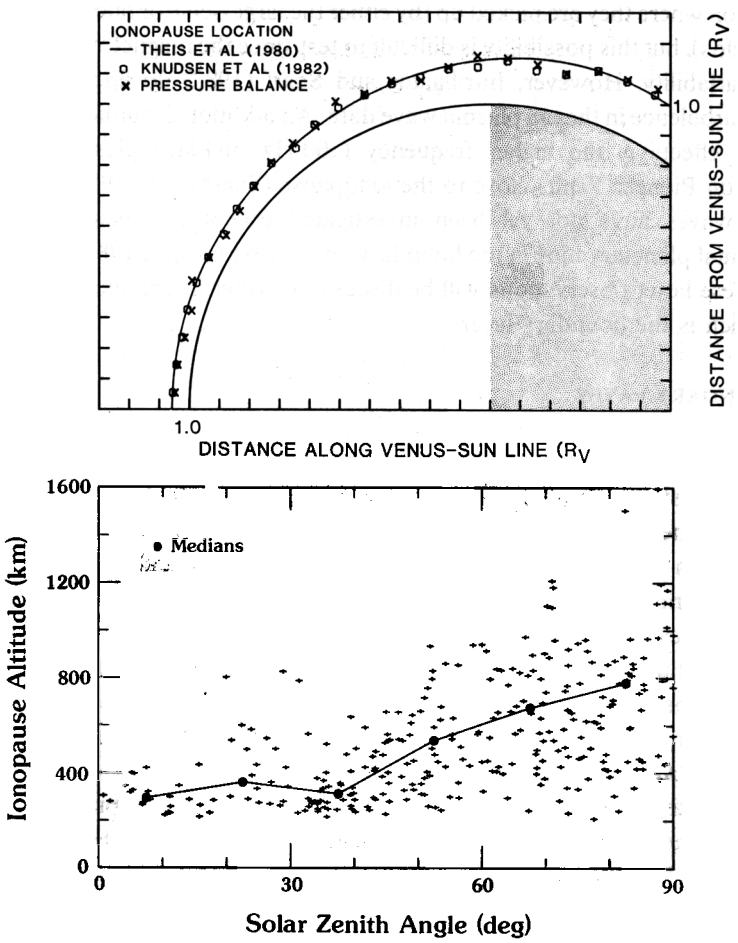

Fig. 24. The average position of the boundary layer current sheet (top) (from Phillips *et al.*, 1984) and the data used to obtain it (bottom).

contained and outside of which the magnetosheath plasma flows around the obstacle. Observations from the Pioneer Venus Orbiter have shown (Elphic *et al.*, 1981; Brace *et al.*, 1983; Phillips *et al.*, 1984) that in its simplest form, this boundary includes a thin ($\sim$ 10s of km) current layer located, on the average, at the altitudes shown in Figure 24. As illustrated by Figure 25, this current layer produces a transformation between

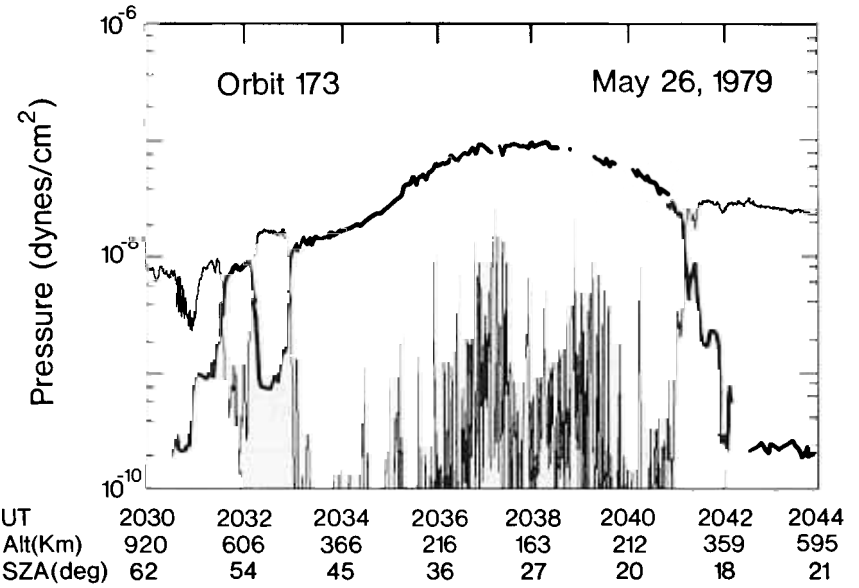

Fig. 25. Time series of magnetic pressure (light line) and ionospheric thermal plasma pressure (heavy line) observed on a typical dayside periapsis, low-to-average solar wind dynamic pressure Pioneer Venus orbit (from Elphic *et al.*, 1980).

magnetic pressure on the magnetosheath side, and the equivalent thermal plasma pressure on the ionosphere side (cf. Elphic *et al.*, 1980). The gradients in field and plasma pressures identify this transition as a dissipationless diamagnetic current layer, with a thickness of a few thermal O^+ gyroradii (Elphic *et al.*, 1981). From the observed pressure balance between the magnetosheath magnetic field and the ionospheric thermal plasma, it is known that the boundary layer must begin above the thin current layer where processes evidently remove the magnetosheath plasma component of the total pressure. The part of the boundary layer that is dominated by the magnetic field is the 'magnetic barrier'. Several authors (cf. Brace *et al.*, 1980; Elphic *et al.*, 1980; Vaisberg *et al.*, 1980; Phillips *et al.*'s 1984) have demonstrated that the normal component of the incident solar wind dynamic pressure is almost completely transformed, at a low altitude in the magnetosheath, to magnetic pressure. An example of this relationship is given in Figure 26, which shows Phillips *et al.*'s (1984) comparison of the normal component of the incident dynamic pressure with the sum of the magnetic and ionospheric plasma pressures in the center of the current sheet. Since the ionopause marks the transformation from magnetic to thermal pressure, the magnetic field functions as an inter-

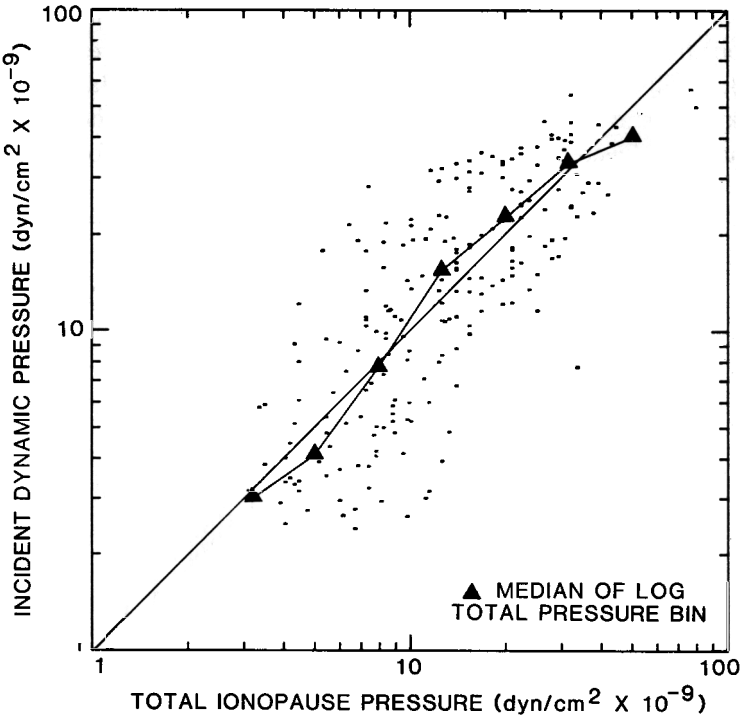

Fig. 26. Relationship of incident (normal) solar wind dynamic pressure to the total (magnetic + thermal plasma) pressure at the center of the boundary layer current sheet (from Phillips *et al.*, 1984).

mediary by which the solar wind dynamic pressure is balanced or 'stood off' by the ionosphere.

4.3.2. *Mantle and Magnetic Barrier*

Spenner *et al.* (1980) equated the 'magnetic barrier' with their 'mantle' where the Retarding Potential Analyzer on the Pioneer Venus Orbiter measured a mixture of solar wind-like and ionospheric photoelectron-like superthermal ($\sim$ 10–40 eV) electrons. The location of the mantle as inferred from these observations is indicated schematically in Figure 27. The tailward extension of the mantle was also seen on Venera by Verigin *et al.* (1978), who referred to it as the penumbra. Attempts to understand the formation and properties of this region have been made by Lipatov (1978) and later by Vaisberg and Zeleny (1984), who considered the role that the production of heavy planetary photoions in the low-altitude magnetosheath might play in its formation. Indeed, the ionopause would not exist if the photoions above it were not removed from this region. Yet the self-consistent details of how the pressure transformation occurs, and of why fresh photoions and photoelectrons in the inner magnetosheath do not seem to contribute substantially to the pressure balance, present problems that have not been solved. For example, Zwan and Wolf (1976) describe how a magnetic barrier configuration can form near a planetary obstacle simply by the depletion of solar wind particles in magneto-

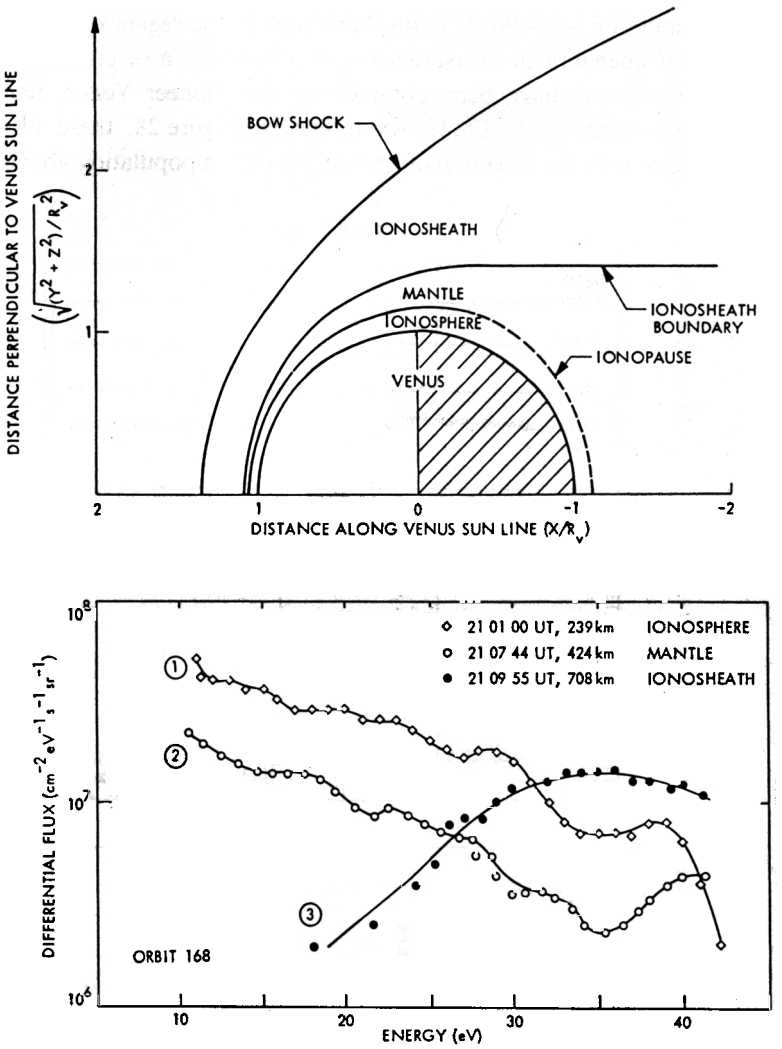

Fig. 27. (T) Schematic illustration of the location of the mantle region where a mixture of ionospheric photoelectrons and solar wind electrons is observed. (B) Examples of electron spectra obtained in the ionosphere, mantle, and magnetosheath or ionosheath, showing the transition between populations (from Spenner *et al.*, 1980).

sheath magnetic flux tubes which are compressed near the stagnation point. It may be that this 'squeezing' of particles out of the low-altitude magnetosheath flux tubes is sufficient to produce the observed magnetic barrier since this effect should also deplete the ionospheric particles produced locally.

The Pioneer Venus plasma analyzer cannot sample sufficiently rapidly to resolve the depletion layer, but other observations including Spenner *et al.*'s mantle measurements of both solar wind electrons and photoelectrons indicate that there are indeed particles in the magnetic barrier. The Pioneer Venus experiment of Taylor *et al.* (1980, 1981)

detects a population of ~10–90 eV ionospheric ions in the region of the mantle (see Figure 3). Similar uncalibrated measurements of a population of energetic (>40 eV) ions near the ionopause have been obtained by the Pioneer Venus neutral mass spectrometer (Kasprzak *et al.*, 1982). As shown by Figure 28, these observations sometimes coincide with the detection of a thermal electron population above the main

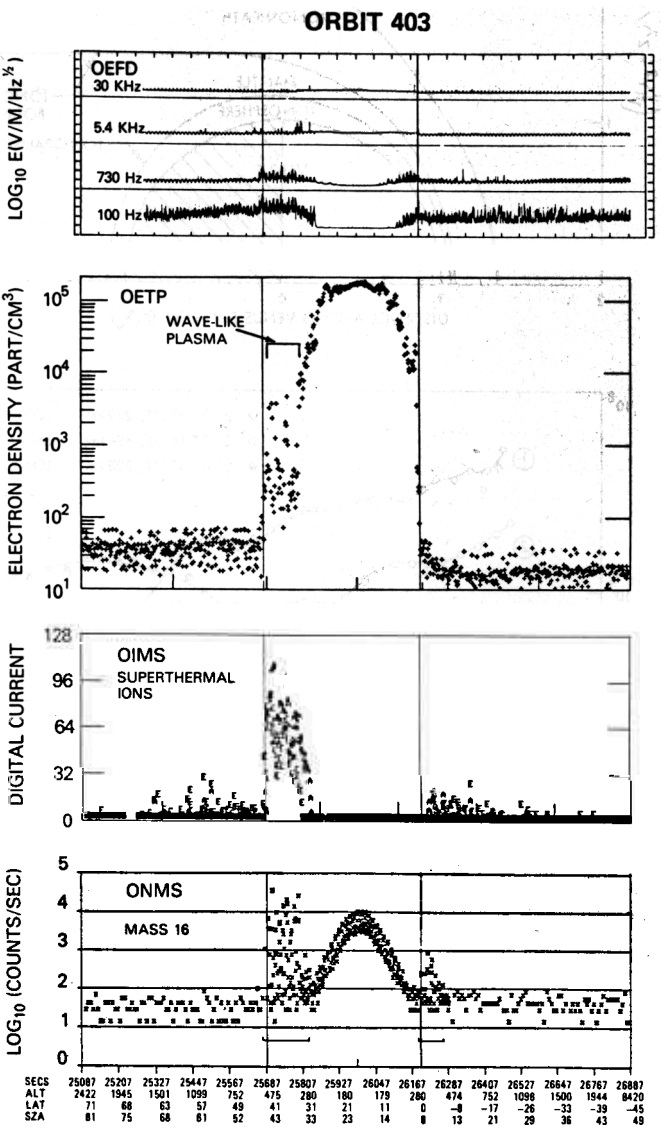

Fig. 28. Time series of near-periapsis data from the Pioneer Venus Orbiter showing the thermal ionospheric plasma (second from top), 10–90 eV and >40 eV superthermal ions occasionally observed in conjunction with the thermal 'wave-like' plasma (two lower panels) and coincident plasma wave activity (top). The hump in the bottom trace is from the measurement of low altitude neutral oxygen. (From Kasprzak *et al.*, 1983.)

ionopause electron density gradient which Brace *et al.* (1982) have called plasma 'clouds'. The source of the super-thermal ion population is generally considered to be ionospheric ions which have been or are in the process of being accelerated anti-sunward. Since both measurements in this energy range are not fully interpretable, one cannot say with certainty how the superthermal ion population contributes to the overall pressure balance. The plasma in the clouds, which may represent thermal plasma scavenged from the top of the ionosphere by instabilities at the ionopause (cf. Wolff *et al.*, 1980; Elphic and Eskovitch, 1984) or in response to sudden changes in incident solar wind dynamic pressure (cf. Brace *et al.*, 1982), could provide the seed population. Kasprzak *et al.*'s map of superthermal ion occurrence does resemble Brace *et al.*'s map of thermal electron clouds as shown in Figure 29. However, another viable source is simply the new planetary photoions that are constantly being produced above the ionopause current sheet. The apparent thickening of the layer of superthermal ions when the ionopause altitude decreases (cf. Taylor *et al.*, 1981) supports this latter view.

If the behavior of these picked up planetary ions in the mantle can be approximated, as in Figure 15, by test particles in the gas dynamic model of the magnetosheath, one can obtain energy spectra and bulk flow directions in addition to trajectories. Because of the steep density gradient in the cold neutrals (see Figure 2), most of the picked up O^+ is produced at low altitudes where the magnetosheath magnetic field magnitude is strongest but the flow velocity is low so that the ion energies are confined to values below a kilovolt. As the trajectories on the right-hand side of Figure 15 show, near the ionopause boundary the gyroradii are small and the bulk motion is anti-sunward in the general direction of the background plasma convection. It is not clear to what extent this modelling exercise describes the properties of the observed superthermal ions. However, if the presence of the photoelectrons and superthermal ions can be explained by this simple picture of planetary ions produced just above the ionopause, some other observations fall into place. For example, Taylor *et al.* (1981) and Kasprzak *et al.* (1982) discuss the apparent correlation of the superthermal ions with 100 Hz–30 kHz noise in the electric field measured near the ionopause on the Pioneer Venus Orbiter (see Figure 28). Taylor *et al.* suggest that these emissions could result from plasma instabilities associated with the picked up planetary ion population such as those anticipated by Hartle *et al.* (1973). Both ion-acoustic and whistler mode waves are considered to be present in the Venus boundary layer (Taylor *et al.*, 1981), although detailed analyses and interpretations of the data including the wave generation and propagation characteristics have not yet been carried out. In this regard, it is notable that observations from the AMPTE experiments (cf. Gurnett *et al.*, 1986) and the ICE encounter with comet Giacobini–Zinner (Scarf *et al.*, 1986) have shown that plasma waves are indeed a signature of ion pickup processes in the solar wind. This mechanism would explain why superthermal ions and plasma waves are enhanced when the ionopause is low (Elphic *et al.*, 1981; Taylor *et al.*, 1981) since the likelihood of wave generation increases as the density of picked up ions increases. Landau damping of the whistler waves by the thermal electrons in the upper ionosphere can heat the electrons as observed (cf. Taylor *et al.*, 1979; Scarf *et al.*, 1980). Still, one cannot at this point

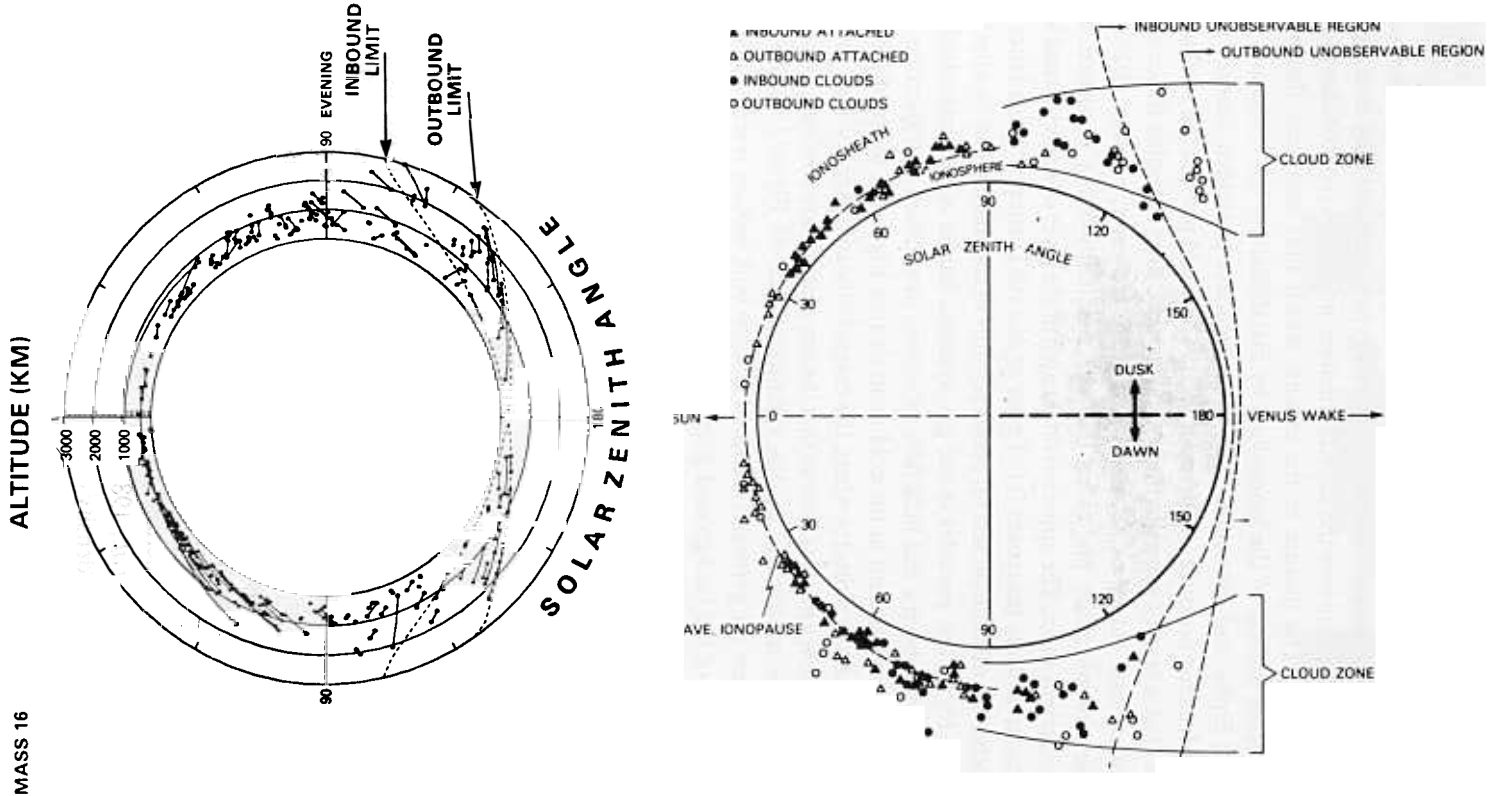

Fig. 29. Comparison of locations of observations of superthermal ions (left, from Kasprzak *et al.*, 1983), and ionospheric thermal plasma intrusions or 'clouds' in the magnetosheath (right, from Brace *et al.*, 1983), projected onto the ecliptic plane.

completely rule out the bow shock, or even the current layer itself, as the source for these plasma waves.

The manner in which the thermal plasma 'clouds' are generated and how they fit into the boundary layer physics is not readily apparent. It seems that macroscopic instabilities such as the Kelvin–Helmholtz instability should easily develop in the sheared plasma flow between the ionosphere, which flows anti-sunward at a few km s^{-1}, and the overlying magnetosheath, which flows at up to several hundred km s^{-1}, especially where the flow and field are perpendicular (cf. Wolff *et al.*, 1980; Elphic and Erskovitch, 1984). This instability could produce ripples on the boundary layer at high solar zenith angles where most of the clouds are observed (see Figure 29). These in turn could cause the viscous interactions advocated by Perez-de-Tejada *et al.* (1983, 1985, 1986) who argue that pressure gradients alone cannot drive the antisolar flow in the upper ionosphere. Still, understanding how the Kelvin–Helmholtz instability occurs in the magnetic barrier in the presence of ongoing ion pick up and magnetohydrodynamic forces associated with the local magnetic field geometry is nontrivial. From this viewpoint, Brace *et al.*'s (1982) clouds may be ionospheric plasma produced above the ionopause in the early stages of being picked up by the magnetosheath convection electric field, or in local flow and field geometries where the convection electric field happens to be small, or in regions where the macroscopic body force ($\bar{J} \times \bar{B}$) of the draped magnetosheath field is important. If one is to adopt one of these interpretations with confidence, however, more work needs to be done on establishing the connection between the magnetosheath field geometry and the superthermal planetary ion populations and clouds as in the case study by Russell *et al.* (1982). One also must endeavor to understand how the superthermal planetary ions, photoelectrons and solar wind electrons affect the boundary layer, if at all.

In addition, although the test particle picture of ion pickup used above is useful, the global response of the bow shock shape to ion pickup also requires a consideration of the dependence of the magnetosheath flow and field on the boundary layer processes. Perhaps one can attribute the greater flare in the shock shape under conditions that optimize ion pickup by the convection electric field to the flow adjustment to an obstacle with the shape of the mantle instead of the ionopause (cf. Spenner *et al.*, 1980). As noted above, the shock appears to contract to a shape consistent with an ionopause shaped obstacle when the interplanetary conditions or solar cycle phase change so as to no longer favor ion pickup (e.g., see Figures 13 and 14). A similar condition should be found when the dynamic pressure is sufficiently low to cause a high ionopause and a resulting decrease of neutrals available in the magnetosheath. However, little is known about the details of mantle photoelectron, thermal plasma cloud, and superthermal ion variability. All of these considerations collectively point out the need for studies relating the boundary-layer observations to interplanetary conditions.

4.3.3. *Ionopause*

The foregoing paragraphs have concentrated on what happens above the low altitude boundary of the boundary layer. It was mentioned that the current layer which marks

the transition between predominantly thermal and predominantly magnetic pressure nominally has a thickness of a few ionospheric (O^+) ion gyroradii (cf. Elphic *et al.*, 1981). This finding is understood as a fundamental property of boundaries between a vacuum field (in this case the magentic barrier) and a collisionless thermal plasma (Grad, 1961). Thus the observations of the ionopause thickness are consistent with the presence of the magnetic barrier or layer of plasma depletion above the ionopause. Interestingly, the basic attributes of the ionopause current layer do not appear to be sensitive to the interplanetary field orientation, in spite of the expectation that the magnetic barrier and ion pickup in the boundary layer should depend on the perpendicular component (cf. Phillips *et al.*, 1986b). As Elphic *et al.* point out, however, the characteristics of the current layer change when it forms at altitudes near ~ 220 km instead of the usual altitudes of $\gtrsim 300$ km in response to solar wind conditions with high-dynamic pressure. Figure 30 shows that at ~ 200 km, ion collisions with neutrals

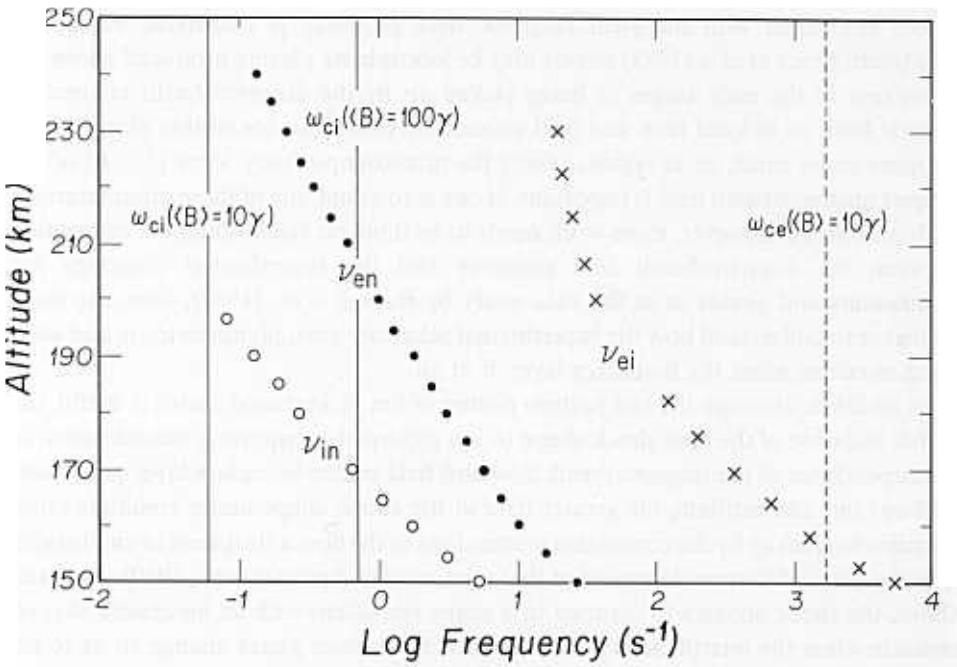

Fig. 30. Altitude profiles of ion-neutral (ν_{in}), electron neutral (ν_{en}), and electron-ion (ν_{ei}) collision frequencies in the subsolar ionosphere compared with the ion (ω_{ci}) and electron (ω_{ce}) gyrofrequencies for various average magnetic field magnitudes.

become important for typical values of the local magnetic field (~ 10–100 nT). The consequence is that, at these low altitudes, the current layer thickens as seen in Figure 31. The rapidly increasing neutral density with decreasing altitude causes the duality of the ionopause behavior. Because this behavior is closely tied to the production of large-scale magnetic fields in the dayside ionosphere, the special cases of thick ionopause current layers will be discussed later in conjunction with ionospheric fields.

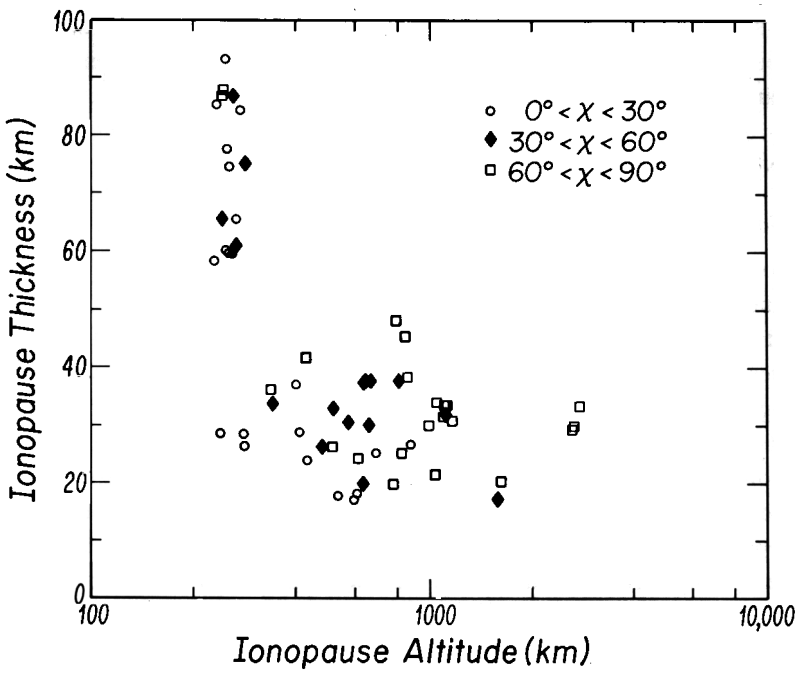

Fig. 31. Boundary-layer current sheet thickness at various (central) altitudes (from Elphic *et al.*, 1981).

In brief, collisional diffusion and the prevailing ionospheric convection mentioned in an earlier section seem to explain this altered appearance of the current layer when it forms in the resistive region of the ionosphere.

4.3.4. *Terminator Region*

Finally, the near-terminator boundary layer deserves special mention. Brace *et al.*'s (1982) clouds appear different in this region in that they tend to be located at greater distances from the main body of ionospheric plasma than do subsolar clouds (see Figure 29). The superthermal ion populations become more common (Taylor *et al.*, 1981; Kasprzak *et al.*, 1981) but the dependence of the details of their appearance on solar zenith angle has not been examined. Because the ionopause in this region has a much more irregular appearance than in the subsolar region, boundary-layer analyses become complicated. Even the greater altitude variability of the high solar zenith angle current layer, illustrated in the lower part of Figure 24, is not well understood. As mentioned above, the Kelvin–Helmholtz instability provides one interpretation (Wolff *et al.*, 1980). However, the picked up planetary ions, which have gradually accumulated from the subsolar point, probably have sufficient momentum near the terminator to also influence the boundary layer. Alternatively, there could be other scavenging processes at work which involve the magnetohydrodynamics of the interaction between the magnetosheath draped field and the ionosphere (cf. Russell *et al.*, 1982) in the form of the $\bar{J} \times \bar{B}$ body force. Given the picture of ion pickup formed earlier in this discussion,

it would seem useful to examine the terminator ionopause and mantle for interplanetary field orientation responses. Once again, the need arises for more coordinated ionosphere and solar wind data analyses in this comet-like planetary region.

4.4. Ionosphere features

4.4.1. *Solar Wind Interaction Effects on Temperatures*

The ionosphere below the boundary layer deserves to be included in a discussion of the solar wind interaction with Venus because it exhibits many special characteristics that it would not have in the absence of the solar wind. An earlier section describes the properties that the dayside ionosphere has in spite of the solar wind interaction, including a peak ion density at ~ 140 km, flow that is a combination of a zonal superrotation and antisolar motion in the horizontal direction, and downward in the vertical direction, and a composition that reflects the results of photoionization of the neutral constituents, recombination and transport. The nominal ionospheric plasma drifts appear to result from the combination of photochemistry, gradients in the plasma pressure, gravity, vertical polarization electric fields, and collisional coupling to the neutrals in the thermosphere.

Early in the Pioneer Venus Orbiter mission, it was perceived that another energy source besides the solar illumination was necessary to produce the observed electron and ion temperature profiles in the dayside ionosphere (cf. Cravens *et al.*, 1980; Miller *et al.*, 1980). The average weak magnetic fields observed in the ionosphere could restrict the electron motions, but could not by themselves explain the electron temperature anomaly. However, the plasma waves measured at the ionopause appear to provide a sufficient heat source for the electrons if they undergo Landau damping at the top of the ionosphere (Taylor *et al.*, 1979). As was noted above, these waves may arise from plasma instabilities caused by ion pickup in the boundary layer or driven by the ionopause curent itself. Alternatively, the bow shock may be the source since plasma waves are easily produced there (Scarf *et al.*, 1980), but the waves' propagation into the inner magnetosheath remains to be demonstrated. In either case, the solar wind interaction provides this energy input. For ions, Gombosi *et al.* (1980) examined the possibility that solar wind proton absorption could cause the observed heating with negative results. Although Cravens *et al.* (1980) consider that local chemical heating is a viable explanation for the additional heating in the ~ 160–200 km range required by the ion temperature observations, the upper boundary heat source for the ions remains to be determined. Both joule heating related to boundary layer ion dynamics, and the influx of planetary ions picked up by the solar wind (see Figure 15), would increase the topside heat flux. If either of these provide the source, then both additional electron and ion heat inputs to the Venus ionosphere can be attributed to the solar wind interaction.

4.4.2. *Ionospheric Magnetic Fields*

Another ionospheric feature that is attributable to the solar wind interaction is the ionospheric magnetic field. From the Pioneer Venus Orbiter data, the dayside

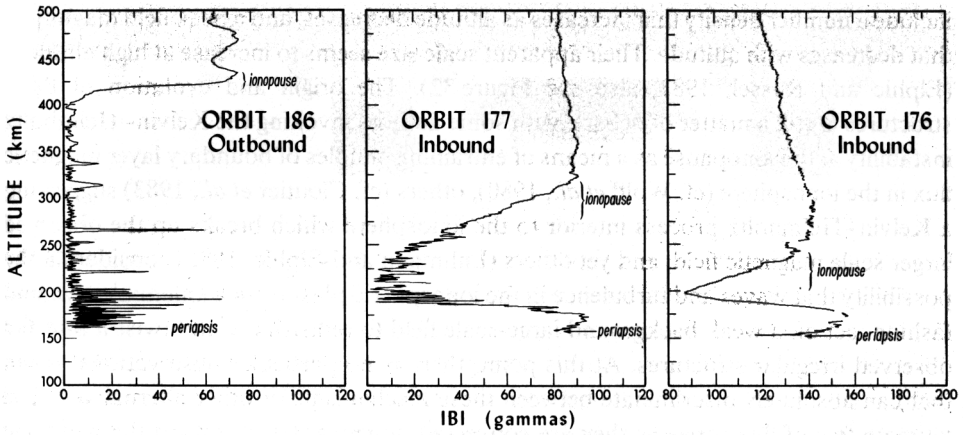

Fig. 32. Examples of altitude profiles of the magnetic field magnitude observed in the subsolar region near periapsis on the Pioneer Venus Orbiter. The location of the boundary-layer current sheet, where the magnetic pressure decreases and the thermal plasma pressure becomes dominant, is indicated. (From Luhmann *et al.*, 1980.)

ionospheric magnetic field, at altitudes above the spacecraft periapsis of ~150 km, is known to possess a dual nature. As illustrated in Figure 32, the field can take the form of turbulent, twisted structures with scale sizes of ~1 to 10 km, and peak fields of up to ~10 nT separated by much smaller (a few nT) fields, or appear as a large-scale horizontal field with magnitudes up to the values typically found in the overlying magnetosheath.

Elphic and Russell (1983) carried out a detailed analysis of the highly structured fields which have come to be known as 'flux ropes' due to their apparent twisted or helical field line configurations. Figure 33 displays some of the properties of these entities which

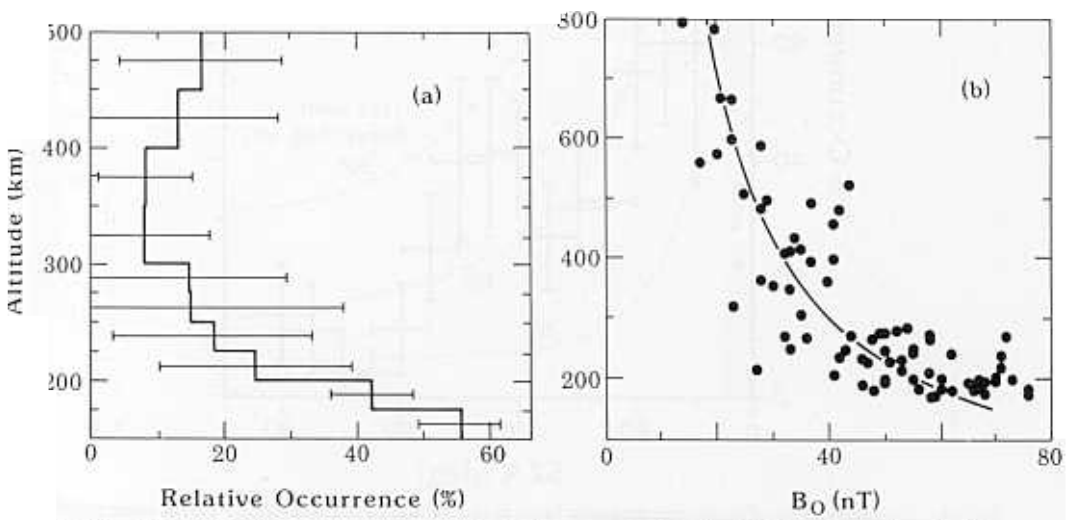

Fig. 33. Properties of the small scale magnetic structures seen in the dayside Venus ionosphere include an occurrence rate that increases with decreasing altitude (left) and a peak field magnitude that also increases with decreasing altitude (right). (From Luhmann and Elphic, 1985.)

include a number density that increases as altitude decreases, and a peak field magnitude that decreases with altitude. Their apparent scale size seems to increase at high altitudes (Elphic and Russel, 1983, also see Figure 32). The origin and evolution of these structures is still a matter of debate, with some authors invoking the Kelvin–Helmholtz instability at the ionopause as a means of entraining bundles of boundary layer magnetic flux in the ionosphere (cf. Wolff *et al.*, 1980), others (cf. Cloutier *et al.*, 1983) suggesting a Kelvin–Helmholtz process interior to the ionosphere which breaks up the observed larger scale magnetic field, and yet others (Luhmann and Elphic, 1985) considering the possibility that waves and turbulence in the ionospheric plasma, in a kinematic-dynamo fashion, act on a weak background large-scale field to redistribute and twist it into the observed irregular structures. At this point, there is no particular observational result that can absolutely discriminate between these mechanisms or other alternatives. The ultimate fate of flux ropes as they are convected downward and toward the nightside with the ionospheric plasma is also an unresolved question. Surely the same dissipative processes that will be seen to govern the large-scale field must play a part in their evolution.

The large-scale dayside horizontal ionospheric field appears in the Pioneer Venus Orbiter observations when the incident solar wind pressure lowers the pressure balance surface of the boundary layer to altitudes <250 km (Luhmann *et al.*, 1980; Phillips

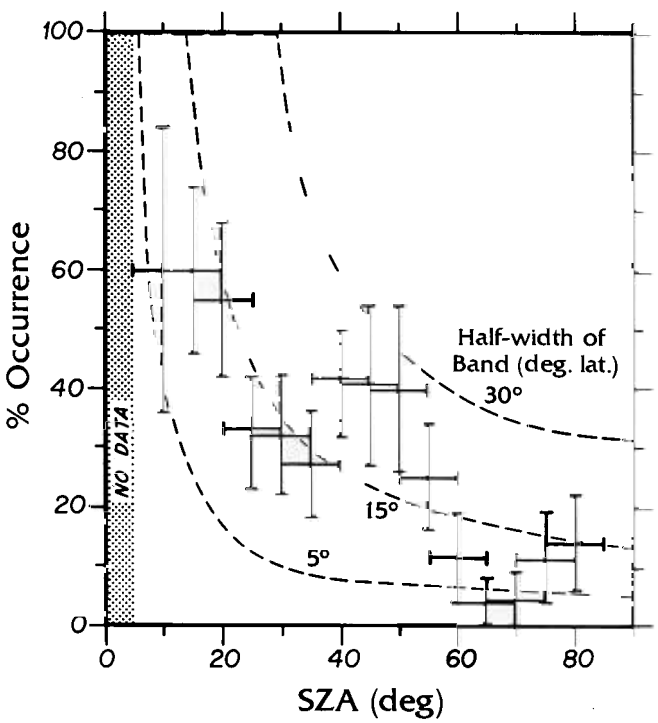

Fig. 34. Occurrence rate of large scale magnetic fields in the Venus dayside ionosphere versus solar zenith angle (from Luhmann *et al.*, 1980). The dashed lines show the distributions expected for latitudinal belts of various constant widths.

et al., 1984). This field occurs in conjunction with a thickened boundary current layer, so that the overall altitude profile is typically one having a characteristic minimum in the field magnitude at and above ~200 km, and a maximum at about 170 km. The examples given in Figure 32 illustrate the persistence of these features in spite of differences in the boundary-layer height and in the strength of the large-scale field (cf. Russell *et al.*, 1983). In the subsolar region (solar zenith angles $< 50°$), the large-scale field orientation usually reflects that of the overlying magnetosheath field. In fact, the large-scale field is most often observed in the subsolar region as is indicated in Figure 34. Although several authors have envisioned a 'belt' of field around the dayside ionosphere (cf. Luhmann *et al.*, 1980; Russell *et al.*, 1983), this solar zenith-angle distribution of occurrence actually suggests that the large-scale fields occur in a somewhat circular region centered near the subsolar point. In this regard, it is notable that Cloutier *et al.* (1983) propose the existence of a belt-like ionospheric field geometry with a somewhat circularized shape at small solar zenith angles, but it is difficult to reconcile their field line geometry with the existence of the strong fields in the subsolar region (cf. Luhmann *et al.*, 1986). Because of the infrequent occurrence of encounters with large-scale ionospheric fields at high-solar zenith angles, it has been difficult to formulate a global empirical model of this structure. Nevertheless, some degree of understanding of the large-scale ionospheric fields has been derived from one-dimensional modelling efforts.

For cases where the ionopause is at ~230 km or higher, the characteristic altitude profiles of the large-scale field can be explained as the result of the combination of

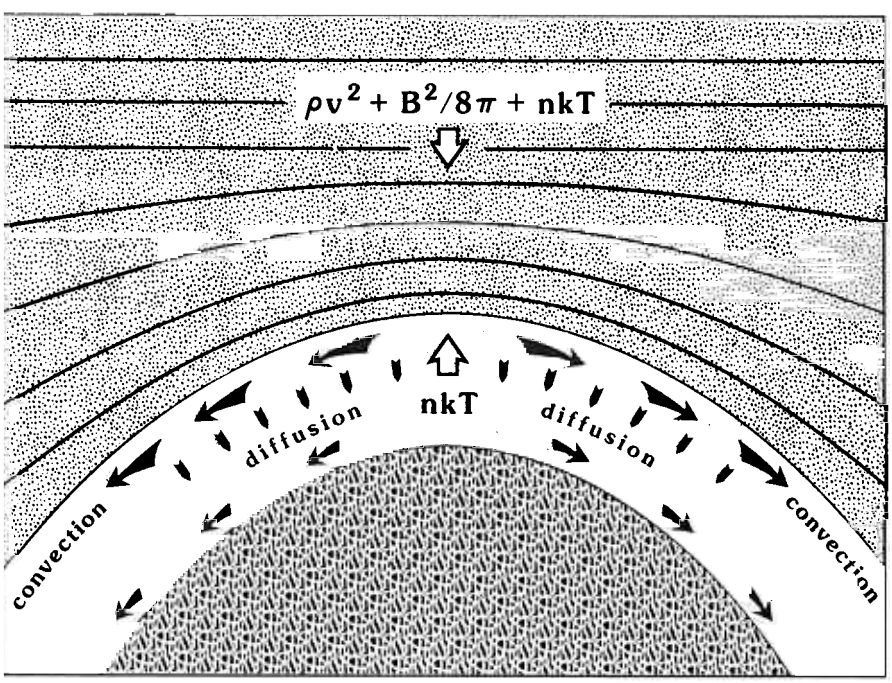

Fig. 35. Schematic of the subsolar ionosphere illustrating the convection/diffusion model for the generation of the large-scale dayside ionospheric magnetic field.

diffusion and vertical convection of magnetic flux from the ionopause downward into the ionosphere and collisional dissipation at the lower altitudes (cf. Luhmann *et al.*, 1984; Cravens *et al.*, 1984; Phillips *et al.*, 1984). This process is illustrated schematically in Figure 35, which depicts the subsolar ionosphere and its neighborhood. The altitude profile of the vertical velocity (Cravens *et al.*, 1984, also see Figure 8) produces the persistent field minimum at ~200 km where the downward velocity is a maximum. The 'stagnating' magnetic flux accumulates at the bottom of the ionosphere where the vertical transport is slow, but it does not accumulate indefinitely because collisions between ionized and neutral constituents damp out the charged particle drifts and hence the currents. Figure 36 from Phillips *et al.* (1984) illustrates how the ionopause position controls the degree of magnetization for the fixed vertical velocity profile. Note that the boundary magnetic field magnitude is larger for low ionopauses since, in their model, the magnetic pressure is equal to the ionosphere pressure at the ionopause. Of course,

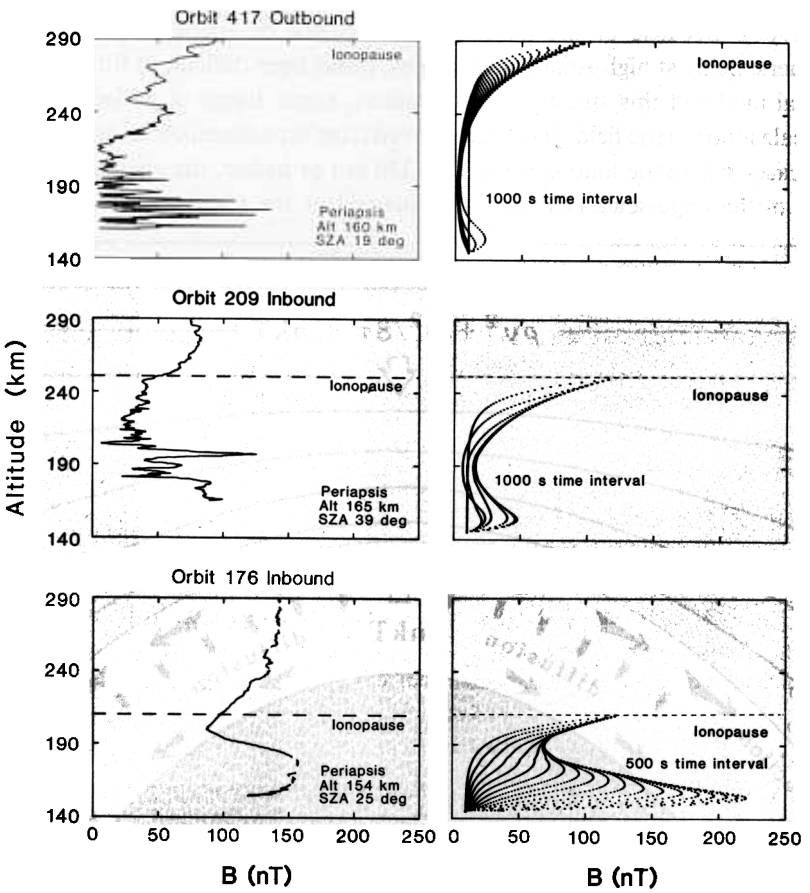

Fig. 36. Observations of the dayside ionospheric magnetic field magnitude for various solar wind conditions (left) compared with corresponding altitude profiles computed from the one-dimensional diffusion/convection model (right). (From Phillips *et al.*, 1984.)

the horizontal velocities must also participate in redistributing the magnetic flux, as suggested in Figure 35, but these effects are more difficult to model.

While successful for most observations, the above explanation for the large-scale ionospheric field fails when the incident solar wind dynamic pressure becomes so great that the projected boundary position, from pressure balance arguments, is below ~230 km. As Figure 37 suggests, the altitude where magnetic and thermal pressures

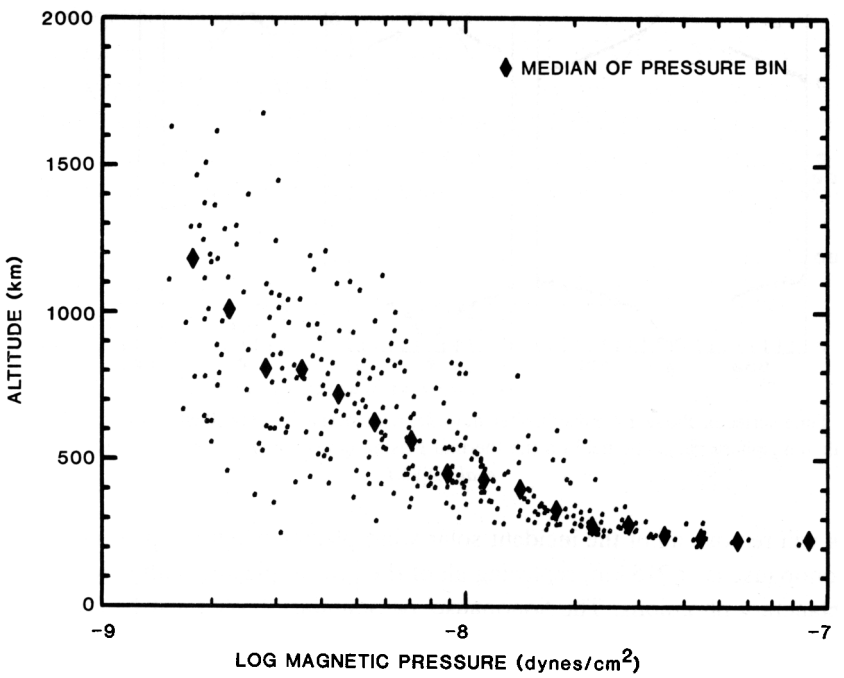

Fig. 37. Altitude of boundary layer current sheet versus the magnetic pressure in the boundary layer (a measure of the incident solar wind dynamic pressure as shown by Figure 26). (From Phillips *et al.*, 1984.)

first become equal has a limiting value of ~220 km (cf. Brace *et al.*, 1980; Phillips *et al.*, 1984). Under these conditions, the basic nature of the Venus-solar wind interaction must change because significant absorption of solar wind plasma by the atmosphere becomes inevitable. The magnetic field structure is no longer predictable by the simple kinematic dynamo treatment because, as Figure 38 demonstrates, the ionosphere's usual temperature and density (cf. Hartle *et al.*, 1980; Luhmann *et al.*, 1983b) and, hence, pattern of convection (Cravens *et al.*, 1984; Shinagawa *et al.*, 1986) are themselves altered by the solar wind interaction as the thermal ions become strongly magnetized (see Figure 30). Cloutier *et al.* (1983) have argued that a significant fraction of the incident solar wind is absorbed by the ionosphere in a manner that drives anti-sunward ionospheric convection and a large-scale ionospheric current system. Indeed, Gombosi *et al.* (1981) carried out a calculation which showed that charge exchange with planetary

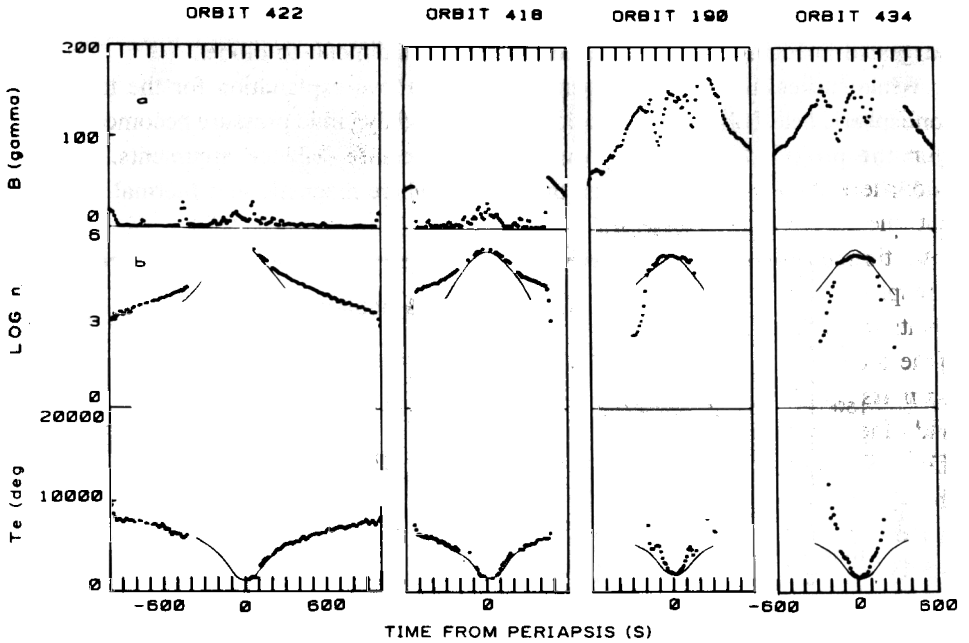

Fig. 38. Time series of Pioneer Venus Orbiter dayside, near periapsis data illustrating the effects of the large scale ionospheric magnetic field on the thermal plasma density and temperature. (From Luhmann *et al.*, 1983.)

neutrals will remove all of the incident solar wind plasma when the projected altitude of the ionopause is <215 km, replacing all of the proton plasma with cold (~ 10 eV), heavy planetary photoions. The 'ionopause' or boundary layer must be redefined on these occasions as the altitude where the thermal plasma pressure or density attains some nominal value. It is evident in these cases that the solar wind convection electric field is imposed across the collision-dominated plasma of planetary origin as was pointed out by Cloutier and Daniell (1979) and Cloutier *et al.* (1985), and that Ohmic currents with their resulting Joule heating must be driven inside of the ionosphere. However, as Vaisberg and Zeleny (1984) have noted, there are some problems with Cloutier and coworkers' treatment of currents from gradient-induced drifts. Moreover, these authors presume that the ionosphere adopts the convection pattern of the magnetosheath flow, an assumption that is probably not appropriate (cf. Cravens *et al.*, 1984). Shinagawa *et al.* (1986) have begun to take a more self-consistent approach, but they are still limited to a one-dimensional treatment, whereas this problem (unlike the low-to-medium dynamic pressure cases) is inherently global in nature. Thus, while solar wind electric fields must certainly drive resistive currents in the subsolar ionosphere when the solar wind dynamic pressure is very high, this subset of the observed large-scale ionospheric fields has yet to be modelled accurately. This limit of the solar wind interaction with Venus is of special interest because it is expected to be generally applicable to Mars, where the solar wind dynamic pressure typically exceeds the peak ionospheric pressure (cf. Slavin and Holzer, 1982).

Because the varying incident solar wind dynamic pressure does not always change in a quasi-steady manner, the transient response of the dayside ionosphere to sudden changes of the ionopause height (cf. Dryer *et al.*, 1982) is also of interest. Wolff *et al.* (1982) and Stein and Wolff (1982) have addressed this problem using a one-dimensional hydrodynamic model within the limitations of their model, which does not include the ionospheric magnetic fields or collisions with neutral atmosphere constituents, they find that when compression or expansion occurs on a time-scale that is faster than the sound travel time through the ionosphere, shock fronts and rarefaction fronts can form in the ionospheric plasma. These authors suggest that heating and cooling of the ionosphere results from the passage of these transient disturbances. They also suggest that some of the fine structure observed in ion density altitude profiles by the Pioneer Venus Orbiter ion mass spectrometer may be produced in this way. However, addition of magnetic fields and neutrals to these models seems essential for an accurate assessment of these effects. When there is a strong compression of the ionosphere, as in the cases discussed above, one expects the magnetic field and the neutral atmosphere to play crucial roles in the ionosphere dynamics. Indeed, even the solar wind interaction for the limit of steady high compression is not well understood.

4.4.3. *Terminator and Nightside Characteristics*

The terminator and nightside ionospheres are areas where observations exceed understanding to an even greater degree than for the dayside, but studies of these have been limited. For example, the phenomenology of wavelike fluctuations in ion density and temperature observed near the terminator on the Pioneer spacecraft in conjunction with wavelike magnitude variations in the weak horizontal ionospheric magnetic field was described in detail by Brace *et al.* (1983b) but possible connections with interplanetary conditions were not investigated. Similarly, Elphic *et al.* (1984) used the Pioneer Venus Orbiter Langmuir probe data to model empirically the transterminator flow of the ionospheric plasma without consideration of possible solar wind control. In connection with the latter, Brace *et al.* (1983a) noted that an observed difference in the dawn and dusk ionospheres might be caused by the preferred interplanetary field configuration of the Parker spiral and the resulting asymmetry in magnetosheath planetary ion pickup efficiency, although the ionosphere superrotation provides an alternative and perhaps more straightforward explanation. Nevertheless, organization of the data according to solar wind conditions may have given information relevant to the boundary layer control of the ionospheric convection (e.g., Perez-de-Tejada, 1986) which is difficult to resolve in the direct flow measurements of Knudsen *et al.* (1981).

It is generally accepted that the height of the terminator ionopause affects the transport of ionospheric plasma to the nightside (Cravens *et al.*, 1982). A lower ionopause on one side, from either external conditions or superrotation, could produce the observed local-time dependence in the nightside ionosphere properties (cf. Theis *et al.*, 1980). Similarly, a lower ionopause should affect the observed anomalously high nightside topside ion temperature if it is indeed caused by thermalization of the converging antisolar flow (Miller *et al.*, 1980). Such relationships have yet to be

established. On the other hand, Cravens *et al.* (1982, 1983), using the concept of the nightside ionosphere supply controlled by the terminator ionopause height (see also Johnson and Hanson, 1979), were able to explain the phenomenon of the 'disappearing ionosphere'. On occasions when the solar wind dynamic pressure is high enough to substantially lower the terminator ionopause altitude, the nightside ionosphere observed on the Pioneer Venus Orbiter is found to be greatly depleted as illustrated by Figure 39. This phenomenon proves the importance of transport from the dayside as a source. This state is evidently the nightside counterpart of the aforementioned high dynamic pressure-related dayside condition wherein magnetic field-generating currents are

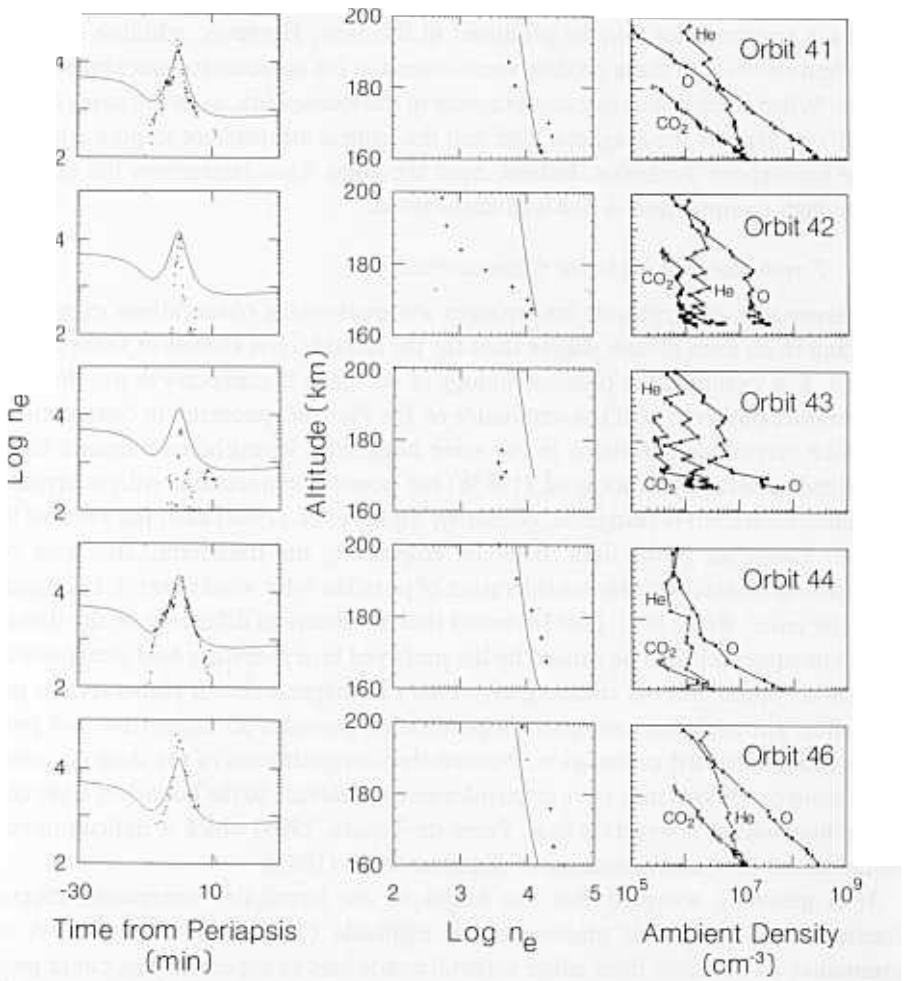

Fig. 39. Ionospheric density measurements from the Langmuir probe for a sequence of Pioneer Venus orbits in the form of time series (left) and outbound altitude profiles (center) during an episode of the 'disappearing ionosphere' phenomenon. The lines describe the Theis *et al.* (1984) ionospheric model for comparison. The corresponding neutral density behavior (from Niemann *et al.*, 1980) is shown on the right.

driven in the ionosphere by solar wind convection electric fields. When the ionospheric plasma is absent at night, stronger magnetic fields than usual are also present. The possible connection of these largely horizontal fields to the magnetosheath or to the dayside current system is at present an open question.

While the existence of disappearing nightside ionospheres strengthens the case for a transport-dominated source of the nightside ionosphere, the significant contribution of energetic particle precipitation (cf. Gringauz, 1983) has not yet been ruled out. Like a complementary experiment on the Venera spacecraft (cf. Verigin *et al.*, 1978), the retarding potential analyzer on the Pioneer Venus Orbiter (Knudsen *et al.*, 1980) detected sufficient fluxes of superthermal ($\sim$10–40 eV) electrons in the wake of the planet to cause a small but significant fraction of the nightside ionization. It is interesting to note that the horizontal magnetic fields which accompany the disappearing ionosphere would discourage vertical motion of these electrons into the atmosphere, thus cutting off both transport and precipitation sources (Cravens *et al.*, 1982). A related phenomenon is the 1304 Å nightside auroral emission discovered in the ultraviolet spectrometer images from the Pioneer Venus Orbiter as discribed by Phillips *et al.* (1986). Examples of this phenomenon, shown in Figure 40, illustrate its patchy

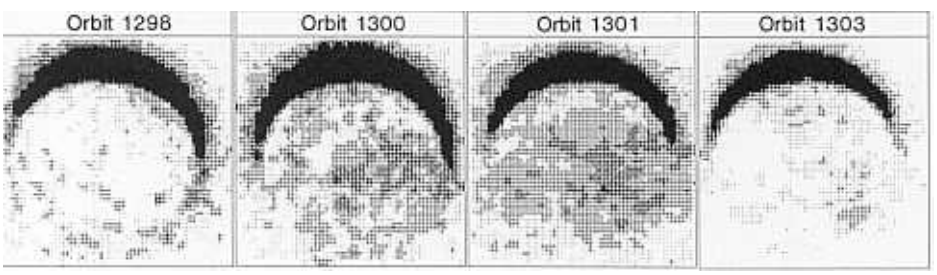

Fig. 40. Sequence of Pioneer Venus ultraviolet spectrometer (negative) images of the nightside showing auroral variations observed in the 1304 Å line of atomic oxygen. The black crescent is the visible section of the sunlit hemisphere. (From Phillips *et al.*, 1986.)

appearance and variable intensity ($\sim$10 to $\sim$100 Rayleighs). The electrons measured by Knudsen *et al.* (1985) in the wake are not sufficiently numerous or energetic to cause the brightest of these emissions, although they may explain the fainter background glow (Fox, 1986). Given this enigma, it is notable that Scarf *et al.* (1985) find evidence for an undetected high-energy electron population in the Pioneer Venus plasma wave and magnetic field data. These latter authors propose that some of Brace *et al.*'s (1982) clouds are connected with tail current sheets, current driven instabilities, and particle acceleration. It has also been suggested by Phillips *et al.* (1986) that the aurora arises from yet other corpuscular nightside ionization sources, namely, precipitating energetic ($>$ keV) particles of interplanetary or solar origin. However, Fox (1986) points out that the electron impact cross sections are so uncertain that even the limits on the lower energy electron precipitation source are not well determined. Thus, processes completely internal to the Venus interaction region cannot be ruled out.

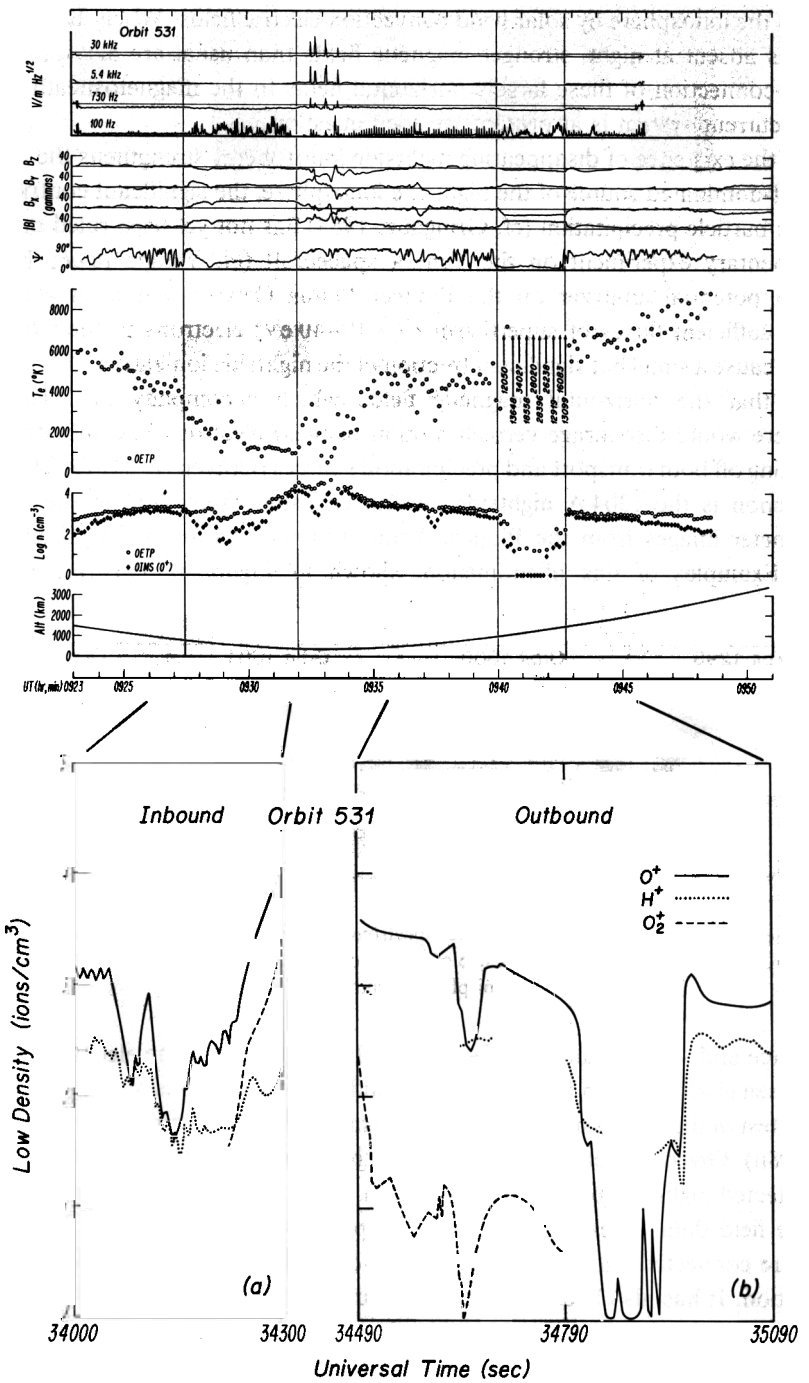

Fig. 41. Time series of Pioneer Venus Orbiter data obtained during a nightside periapsis pass showing two localized 'holes', or depletions in thermal plasma density, at ~09 : 28–09 : 32 and ~0.9 : 40–0.9 : 43 UT. These depletions are accompanied by unusually strong, sunward and antisunward directed magnetic fields and 100 Hz plasma wave activity. The inset at the bottom shows how the composition also changes within these features. (From Luhmann *et al.*, 1982.)

The aurora notwithstanding, the most unexpected feature of the nightside ionosphere has probably been the phenomenon of 'holes'. Observationally, the holes observed on the Pioneer Venus Orbiter appear as deep troughs in the electron (Brace *et al.*, 1982a) and ion (Taylor *et al.*, 1985) densities in the antisolar ionosphere which occur in conjunction with enhanced ($\sim$10–30 nT) sunward or anti-sunward directed magnetic fields. The collected data for one example in Figure 41 illustrates that these plasma troughs are also characterized by an anomalous composition which favors the light ions (H^+ and He^+) over the usual O^+, a superthermal electron component together with a colder than usual ionospheric electron population, and low-frequency (100 Hz) plasma wave activity (cf. Luhmann *et al.*, 1983). Holes are seen to extend from the Pioneer spacecraft periapsis at $\sim$150 km altitude, upward. Unlike the dayside large scale fields, they do not occur in response to extraordinarily high solar wind dynamic pressure (Luhmann *et al.*, 1981). Their apparent spatial distribution is such that they often appear in north–south pairs, with oppositely directed magnetic fields, in the local time interval between about 23 : 00 and 02 : 00 hr (cf. Brace *et al.*, 1982b). Figure 42, from Marubashi

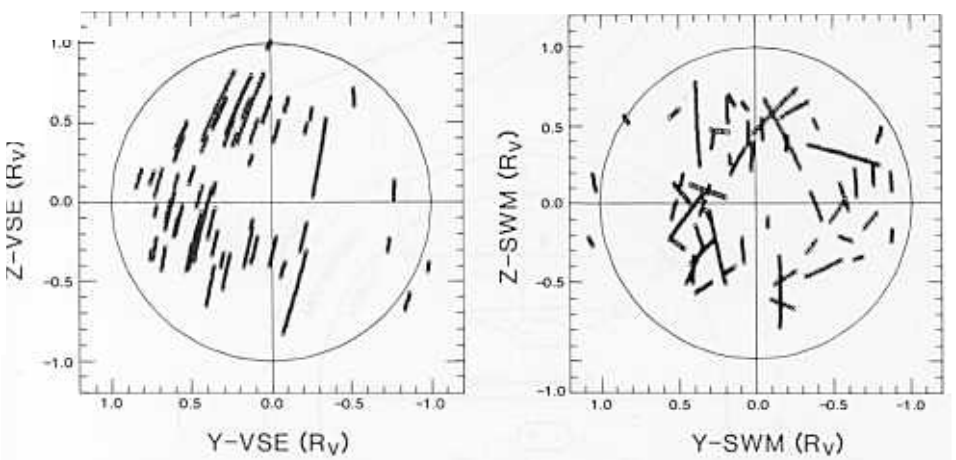

Fig. 42. Pioneer Venus Orbit segments where holes were observed projected onto the nightside of the planet (left), and these same data after they are rotated according to the external magnetic field direction (right). The two types of lines on the right indicate positive and negative (toward and away) magnetic field polarity. The external fields point along the y axis after rotation, so that the polarity division is consistent with that expected form magnetosheath field draping. (From Marubashi *et al.*, 1983.)

et al. (1985), shows the projected locations where holes were observed during a number of orbits with nightside periapsis. Analyses of the magnetic polarity of these features (Marubashi *et al.*, 1985; Luhmann and Russell, 1983), one of which is reproduced in Figure 42, support the hypothesis that they are controlled by the interplanetary magnetic field orientation rather than by some intrinsic planetary field (Knudsen *et al.*, 1982). Brace *et al.* (1982b) suggested the conceptual picture in Figure 43 for the evolution of the magnetic fields of holes from the draped interplanetary field, but theoretical ideas regarding the details of their origin by transport and either subsidence or escape of

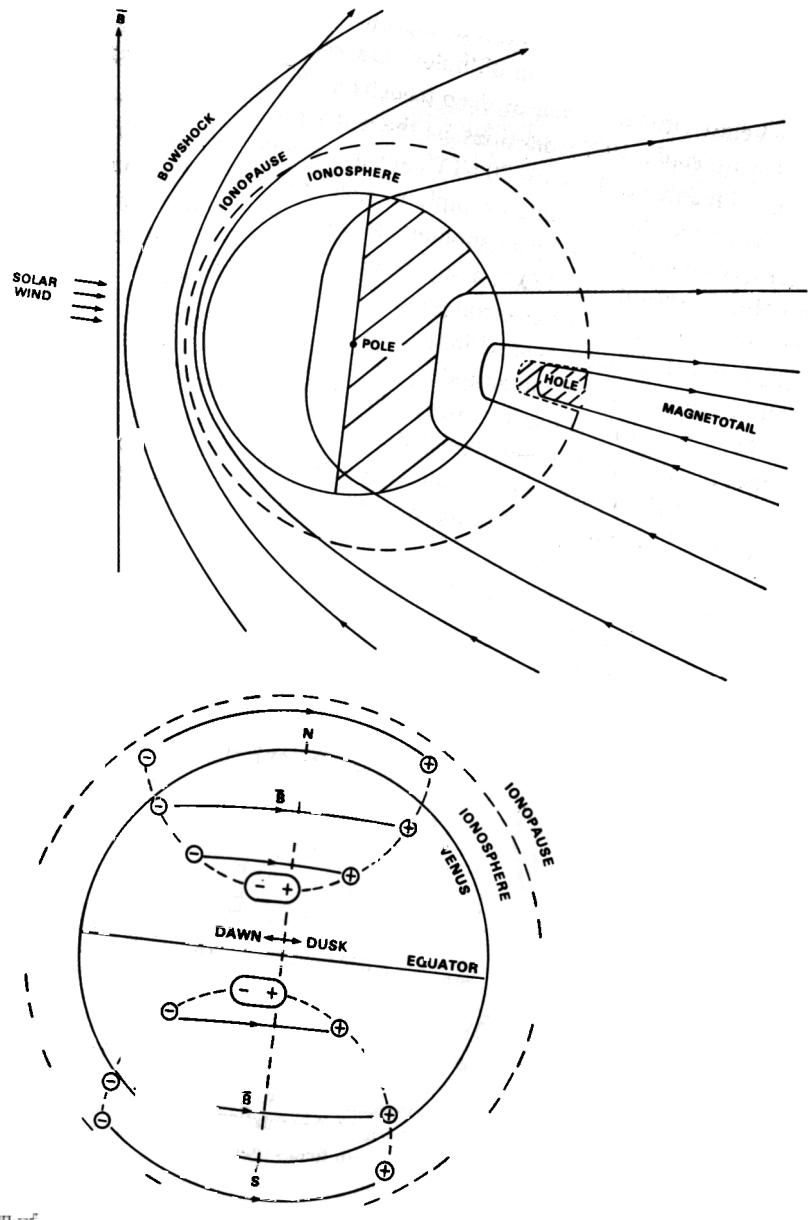

Fig. 43. Illustration of a possible scenario for the formation of holes, wherein low altitude magnetosheath flux tubes are anchored in the lower nightside ionosphere prior to being pulled away by the ongoing solar wind flow (from Brace *et al.*, 1983).

ionospheric plasma have been few. Grebowsky and Curtis (1981) proposed that parallel electric fields similar to those found in the earth's auroral zone could evacuate the magnetic flux tubes of the holes which were in turn maintained by the anti-sunward convection of the magnetized ionosphere. Another possible signature of such parallel

electric fields in holes might be the observed plasma waves, if produced in conjunction with accelerating particles, but at least the impulsive component of these waves could be generated at low altitudes by lightning (Scarf *et al.*, 1980; Scarf and Russell, 1983, Singh *et al.*, 1986). Plasma instabilities related to the sharp gradients of the holes' structure have also been invoked to explain the associated electric field emissions (Taylor *et al.*, 1985). Scarf *et al.* (1985) find signatures of anomalous electron distribution functions in the Pioneer Venus Langmuir probe data obtained in the near wake of the planet in association with other current layers. Nevertheless, there has been no hard evidence of energetic (keV) particles in conjunction with the holes nor is there evidence that the holes map to the patchy regions of 1304 Å auroral emissions.

It seems that many aspects of the nightside Venus ionosphere, including its dayside source in high altitude transport across the terminator, ionospheric holes, and probably the 1304 Å aurora on the nightside of Venus, are controlled by interplanetary conditions. If there was no solar wind, one would expect that antisolar pressure gradients would still supply a nightside ionosphere, which would exhibit some high altitude heating near the antisolar point from the colliding, converging ionospheric flow, but there would be not disappearing ionospheres, no holes, and most probably no aurora.

4.5. Neutral Atmosphere Features

4.5.1. *Loss of Constituents*

Most authors agree that the atmosphere of Venus started out with about the same constitution as that of the Earth, and that the $\sim 2 \times 10^{23}$ g of water in that original atmosphere has disappeared over the course of the planet's evolution (cf. Walker, 1975; Donahue and Pollack, 1983). There is little agreement, however, on the manner in which it disappeared. On explanation that involves only internal processes envisions destruction of the water vapor by photodissociation and the free escape of exospheric hydrogen, and then removal of the remaining oxygen by reaction with surface rocks over a period comparable to the age of the solar system. However, other hypotheses invoke the solar wind interaction for the removal of the hydrogen and oxygen constituents of water. This is tempting to do considering that the absence of an intrinsic field is a major difference between the Earth and Venus.

A number of authors (cf. Wallis, 1972;, Cloutier *et al.*, 1975) realized very early that, at Venus, photoionization and charge exchange of atmospheric atoms with solar wind protons will produce ions of planetary origin in the magnetosheath and upstream where they will be picked up and carried away. This same process was discussed above where its effects on the magnetosheath plasma, rather than the atmosphere, were of interest. It was noted that the rate of production of these ions, and therefore the rate of atmospheric escape, can be estimated by integrating the neutral exosphere density above an assumed ionopause at 250 km (see Figure 2) and multiplying by $4 \times 10^{-6}\ s^{-1}$. The latter rate reflects the contributions of both photoionization and charge exchange production mechanisms, which are thought to be of roughly equal importance. With this recipe, one finds that $\sim 10^{26}\ O^+$ ions and $\sim 10^{25}\ H^+$ ions are created above the

ionopause every second. Since hydrogen escape by other processes is most easily accomplished (cf. Hunten, 1982), one can consider the escape rate of oxygen as the key parameter in assessing the solar-wind effect. Thus, if 16/18 of the 2×10^{23} g of original water on Venus was photodissociated, and then its O^+ was ionized and lost to the solar wind at a rate of 10^{26} ions s^{-1}, it would take $\sim 10^{12}$ yr for the water to disappear. Given that the age of the solar system is only $\sim 5 \times 10^9$ yr, this loss rate appears to slow. Of course, the exosphere model (Figure 2) used to evaluate the ion production rate above the ionopause would not necessarily apply to all of the planet's history. This rate also presumes that Venus never had an appreciable intrinsic magnetic field, and that the lower atmosphere was similar enough over time to maintain the ionopause near its current altitude. However, if these additional considerations are overlooked, the ion-pickup process seems as if it could not have been significant in the disappearance + of Venus' water.

Another potential atmosphere loss process related to the solar wind interaction is even more difficult to evaluate. Brace *et al.* (1982a) considered the phenomenon of the 'clouds' observed in the boundary layer from the Pioneer spacecraft as a manifestation of the scavenging of substantial volumes of ionospheric plasma by the solar wind in addition to the exospheric ion pickup loss. Because of the appearance of these features, they have not been attributed to the usual production of planetary ions (although this possibility was raised above), but rather to some bulk removal mechanism like the action of the hydromagnetic body force $(\bar{J} \times \bar{B})$ of the draped boundary-layer field on the thermal plasma at the ionopause (cf. Russell *et al.*, 1982). The estimated current O^+ loss rate from this process, which for reasons of observational limitations involves many assumptions about the shape and distribution of the clouds and the dynamics of their removal, is about 10^{25}–10^{26} s^{-1} (Brace *et al.*, 1986) or comparable to the loss due to ion pickup. Although this rate, like that of ion pickup, is too small to be important, more must be learned about the cloud features before they are dismissed as an alternative mechanism for water removal by the solar wind interaction.

4.5.2. *Ion-Neutral Coupling*

Although long-term, evolutionary effects of the solar wind interaction on the Venus atmosphere appear to have attracted the most interest, there may also be significant day-to-day effects. In the upper atmosphere below the ionopause, there is likely to be some exchange of energy between the colliding neutral and ionized species. The effects of ion drag may be seen in the apparent superrotation of the ionosphere if it is indeed somehow driven by the inferred thermospheric zonal wind (Miller *et al.*, 1984). Moreover, this frictional force should have effects on the thermospheric wind itself. In addition, when ohmic currents are generated in the lower ionosphere during periods of high solar wind pressure, as discussed earlier, some of the dissipated heat will go into the neutrals. Yet little has been done to correlate the behavior of the neutrals observed between ~ 150 km and 200 km with the ionospheric and solar wind conditions. There are some intriguing prospects for such studies suggested by the observations. For example, Figure 39 shows corresponding unusual altitude profiles in the nightside

Pioneer Venus Orbiter data form the neutral mass spectrometer (Niemann *et al.*, 1980) and the Langmuir probe (Brace, personal communication). The electron density data are characteristic of the state described previously as the 'disappearing ionosphere' which is related to high solar wind pressure. The reason why the nightside neutral atmosphere should be affected by the processes which produce this ionospheric state is not understood, but it may reflect a change in the global heat or momentum transfer between the neutral and ionized constituents. It has also been suggested (Luhmann and Elphic, 1985) that some of the structures that are observed in the ionospheric magnetic field are a manifestation of small scale neutral motions (e.g., gravity waves) coupled to

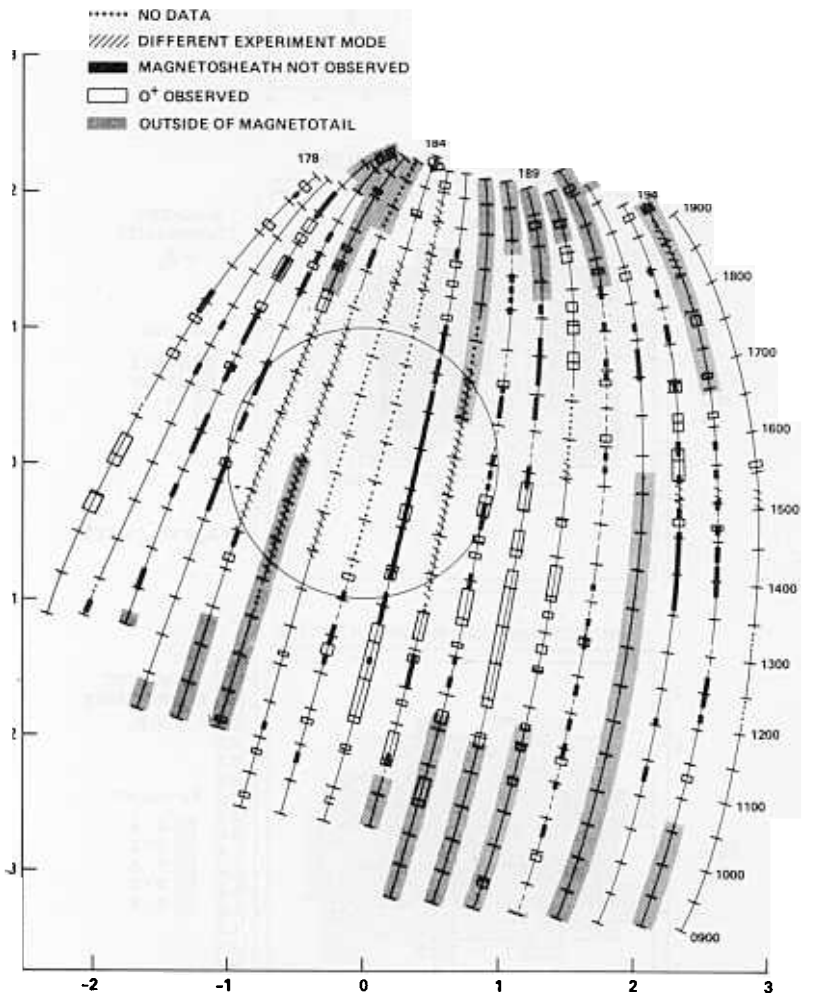

Fig. 44. Projections of Pioneer Venus nightside apoapsis Orbit segments on the terminator plane showing where the plasma analyzer observed the wake ion plasma cavity (black bars) and picked up O^+ (white bars) near $\sim 12\ R_v$ (from Mihalov and Barnes, 1981). The oxygen appears in the energy/charge spectra as in Figure 22.

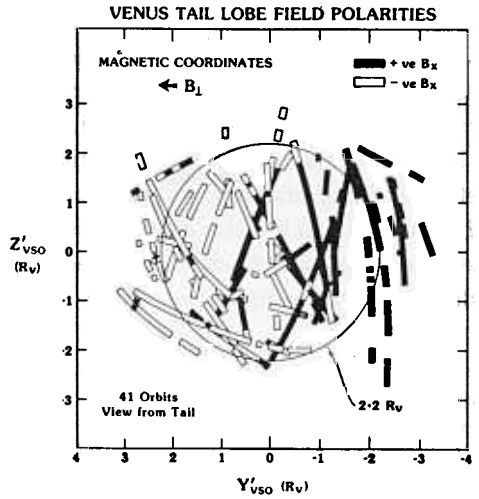
VENUS TAIL LOBE FIELD POLARITIES
MAGNETIC COORDINATES
← B⊥
+ ve Bx
− ve Bx
41 Orbits
View from Tail
2·2 Rv
Z'VSO (Rv)
Y'VSO (Rv)

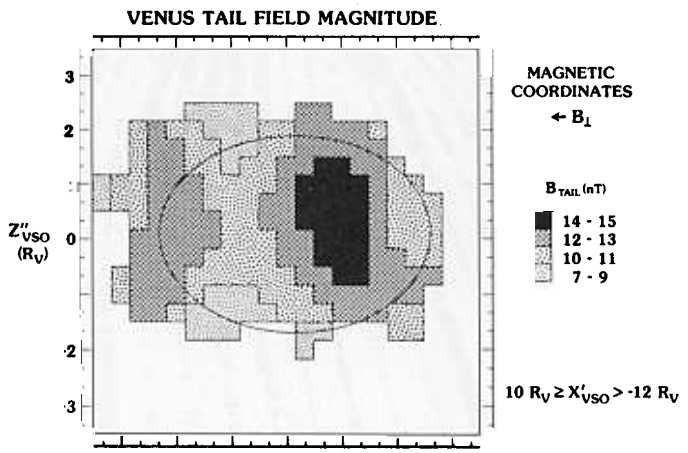
VENUS TAIL FIELD MAGNITUDE
MAGNETIC COORDINATES
← B⊥
BTAIL (nT)
14 - 15
12 - 13
10 - 11
7 - 9
10 RV ≥ X'VSO > -12 RV
Z''VSO (RV)

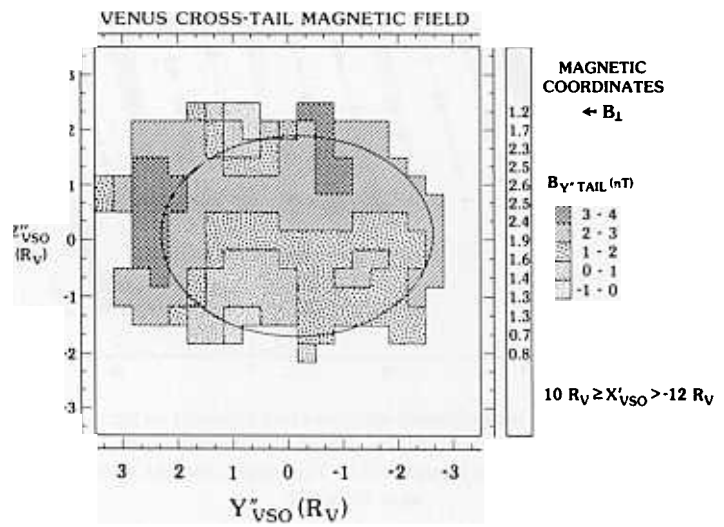
VENUS CROSS-TAIL MAGNETIC FIELD
MAGNETIC COORDINATES
← B⊥
BY' TAIL (nT)
3 - 4
2 - 3
1 - 2
0 - 1
-1 - 0
10 RV ≥ X'VSO > -12 RV
Y''VSO (RV)

the ionosphere. Overall, the influence of neutral dynamics on the ion dynamic, and vice versa, is something that has not been fully assessed.

4.6. Wake and Magnetotail

4.6.1. *Plasma and Magnetic Tail*

Observations at Venus tell us that, at least out to the 12 R_v distance of the Pioneer Venus Orbiter apoapsis, a cavity in the solar wind ion plasma persists. A cross-section of this region as described by Mihalov and Barnes (1982), in terms of both plasma and magnetic field measurements along the Pioneer Venus orbit, is reproduced in Figure 44. Venera experiments had also detected an ion cavity (cf. Gringauz, 1983), but found that superthermal electrons (10 to 10 s of eV) were present in agreement with some other Pioneer Venus observations by Knudsen *et al.* (1984)., thereby raising the possibility that solar wind electrons do enter the wake. The plasma flow and draped magnetic field outside the ion cavity appear to be well described by the post-terminator gas dynamic magnetosheath model (cf. Russell and Vaisberg, 1983). However, inside is a classical double-lobed induced magnetotail structure wherein the field magnitude is enhanced above magnetosheath levels and points in nearly sunward or anti-sunward directions (Russell *et al.*, 1981) in a manner analagous to a comet's tail.

Since the publication of *Venus*, much effort has gone into the analysis of the Pioneer Venus magnetotail magnetic field data. Slavin *et al.* (1984) determined the average ($\sim$5–10 nT) lobe field strengths and directions. Russell *et al.* (1985) presented a picture of the tail lobe polarity structure shown at the top of Figure 45, which demonstrated the anticipated comet tail-like organization by the cross flow or perpendicular component of the interplanetary magnetic field as found earlier in the Venera data by Eroshenko (1979). This picture also indicated that the magnetotail cross-section at $\sim$10–12 R_v distance is flattened in the direction of the perpendicular interplanetary field as sketched earlier by Vaisberg and Zeleny (1984). Flattening like this is expected from magneto-hydrodynamic effects, but mass loading may also be a factor in producing this shape. The tail field polarity distribution is found to be unequal, on the average, due to the significant flow-aligned component of the average Parker spiral field at Venus (cf. McComas *et al.*, 1986).

Saunders and Russell (1986) determined the contours of the average field magnitude and cross-tail field (in the direction of the perpendicular interplanetary field) which are also shown in Figure 45. The result for the cross-tail field is important because it shows that the cross tail field, together with the lobe fields, produce bent field lines that generally cross the current sheet in the tail region behind the planet, rather than near

←Fig. 45. (Top) Some Pioneer Venus Orbit segments, rotated to coalign the upstream magnetic fields in the y direction and projected on the terminator plane, showing where positive and negative magnetotail lobe fields are observed. As in the case of the hole field polarities (Figure 42), this pattern of polarites is consistent with what is expected for interplanetary field draping (from Russell *et al.*, 1983). Also shown are contours of magnetic field magnitude in the magnetotail (center), and contours of the magnitude of the cross-tail component of the Venus magnetotail field (bottom) at $\sim$12 R_v. (From Saunders and Russell, 1986.)

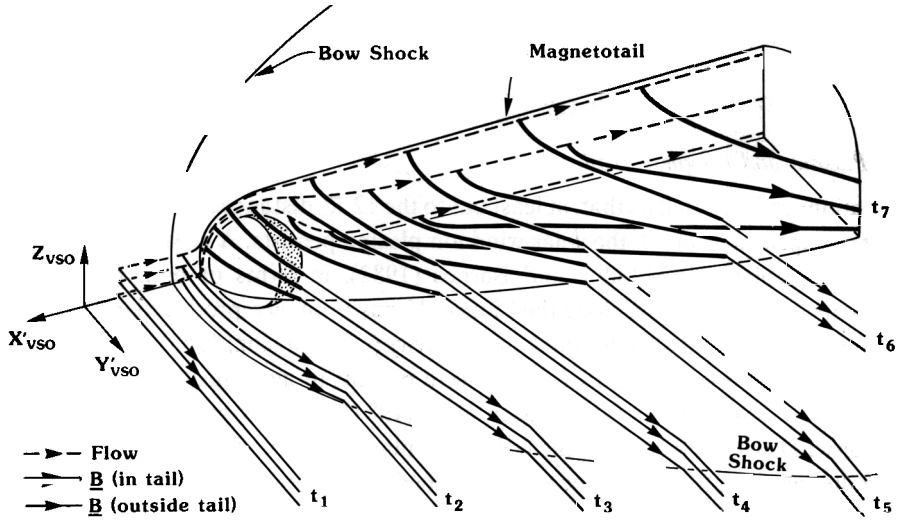

Fig. 46. Magnetotail field line geometry deduced by Saunders and Russell (1986) from Pioneer Venus Orbiter observations.

or in front of the planet. The deduced magnetotail field line configuration as illustrated by Saunders and Russell is given in Figure 46. Notice that the bending of field lines is most severe near the center of the tail where the flux tubes which have been most heavily mass loaded (by virtue of their passage closest to the planet) are found. Slavin *et al.* (1985) separated out the regions which were near this current sheet (e.g., near-polarity reversals in the lobes) in their investigation of the tail field properties. Subsequently, McComas *et al.* (1986) found that analysis of the current sheet could be improved if one made use of an empirical relationship between the field magnitude and orientation, and the assumption that the cross-tail magnetic field was in the direction of the upstream perpendicular field. The thickness of the current sheet inferred from their empirical model is shown in Figure 47. These authors also used their description of the magnetic field in the lobes and current sheet to estimate the plasma density and temperature in the equatorial plane of the magnetotail. They deduced that the current sheet could range from a $0.9\,cm^{-3}$, 6×10^6 K proton plasma to a $0.06\,cm^{-3}$, 9×10^7 K oxygen ion plasma, neither of which were measurable by available spacecraft instrumentation. This current sheet plasma is inferred to be accelerating toward the solar wind speed as it moves down the tail. It is notable that these authors estimate an escape rate for oxygen ions that is approximately equal to the aforementioned rate of ion production in the magnetosheath.

In general, the interpretations that are given with the observations have involved only rough calculations because there are still many unknowns in the Venus magnetotail formation process. Russell *et al.* (1985) and Saunders and Russell (1986) point out that the observed tail magnetic flux of 3 megawebers far exceeds the flux observed to thread the dayside ionosphere. In addition, they argue that since the normal component of the

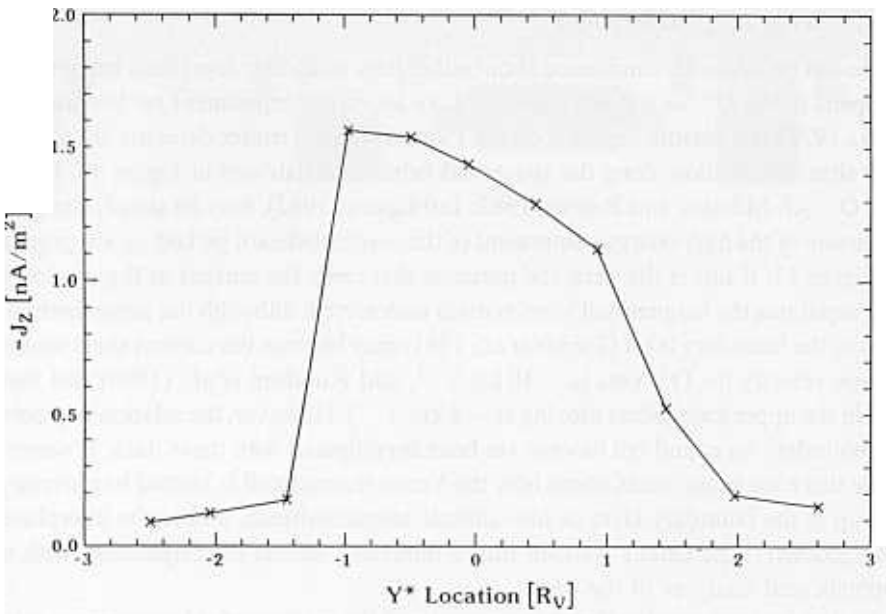

Fig. 47. Average current density across the magnetotail deduced by McComas et al. (1986) from Pioneer Venus Orbiter magnetometer observations.

field across the tail magnetopause is small (~ 1 nT), and the solar wind flows at $\sim 4\,R_v$ per minute, the resupply of flux must come from the magnetosheath below $\sim 0.5\,R_v$ altitude every few minutes. This approximation is in fact consistent with some of the ideas put forth by Vaisberg and Zeleny (1984), who consider the region of planetary ion pickup on low altitude magnetosheath field lines as the source of the magnetotail. As was discussed earlier, O^+ ions created and picked up in the innermost magnetosheath or boundary layer will have small gyroradii which allow them to escape absorption by the lower atmosphere (see Figure 15). These ions will be accelerated up to the speed of the low altitude magnetosheath protons, but they will be 16 times heavier, and by conservation of momentum should retard the average flow from which their energy was derived. This boundary layer may be sufficient in its extent to supply the needed magnetotail magnetic flux (see also Breus, 1979). However, with this scenario one still does not have a picture of how the magnetic flux from the heavy ion-laden boundary layer gets inside of the magnetotail. Possibly the boundary-layer magnetic field leaks into the void of the wake by diffusion, but the magnetohydrodynamic body force ($\bar{J} \times \bar{B}$) may also help to drag boundary-layer flux tubes into the wake since these draped tubes are still connected to the flowing solar wind. Venera measurements of a thick boundary layer over the magnetic 'poles' compared to the magnetic 'equator' (cf. Russell and Vaisberg, 1983) suggest that the most heavily mass-loaded boundary-layer flux tubes might sink toward the equatorial plane after they pass over the polar terminator because gravity exerts some control over their motion.

4.6.2. *Picked Up Planetary Ions*

Little can be said with confidence about either how boundary-layer ions behave or what happens to the O^+ as it flows tailward. Like an earlier experiment on Venera (Verigin *et al.*, 1978), the plasma analyzer on the Pioneer Venus Orbiter detected O^+ in the tail. The sites of detection along the spacecraft orbit are illustrated in Figure 44. However, this O^+ (cf. Mihalov and Barnes, 1982; Intriligator, 1982), may be simply the tailward extension of the high-energy component of the magnetosheath picked up ion population of Figure 15. If this is the case, the particles that carry the current in the current sheet that separates the magnetotail lobes remain undetected, although the superthermal ions seen in the boundary layer (Taylor *et al.*, 1981) may become the current sheet ions. (The escape velocity for O^+ ions is ~ 10 km/s^{-1}, and Knudsen *et al.*, (1980) find thermal O^+ in the upper ionosphere moving at ~ 8 km/s^{-1}). However, the relationship between the boundary layer and tail has not yet been investigated with these data. It seems that while there are rough ideas about how the Venus magnetotail is related to planetary ion pickup in the boundary-layer or low-altitude magnetosheath, and to the interplanetary field geometry, the details warrant future modelling efforts in conjunction with more sophisticated analyses of the data.

To date, the only studies that have considered the magnetic field geometry in relation to the observed O^+ ions are those of Verigin *et al.* (1978) who found the energetic ions to sometimes be correlated with reversals in the tail-lobe field polarities, and Perez-de-Tejada *et al.* (1982) who determined that the O^+ in the wake was generally moving in the direction of the local solar wind plasma flow and not along the magnetic field. It has not yet been demonstrated whether the energetic O^+ seen in the Pioneer Venus Orbiter plasma analyzer data is organized by the interplanetary field direction in a manner analogous to Figure 15, although an analysis of this type is in progress (Slavin, personal communication).

Further observational studies that are currently underway include analysis of the region of magnetotail formation previously unobservable from the initial Pioneer Venus spacecraft orbit. Brace *et al.* (1986) are examining periapsis data obtained in the wake during the past few years which give information about the high-altitude evolution of holes and clouds, and the roots of the magnetotail. These data, unfortunately, show a degree of complexity that is difficult to unravel. Highly-structured ionospheric thermal electron and both thermal and superthermal ion intrusions are found a few thousands of kilometers downstream in conjunction with magnetic fields with large sunward or antisunward components and alternating directions. The plasma configuration here seems to be largely magnetic field-dominated. In another new study, Russell (1986) is examining changes in the magnetotail magnetic field characteristics at different phases of the solar cycle. A less developed structure is seen at solar minimum, in agreement with the idea that planetary ion pickup in the boundary layer is important in tail formation. The goal, of course, is to synthesize a picture of the observations which will bring the physics of the Venus magnetotail to light.

5. Some Outstanding Questions

For Venus, as for most subjects of research, observations have raised as many questions as they have provided answers. Figure 48 contains a summary illustration of Venus in the solar wind with many of the attributes of the interaction, mentioned in this review, shown schematically. The complexity of the system and of the relevant physical

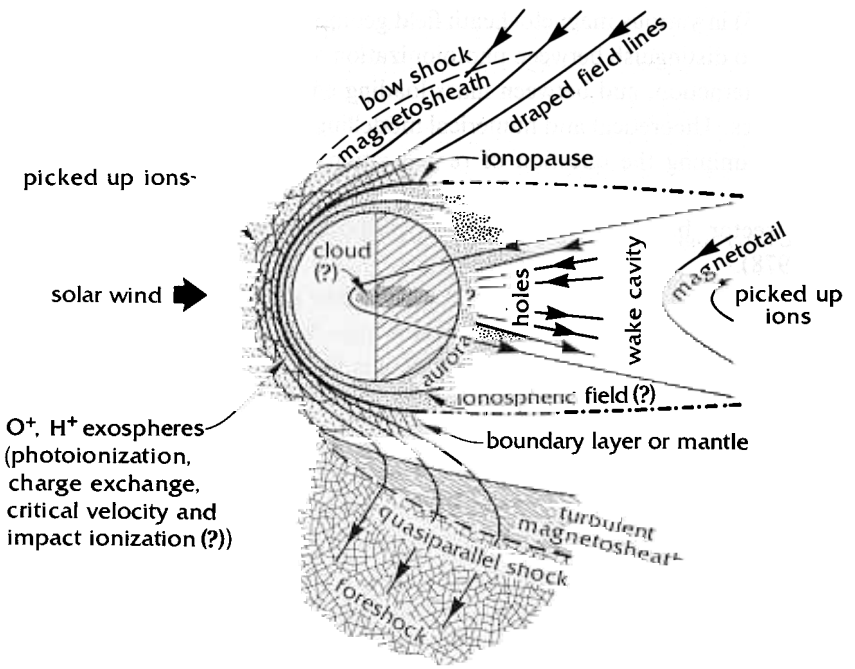

Fig. 48. Schematic illustration of the solar wind interaction with Venus including some of the features mentioned in this review.

processes is evident from even this highly simplified diagram. Of course, all of the processes shown will vary with the solar cycle, with solar wind parameters such as the dynamic pressure, and with changes in the orientation of the interplanetary magnetic field. Outstanding questions on which reasonable progress can be expected in the next few years can be grouped roughly into three basic areas: boundary layer and tail formation, global models, and the high-dynamic pressure interaction.

In particular, the available observations might tell us considerably more about mass loading and tail formation if emphasis was placed on looking at the behavior of the plasmas in relation to the global magnetic geometry in the magnetosheath and the upstream solar wind conditions. The observations that would be of most interest in this regard would be the thermal-ion clouds, the superthermal ions, and the energetic oxygen ions. Observations in the Pioneer Venus Orbiter extended mission phase will fill in some of the sampling gaps that currently exist. The relative importance of not only photoionization and charge exchange, but also of critical velocity ionization and electron impact

ionization of planetary atoms in the boundary layer must also be addressed. In this regard, the plasma waves observed there might provide some clues. Local models of the ionopause current layer, with finite gyroradius ions, are within the capabilities of current simulation techniques. It is expected that global 'mass-loaded' gas dynamic models (e.g., Breus *et al.*, 1986) and magnetohydrodynamic models (which unlike the gas dynamic models, will include a magnetotail) will become available for comparisons with the observations, and that a better understanding of the behavior of energetic pick up ions (see Figure 15) in various magnetosheath field geometries will be gained. These models will allow us to distinguish between photoionization and charge exchange effects on the solar wind interaction, and between mass loading effects and these of magnetohydrodynamic forces. Theoretical and numerical modelling efforts would also be particularly useful for examining the question of reconnection across the tail current sheet (cf. Kivelson and Russell, 1983) and phenomena such as tail disconnection during interplanetary sector boundary crossings as proposed for comets by Niedner and Brandt (1978).

Lastly, in anticipation of the Mars missions of the next decade, some concentrated efforts will be aimed toward understanding the high-dynamic pressure limit of the solar wind interaction observed by the Pioneer Venus Orbiter experiments. Since Mars is essentially always experiencing this limit because of its weaker ionosphere, (cf. Slavin and Holzer, 1982), many of the same processes that characterize the extreme Venus interaction should apply at Mars most of the time (as long as Mars also has a negligible intrinsic magnetic field). Thus, highly magnetized ionospheres, wherein the magnetic field governs the ion dynamics and energies as well as the electron properties, and where the 'ionopause' is formed by a process other than pressure balance with the ionosphere thermal pressure, should be the norm. It should also be the case that this limit is more prevalent at Venus at solar minimum when the ionospheric pressure is likely to drop by $\sim 50\%$ as the solar ionizing radiation flux falls. Analysis and modelling of the Venus ionosphere and solar wind interaction under high dynamic pressure conditions will allow us to make educated predictions which will hopefully be put to the observational test at Mars within the next decade. Such studies are an ideal example of how we can extrapolate between the hierarchy of solar wind interactions with the bodies in our solar system.

Acknowledgements

The writing of this review was supported by NASA grants NAS 2-12383 and NAGW 69.

This review benefitted from suggestions by many members of the Venus community, including C. T. Russell, R. C. Elphic, J. L. Phillips, J. A. Slavin, T. E. Cravens, L. Brace, F. L. Scarf, and J. Fox.

References

Alexander, C. J. and Russell, C. T.: 1985, *Geophys. Res. Letters.* **12**, 369.

Alexander, C. J., Luhmann, J. G., and Russell, C. T.; 1986, *Geophys. Res. Letters*, in press.

Banks, P. M. and Axford, W. I.; 1970, *Nature* **225**, 924.

Bauer, S. J., and Taylor, H. A., Jr: 1981, *Geophys. Res. Letters* **8**, 840.

Brace, L. H., Elphic, R. C., Curtis, S. A., and Russell, C. T., 1983, *Geophys. Res. Letters* **10**, 1116.

Brace, L. H., Taylor, H. A., Jr., Gombosi, T. I., Kliore, A. J., Knudsen, W. C. and Nagy, A. F., 1983, in D. M. Hunten, L. Colin, T. M. Donahue, and V. I. Moroz (eds.), *Venus*, Univ. of Arizona Press, Tucson, Arizona, p. 779.

Brace, L. H., Theis, R. F., Hoegy, W. R., Wolfe, J. H., Mihalov, J. D., Russell, C. T., Elphic, R. C., and Nagy, A. F.: 1980, *J. Geophys. Res.* **85**, 7663.

Brace, L. H., Theis, R. F., and Hoegy, W. R.: 1982, *Planetary Space Sci.* **30**, 29.

Brace, L. H., Theis, R. F., Mayr, H. G., Curtis, S. A., and Luhmann, J. G.: 1982b, *J. Geophys. Res.* **87**, 199.

Brace, L. H., Theis, R. F., Kasprzak, W. T., Taylor, H. A., Jr, Russell, C. T., Barnes, A., Mihalov, J. D. and Hunten, D. M.: 1986, *J. Geophys. Res.*, in press.

Breus, T. K.: 1979, *Space Sci. Rev.* **23**, 253.

Breus, T. K., Krymskii, A. M., and Mitnitskii, V. Ya.: 1986, *Planetary Space Sci.*, in press.

Cloutier, P. A.: 1975, *NASA Special Report NASA SP-397*, National Aeronautics and Space Administration, Washington DC, p. 111.

Cloutier, P. A. and Daniell, R. E., Jr.: 1979, *Planetary Space Sci.* **27**, 1111.

Cloutier, P. A., Daniell, R. E., Jr., and Butler, D. M.: 1974, *Planetary Space Sci.* **22**, 967.

Cloutier, P. A., Tascione, T. F., Daniell, R. E., Jr., Taylor, H. A., Jr., and Wolff, R. S.: 1983, in D. M. Hunten, L. Colin, T. M. Donahue, and V. I. Moroz (eds.), Univ. of Arizona Press, Tucson, Arizona, p. 941.

Cravens, T. E., Brace, L. H., Taylor, H. A., Jr., Russell, C. T., Knudsen, W. L., Miller, K. L. Barnes, A., Mihalov, J. D., Scarf, F. L., Quenmon, S. J., and Nagy, A. F.: 1982, *Icarus* **51**, 271.

Cravens, T. E., Crawford, S. L., Nagy, A. F., and Gombosi, T. I., 1983, *J. Geophys. Res.* **88**, 5595.

Cravens, T. E., Gombosi, T. I., and Nagy, A. F.: 1980a, *Nature* **283**, 178.

Cravens, T. E., Gombosi, T. I., Kozyra, J., Nagy, A. F., Brace, L. H., and Knudsen, W. C.: 1980b, *J. Geophys. Res.* **85**, 7778.

Cravens, T. E., Kliore, A. J., Kozyra, J. U., and Nagy, A. F.: 1981, *J. Geophys. Res.* **86**, 11323.

Cravens, T. E., Shinagawa, H., and Nagy, A. F.: 1984, *Geophys. Res. Letters* **11**, 267.

Donahue, T. M. and Pollack, J. B.: 1983, in D. M. Hinten, L. Colin, T. M. Donahue and V. I. Moroz (eds.), *Venus*, University of Arizona Press, Tucson, Arizona, p. 1003.

Dryer, M., Perea-de-Tejada, H., Taylor, H. A. Jr., Intriligator, D. S. Mihalov, J. D., and Rompolt, B.: 1982, *J. Geophys. Res.* **87**, 9035.

Elphic, R. C. and Ershkovich, A. I.: 1984, *J. Geophys. Res.* **89**, 997.

Elphic, R. C., and Russell, C. T.: 1983, *J. Geophys. Res.* **88**, 58.

Elphic, R. C., Brace, L. H., Theis, R. F. and Russell, C. T.: 1984, *Geophys. Res. Letters* **11**, 124.

Elphic, R. C., Mayr, H. G., Theis R. F., Brace, L. H., Miller, K. L., and Knudsen, W. C.: 1984b, *Geophys. Res. Letters* **11**, 1007.

Elphic, R. C., Russell, C. T., Luhmann, J. G., Scarf, F. L. and Brace, L. H.: 1981, *J. Geophys. Res.* **86**, 11430.

Elphic, R. C., Russell, C. T. Slavin, J. A., and Brace, L. H.: 1980, *J. Geophys. Res.* **85**, 7679.

Eroshenko, E. G.: 1979, *Cosmic Res.* **17**, 77.

Fox, J. L.: 1986, *Canad. J. Phys.*, in press.

Gombosi, T. I., Cravens, T. E., Nagy, A. F., Elphic, R. C., and Russell, C. T.: 1980, *J. Geophys. Res.* **85**, 7747.

Gombosi, T. I., Horanyi, M., Cravens, T. E., Nagy, A. F., and Russell, C. T.: 1981, *Geophys. Res. Letters* **8**, 1265.

Grad, H.: 1961, *Phys. Fluids* **4**, 1366.

Grebowsky, J. M. and Curtis, S. A.: 1981, *Geophys. Res. Letters*, **8**, 1273.

Greenstadt, E. W., Baum, L. W., Jordan, K. F., and Russell, C. T.: 1986, *J. Geophys. Res.*, in press.

Gringauz, K. I., 1983, in D. M. Hunten, L. Colin, T. M. Donahue, V. I. Moroz (eds.), *Venus*, University of Arizona Press, Tucson, Arizona, P. 980.

Gurnett, D. A., Anderson, R. R., Hausler, B., Haerendel, G., Bauer, O. H., Treumann, R. A., Koons, H. C., Holzworth, R. H., and Luhr, H.: 1985, *Geophys. Res. Letters* **12**, 851.

Hartle, R. E., Ogilvie, K. W., and Wu, C. S., 1973, *Planetary Space Sci.* **21**, 2181.

Hartle, R. E., Taylor, H. A., Jr., Bauer, S. J., Brace, L. H., Russell, C. T. and Daniell, R. E., Jr.: 1980, *J. Geophys. Res.* **85**, 7739.
Hoppe, M. M. and Russell, C. T.: 1982, *Nature* **245**, 41.
Hunten, D. M.: 1982, *Planetary Space Sci.* **30**, 773.
Intriligator, D. S.: 1982, *Geophys. Res. Letters* **9**, 727.
Intriligator, D. S. and Scarf, F. S.: 1982, *Geophys Res. Letters* **9**, 1325.
Intriligator, D. S. and Scarf, F. L.: 1984, *J. Geophys. Res.* **89**, 47.
Ip, W. H. and Axford, W. I., 1986, *Nature*, in press.
Johnson, F. S. and Midgely, J. E.: 1969, *Space Res.* **9**, 760.
Johnson, F. S. and Hanson, W. B.: 1979, *Geophys. Res. Letters* **6**, 581.
Kar, J., Mahajan, J. J., Srilakshmi, M. V., and Kohli, R.: 1986, *J. Geophys. Res.* 91, 8986.
Kasprzak, W. T., Taylor, H. A., Jr., Brace, L. H., Niemann, H. B., and Scarf, F. L.: 1982, *Planetary Space Sci.* **30**, 110.
Kivelson, M. G., and Russell, C. T.: 1983, *J. Geophys. Res.* **88**, 49.
Kliore, A. J., Moroz, V. I., and Keating, G. M. (eds.): 1985, *Adv. Space Res.* **5**.
Knudsen, W. C. and Miller, K. L.: 1985, *J. Geophys. Res.* **90**, 2695.
Knudsen, W. C., Banks, P. M. and Miller, K. L.: 1982, *Geophys. Res. Letters* **9**, 765.
Knudsen, W. C., Spenner, K., Michelson, P. F., Whitten, R. C. Miller, K. L., and Novak, V.: 1980a, *J. Geophys. Res.* **85**, 7754.
Knudsen, W. C., Spenner, K., and Miller, K. L., and Novak, V.: 1980b, *J. Geophys Res.* **85**, 7803.
Knudsen, W. C., Spenner, K., and Miller, K. L.: 1981, *Geophys. Res. Letters* **8**, 241.
Kumar, S.: 1982, *Geophys. Res. Letters* **9**, 595.
Lipatov, A. S.: 1978, *Cosmic Res.* **16**, 346.
Luhmann, J. G. and Elphic, R. C.: 1985, *J. Geophys. Res.* **90**, 12047.
Luhmann, J. G. and Russell, C. T., 1983a, *Geophys. Res. Letters* **10**, 409.
Luhmann, J. G. and Russell, C. T., 1983b, *Geophys. Res. Letters* **10**, 409.
Luhmann, J. H., Elphic, R. C., Russell, C. T., Mihalov, J. D., and Wolfe, J. H.: 1980, *Geophys. Res. Letters* **7**, 917.
Luhmann, J. G., Elphic, R. C., Russell, C. T., and Slavin, J. A.: 1981, *Geophys. Res. Letters* **8**, 517.
Luhmann, J. G., Elphic, R. C., Russell, C. T., Brace, L. H., and Hartle, R. E.: 1983, *Adv. Space Res.* **2**, 17.
Luhmann, J. G., Tatrallyay, M., Russell, C. T., and Winterhalter, D.: 1983, *Geophys. Res. Letters* **10**, 655.
Luhmann, J. G., Russell, C. T., Brace, L. H., Taylor, H. A., Jr., Knudsen, W. C., Scarf, F. L., Colburn, D. S., and Barnes, A.: 1982, *J. Geophys. Res.* **87**, 9205.
Luhmann, J. G., Russell, C. T., and Elphic, R. C.: 1984, *J. Geophys. Res.* **89**, 362.
Luhmann, J. G., Russell, C. T., Spreiter, J. R., and Stahara, S. S.: 1985, *Adv. Space Res.* **5**, 307.
Luhmann, J. G., Warniers, R. J., Russell, C. T., Spreiter, J. R., and Stahara, S. S.: 1986a, *J. Geophys. Res.* **91**, 3001.
Luhmann, J. G., Russell, C. T., and Phillips, J. L.: 1986b, *J. Geophys. Res.*, in press.
Luhmann, J. G., Phillips, J. L., and Russell, C. T.: 1986c, *Adv. Space Res.*, in press.
Marubashi, K., Grebowsky, J. M., Taylor, H. A., Jr., Luhmann, J. G., Russell, C. T., and Barnes, A.: 1985, *J. Geophys. Res.* **90**, 1385.
Mayr, H. G., Harris, I., Niemann, H. B., Brinton, H. C., Spencer, N. W., Taylor, H. A. Jr., Hartle, R. E., Hoegy, W. R., and Hunten, D. M.: 1980, *J. Geophys. Res.* **85**, 7841.
McComas, D. J., Spence, H. E., Russell, C. T., and Saunders, M. A.: 1986, *J. Geophys. Res.* **91**, 7939.
Mihalov, J. D. and Barnes, A.: 1981, *Geophys. Res. Letters* **8**, 1277.
Mihalov, J. D. and Barnes, A.: 1982, *J. Geophys. Res.* **87**, 9045.
Mihalov, J. D., Spreiter, J. R., and Stahara, S. S.: 1982, *J. Geophys. Res.* **87**, 10363.
Mihalov, J. D., Wolfe, J. H., and Intriligator, D. S.: 1980, *J. Geophys. Res.* **85**, 7613.
Miller, K. L., Knudsen, W. C., Spenner, K. Whitten, R. C., and Novak, V.: 1980, *J. Geophys. Res.* **85**, 7759.
Miller, K. L., Knudsen, W. C., and Spenner, K.: 1984, *Icarus* **57**, 386.
Nagy, A. F., Cravens, T. E., and Gombosi, T. I.: 1983, in D. M. Hunten, L. Colin, T. M. Donahue, and V. I. Moroz (eds.), *Venus*, Univ. of Arizona Press, Tucson, Arizona, p. 841.
Nagy, A. F., Cravens, T. E., Smith, S. G., Taylor, H. A., Jr., and Brinton, H. C.: 1980, *J. Geophys. Res.* **85**, 7795.
Nagy, A. F., Cravens, T. E., Yee, J. H., and Stewart, A. I. F.: 1981, *Geophys. Res. Letters* **8**, 629.
Niedner, M. B., Jr. and Brandt, J. C.: 1978, *Astrophys. J.* **223**, 655.

Niemann, H. B., Kasprzak, W. T., Hedin, A. E., Hunten, D. M., and Spencer, N. W.: 1980, *J. Geophys. Res.* **85**, 7817.
Omidi, N., Winske, D., and Wu, C. S.: 1986, *Geophys. Res. Letters*, in press.
Perez-de-Tejada, H.: 1986, *J. Geophys. Res.* **91**, 6765.
Perez-de-Tejada, Dryer, M., Intriligator, D. S., Russell, C. T., Brace, L. H.: 1983, *J. Geophys. Res.* **88**, 9019.
Perez-de-Tejada, H., Intriligator, D. S., and Scarf, F. L.: 1985, *J. Geophys. Res.* **90**, 1759.
Perez-de-Tejada, H., Intriligator, D. S., and Russell, C. T.: 1982, *Nature* **299**, 325.
Phillips, J. L. and Russell, C. T.: 1986, *Adv. Space Res.*, in press.
Phillips, J. L., Luhmann, J. G., and Russell, C. T.: 1984, *J. Geophys. Res.* **89**, 10676.
Phillips, J. L., Luhmann, J. G., and Russell, C. T.: 1985, *Adv. Space Res.* **5**, 173.
Phillips, J. L., Luhmann, J. G., and Russell, C. T.: 1986a, *J. Geophys. Res.* **91**, 7931.
Phillips, J. L., Luhmann, J. G., Russell, C. T., and Alexander, C.: 1986b, *Adv. Space Res.*, in press.
Phillips, J. L., Stewart, A. I., and Luhmann, J. G.: 1986c, *Geophys. Res. Letters*, in press.
Podgorny, I. M.: 1983, in D. M. Hunten, L., Colin, T. M. Donahue, and V. I. Moroz (eds.), *Venus*, University of Arizona Press. Tucson, Arizona, p. 994.
Romanov, S. A.: 1978, *Cosmic Res.* **16**, 256.
Russell, C. T.: 1977, *J. Geophys. Res.* **82**, 625.
Russell, C. T.: 1986, *Adv. Space Res.*, in press.
Russell, C. T. and Vaisberg, O., 1983, in D. M. Hunten, L. Colin, T. M. Donahue, and V. I. Moroz (eds.), *Venus*, Univ. of Arizona Press. Tucson, Arizona, p. 873.
Russell, C. T., Elphic, R. C., Luhmann, J. G. and Slavin, J. A.: 1980, *Proc. Lunar Planet. Sci. Conf. 11th*, p. 1897.
Russell, C. T., Elphic, R. C., and Slavin, J. A.: 1979, *Nature* **282**, 815.
Russell, C. T., Luhmann, J. G., Elphic, R. C., Scarf, F. L., and Brace, L. H.: 1982, *Geophys. Res. Letters* **9**, 45.
Russell, C. T., Luhmann, J. G., and Elphic, R. C., 1983, *Adv. Space Res.* **2**, 13.
Russell, C. T., Luhmann, J. G., and Phillips, J. L.: 1985a, *Geophys. Res. Letters* **12**, 627.
Russell, C. T., Saunders, M. A., and Luhmann, J. G.: 1985b, *Adv. Space Res.* **5**, 177.
Saunders, M. A. and Russell, C. T.: 1986, *J. Geophys. Res.* **91**, 5589.
Scarf, F. L. and Russell, C. T.: 1983, *Geophys. Res. Letters* **10**, 1192.
Scarf, F. L., Coroniti, F. V., Kennel, C. F., Gurnett, D. A., Ip, W. H., and Smith, E. J., 1986, *Science* **232**, 377.
Scarf, F. L., Neumann, S., Brace, L. H., Russell, C. T., Luhmann, J. G., and Stewart, A. I. F.: 1985, *Adv. Space Res.* **5**, 185.
Scarf, F. L., Taylor, W. W. L., Russell, C. T., and Brace, L. H.: 1980, *J. Geophys. Res.* **85**, 8158.
Schubert, G., 1983, in D. M. Hunten, L. Colin, T. M. Donohue, and V. I. Moroz (eds), *Venus*, Univ. of Arizona Press, Tucson, Arizona, p. 681.
Shinagawa, H., Cravens, T. E., and Nagy, A. F.: 1986, *J. Geophys. Res.*, in press.
Singh, R. N. and Russell, C. T.: 1986, *Geophys. Res. Letters*, in press.
Slavin, J. A. and Holzer, R. E.: 1981, *J. Geophys. Res.* **86**, 11401.
Slavin, J. A. and Holzer, R. E.; 1982, *J. Geophys. Res.* **87**, 10285.
Slavin, J. A., Elphic, R. C., and Russell, C. T.; 1979, *Geophys. Res. Letters* **6**, 905.
Slavin, J. A., Elphic, R. C., Russell, C. T., Scarf, F. L., Wolfe, J. H., Mihalov, J. D., Intriligator, D. S., Brace, L. H., Taylor, H. A., Jr., Daniell, R. E., Jr.: 1980, *J. Geophys. Res.* **85**, 7625.
Slavin, J. A., Holzer, R. E., Spreiter, J. R., Stahara, S. S., and Chaussee, D. S.: 1983, *J. Geophys. Res.* **88**, 19.
Slavin, J. A., Smith, E. J., and Intriligator, D. S.: 1984, *Geophys. Res. Letters* **11**, 1074.
Spenner, K., Knudsen, W. C., Miller, K. L., Novak, V., Russell, C. T., and Elphic, R. C.: 1980, *J. Geophys. Res.* **85**, 7655.
Spreiter, J. R. and Stahara, S. S.: 1980a, *J. Geophys. Res.* **85**, 6769.
Spreiter, J. R. and Stahara, S. S.: 1980b, *J. Geophys. Res.* **85**, 7715.
Stahara, S. S., Klenke, D., Trudinger, B. C., and Spreiter, J. R.: 1980, NASA Contractor Report, 3267: Application of Advanced Computational Procedures for Modeling Solar-Wind Interactions with Venus-Theory and Computer Code.
Stein, R. F. and Wolff, R. S.: 1982, *Icarus* **51**, 296.

Tatrallyay, M., Russell, C. T., Luhmann, J. G., Barnes, A., and Mihalov, J. D.: 1984, *J. Geophys. Res.* **89**, 7381.
Tatrallyay, M., Russell, C. T., Mihalov, J. D., and Barnes, A.: 1983, *J. Geophys. Res.* **88**, 5613.
Taylor, H. A., Jr., Brinton, H. C., Bauer, S. J., Hartle, R. E., Cloutier, P. A., and Daniell, R. E., Jr.: 1980, *J. Geophys. Res.* **85**, 7765.
Taylor, H. A., Jr., Daniell, R. E., Hartle, R. E., Brinton, H. C., Bauer, S. J. and Scarf, F. L.: 1981, *Adv. Space Res.* **1**, 247.
Taylor, H. A., Jr., Brebowsky, J. M., and Cloutier, P. A.: 1985, *J. Geophys. Res.* **90**, 7415.
Taylor, W. W. L., Scarf, F. L., Russell, C. T., and Brace, L. H.: 1979, *Science*, **205**, 112.
Theis, R. F., Brace, L. H., and Mayr, H. G., 1980, *J. Geophys. Res.* **85**, 7787.
Theis, R. F., Brace, L. H., Elphic, R. C., and Mayr, H. G.: 1984, *J. Geophys. Res.* **89**, 1477.
Vaisberg, O. L. and Zeleny, L. M.: 1984, *Icarus* **58**, 412.
Vaisberg, O. L., Intriligator, D. S., and Smith, E. J.: 1980, *J. Geophys. Res.* **85**, 7642.
Vaisberg, O. L, Romanov, S. A., Smirnov, V. N., Karpinsky, I. P., Khazanov, B. I., Polenov, B. V., Bogdanov, A. V., and Antonov, N. M.: 1976, in D. J. Williams (ed.), *Physics of Solar Planetary Environments*, American Geophysical Union, Washington, D.C., p. 904.
Verigin, M. I., Gringauz, K. I., Gombosi, T., Breus, T. K., Bezrukikh, V. V., Remizov, A. P. and Volkov, G. I.: 1978, *J. Geophys. Res.* **83**, 3721.
Walker, J. C. G.: 1975, *J. Atmos. Sci.* **32**, 1248.
Wallis, M. K.: 1974, in C. T. Russell (ed.), *Solar Wind Three*, Institute of Geophysics and Planetary Physics, Univ. of California, Los Angeles, California, p. 421.
Wallis, M. K. and Ip, W. H.: 1982, *Nature* **298**, 229.
Whitten, R. C., McCormick, P. T., Merritt, D., Thompson, K. W., Brynsvold, R. R., Eich, C. J., Knudsen, W. C., and Miller, K. L.: 1984, *Icarus* **60**, 317.
Winske, D., 1986, *J. Geophys. Res.*, in press.
Wolff, R. S., Goldstein, B. E., and Kumar, S.: 1979, *Geophys. Res. Letters* **6**, 353.
Wolff, R. S., Goldstein, B. E., and Yeates, C. M.: 1980, *J. Geophys. Res.* **85**, 7697.
Wolff, R. S., Stein, R. F. and Taylor, H. A., Jr.: 1982, *J. Geophys. Res.* **87**, 8118.
Wu, C. S., Winske, D. and Gaffey, J. D.: 1986, *Geophys. Res. Letters*, submitted.
Zwan, B. J. and Wolf, R. A.: 1976, *J. Geophys. Res.* **81**, 1636.